THESIS

LIVE-BED FAILURE MODES OF BENDWAY WEIRS AND ROCK VANES IN ALLUVIAL CHANNELS

Submitted by

Parker Maddocks

Department of Civil and Environmental Engineering

In partial fulfillment of the requirements

For the Degree of Master of Science

Colorado State University

Fort Collins, Colorado

Spring 2022

Master's Committee:

Advisor: Robert Ettema
Co-Advisor: Christopher Thornton

Ellen Wohl

ABSTRACT

LIVE-BED FAILURE MODES OF BENDWAY WEIRS AND ROCK VANES IN ALLUVIAL CHANNELS

Bendway weirs and rock vanes have been used and refined for decades to control thalweg location and alignment along alluvial channel-bends and decrease flow velocity along the outer bank of such channels. Since the early 2000s, Colorado State University's Hydraulics Lab has assisted the U.S. Bureau of Reclamation (USBR) in refining design guidelines for bendway weirs, rock vanes, and other in-stream rock structures. This effort has entailed optimizing the layout of configurations of bendway weirs and rock vanes. The present study, however, focuses on the failure modes of bendway weirs and rock vanes, and led to the development of refinements to the design recommendations for individual bendway weirs and rock vanes so that such structures can perform as intended, even though the structures have encountered scour. Live-bed conditions were selected for the experiments, as such conditions involve active bed-sediment transport and, thereby, pose more severe conditions than do clear-water conditions in which little bed-sediment transport occurs.

To investigate live-bed failure modes at bendway weirs and rock vanes, two flumes were used: a straight flume and a curved flume. The experiments used different parameters suggested in technical literature as documents as affecting bendway-weir and rock-vane performance (e.g., structure geometry, spacing, flow condition, and angle relative to a channel's outer bank). The straight flume was chosen for its capacity to create the constrained flow conditions needed to illuminate the failure modes, which then were verified using the curved flume, which was wider

and subject to the effects of flow curvature. Each experiment involved a series of three bendway weirs or rock vanes. Preliminary experiments indicated that three structures were needed, because of observed differences in the failure modes at the three structures in a series.

Experimental results revealed that failure modes of bendway weirs and rock vanes were primarily driven by rock dislodgement due to contraction scour at the tip of such structures, and by dune-trough presence at the upstream face (the first rock structure) and flow impingement (against the second rock structure). Also, flow swept some rock from the crest of bendway weirs and rock vanes. The observed failure modes in the straight flume were confirmed by the experiments using the curved flume, though the curved flume's curvature of flow and greater width partially obscured the failure modes.

The failure modes led to refinements regarding the design recommendations for the structure of bendway weirs and rock vanes. The recommendations essentially specify the widening and lengthening of the crest of bendway weirs and rock vanes, so that these rock structures may experience controlled failure to accommodate scour but preserve their main dimensions.

ACKNOWLEDGEMENTS

I would first like to thank my advisor, Dr. Robert Ettema who helped guide me through a majority of this study. Dr. Ettema has spent countless hours teaching, problem solving, reviewing, and discussing results. I greatly appreciate his time and energy put into this project. I would also like to thank Dr. Ettema for guiding me through my master's at CSU and teaching me about hydraulics in numerous fields. I would not be in the academic and professional position that I am in today without him.

Thanks are also due in high order to Dr. Chris Thornton for giving me the opportunity to work at the CSU hydraulics lab and guiding me through various parts of this study. I greatly appreciate his time spent developing me into a better person and engineer. I would also like to thank my third committee member Dr. Ellen Wohl for her time and input.

I also thank my colleagues at the Engineering Research Center for their collaboration on this project, specifically Taylor Hogan, Jeff Ellis, and Alex Wittmershaus. Their support and knowledge helped me significantly throughout the course of this study.

Finally, I would like to thank God and my family for their continuous support. They have given me invaluable encouragement and advice throughout my studies at Colorado State University. I would specifically like to thank my parents, Jason and Sandra Maddocks for helping me grow and reach my goals in life.

TABLE OF CONTENTS

LIST OF TABLES

LIST OF FIGURES

LIST OF SYMBOLS

A^* = percentage of baseline cross-sectional flow area blocked by structure

D_b = average thalweg depth in bend before the installation of structures

D = hydraulic depth

d_{50} = median particle diameter

H = height of BW crest, or height of crest at tip of RV

Δz = elevation difference between the baseline water surface and structure crest at the tip

L_c = length of the structure crest, measured as the distance along the structure crest from the waterline at the design flowrate to the tip of the crest

L_{proj} = projected length of the structure, defined as the shortest distance from the tip of the structure crest to the waterline along the outer bank

L_{arc} = arc length along the bank between the centerline of adjacent structures

m = slope of the structure toe, given as mH:1V (1 for bendway weirs)

$tan\phi$ = slope of the structure crest; $tan\phi = 0$ for bendway weirs

R_c = radius of curvature of channel bend centerline

T_w = average top-width of channel in the bend at the design flowrate before the installation of structures

α or θ = structure planform angle measured from the bank on the upstream side of the structure to the structure crest

W = width of structure crest

y = flow depth

Δy = change in flow depth

Y = flow depth at top of bank

CHAPTER 1. INTRODUCTION

1.1 Introduction

Since the early 2000s, Colorado State University (CSU) has been working with the United States Bureau of Reclamation (USBR) to improve the design layout and dimensions of rock structures used as in-stream structures to control the thalweg alignment of alluvial-channel bends (Heintz 2002; Darrow 2004; Cox 2005; Kasper 2005; Kinzli 2005; Schmidt 2005; Walker 2009; Scurlock et al. 2014; Shin et al. 2018; Garfield 2019; Hogan 2019; Siefken et al. 2021). The rock structures researched were bendway weirs and rock vanes (sometimes called barbs). During this time, CSU used hydraulic and numerical models to investigate the effectiveness of configuration layouts of these structures. The models were developed using field data from two bends along a sinuous reach of the Middle Rio Grande River, New Mexico. USBR's Albuquerque, New Mexico Office funded the present study and was focused especially on alluvial channels similar in geometry to those found along the Middle Rio, the reach in the vicinity of Albuquerque.

Figure 1: CSU's hydraulic model of a reach of the Middle Rio Grande River (Scurlock et al. 2014)

Figure 1, for example, illustrates the main physical model, used to simulate a reach comprising two bends. The model, formed at a length scale of 12 (prototype/model), produced extensive data and insights, including information of the variation of water velocity, water-surface elevation, and general qualitative insights into flow-field behavior. This information was used to calibrate a series of numerical computational fluid dynamic (CFD) models using the commercially available codes FLOW-3D and SRH-2D (Scurlock et al. 2014; Garfield and Ettema 2019; Hogan 2019; and Siefken et al. 2021). The first code simulated the flow fields as steady, three-dimensional flows, and the second code simulated the flows as two-dimensional (depth-averaged) flow.

Whereas the prior studies investigated the layout of configurations of bendway weirs and rock vanes to manage the thalweg alignment of an alluvial channel, the present study focused on the dimensions of bendway weirs and rock vanes required to ensure the stability and ongoing performance of these rock structures during live-bed conditions in an alluvial channel. The experiments with flow in CSU's outdoor flume, where the stability of a single bendway weir was examined only for conditions of clear-water scour. The bendway weir for the outdoor flume was built on a sediment recess filled with a uniform coarse sand whose median particle diameter, d_{50}, was 0.8 mm. The angular, quarry-run rock forming the bendway weir had an average diameter of 0.5 ft (0.15 m). Figure 2 is a view of flow at a single bendway weir in that flume. However, it was found that clearwater scour produced only a relatively minor failure of the bendway weir; rock failed locally at the base of the end or tip of the bendway weir, and such scour did not cause the side slope of the bendway to otherwise fail. This result was confirmed by USBR, who noted that more severe failures had been observed in the field and that such failures typically coincided with live-bed conditions (active bed-sediment transport) in the curved channel containing the bendway weirs.

Figure 2: A view of the single bendway weir formed in the sediment recess of CSU's large (20.0 ft wide, 8.0 ft deep) flume located outdoors. In this experiment, *y/H* = 1.25

From the results obtained from the preliminary experiments conducted with the large outdoor flume, CSU and the USBR decided that further experiments focused on bendway-weir or rock-vane failure needed to place such rock structures in a flume that could produce live-bed conditions capable of replicating the much harsher field conditions representative of the swifter currents, more dramatic bed conditions and greater depths of scour observed (but not quantified) in the field.

1.2 Objectives

This study had the following primary objectives:

1. Determine how bendway weirs (BWs) and rock vanes (RVs) fail under live-bed conditions prevailing in the curved channel in which the BWs or RVs are placed;

2. Produce recommendations for the design of BWs and RVs so these rock structures accommodate the failure modes and still perform as required; and
3. As the bulk of the experiments regarding BW and RV failure were investigated in a straight flume fitted with a sand bed, confirm that the failure modes observed in a straight flume also occur in a curved flume that simulates channel bends of proportions comparable to the bends Figure 1 illustrates.

Objective 3 mentions that the bulk of the experiments were done using a straight flume. A straight flume was chosen because it could be controlled to produce the severe live-bed conditions of essentially known properties, such as average bed shear stress of the approach flow. Additionally, the flow field and the bed were much less three-dimensional in their spatial variation than would be the case in a curved flume. As noted above, though, the results from the straight flume had then to be confirmed by means of additional experiments done with a curved flume.

CHAPTER 2. BACKGROUND

Rock vanes (RVs) and bendway weirs (BWs) are instream, rock structures commonly used for channel control or management. This chapter briefly reviews their use and current information regarding their configuration design and how individual RVs and BWs may fail. The review, though, revealed little investigation has been done regarding the manner whereby RVs and BWs fail, especially in live-bed conditions. Design recommendations of individual BWs and RVs then were refined during the present study to mitigate individual failure of RVs and BWs.

2.1 Geometry of Rock Vanes and Bendway Weirs

Rock vanes (sometimes also known as barbs and point dykes) and bendway weirs are rock structures that extend out from the outer riverbank of an alluvial channel. Rock vanes have their crest sloping down toward the center of the channel, as shown in Figure 3. The sloped crest increases the area of flow blocked as the water level increases, providing a progressive hydraulic effect as discharge increases (NRCS 2005). Well-designed rock vanes should provide sufficient velocity reduction along the outer bank of a bend to prevent erosion, usually at a lower cost and with less environmental impact than a riprap revetment (Baird et al. 2015).

Figure 3: Installation of rock vanes (NRCS 2007)

The terminology used in the literature to describe the geometric parameters of rock vanes is somewhat muddled. The following definitions are adopted in this study for the parameters modified slightly (Δy instead of Δz) from Baird et al. (2015).

D_b = average thalweg depth in bend before the installation of structures

L_c = length of the structure crest, measured as the distance along the structure crest from the waterline at the design flowrate to the tip of the crest

L_{proj} = projected length of the structure, defined as the shortest distance from the tip of the structure crest to the waterline along the outer bank

L_{arc} = arc length along the bank between the centerline of adjacent structures

m = slope of the structure toe, given as mH:1V

R_c = radius of curvature of channel bend centerline

T_w = average top-width of channel in the bend at the design flowrate before the installation of structures

W = width of structure crest

Δy = elevation difference between the baseline water surface and structure crest at its tip

θ = structure planform angle measured from the bank on the upstream side of the structure to the structure crest

$\tan\phi$ = slope of the structure crest; $\tan\phi = 0$ for bendway weirs

Previous studies have defined the projected length as $L_{proj} = L_c \sin\theta$. However, for structures installed at small angles to the bank in channels with a small radius of curvature, this definition results in projected lengths which are much greater than the distance from the outer bank to the tip of the structure, as illustrated in Figure 4. For such structures, it is better to use Equation 1, which computes the exact distance from the outer bank to the tip of the structure crest for a channel of constant top-width and radius of curvature;

$$L_{proj} = R_c + \frac{T_w}{2} - \sqrt{L_c^2 + \left(R_c + \frac{T_w}{2}\right)^2 - 2L_c\left(R_c + \frac{T_w}{2}\right)\sin\theta} \quad (1)$$

Note that Equation 1 simplifies to $L_{proj} = L_c\sin\theta$ for $\theta = 90°$, or for R_c approaching infinity.

When laying out rock vanes, it is useful to be able to calculate the crest length required for a given projected length. By manipulating Equation 1 to solve for crest length as a function of projected length, planform angle, top-width, and radius of curvature, one arrives at Equation 2:

$$L_c = \left(R_c + \frac{T_w}{2}\right) sin\theta - \sqrt{L_{proj}^2 - 2L_{proj}\left(R_c + \frac{T_w}{2}\right) + \left(R_c + \frac{T_w}{2}\right)^2 \sin^2\theta} \quad (2)$$

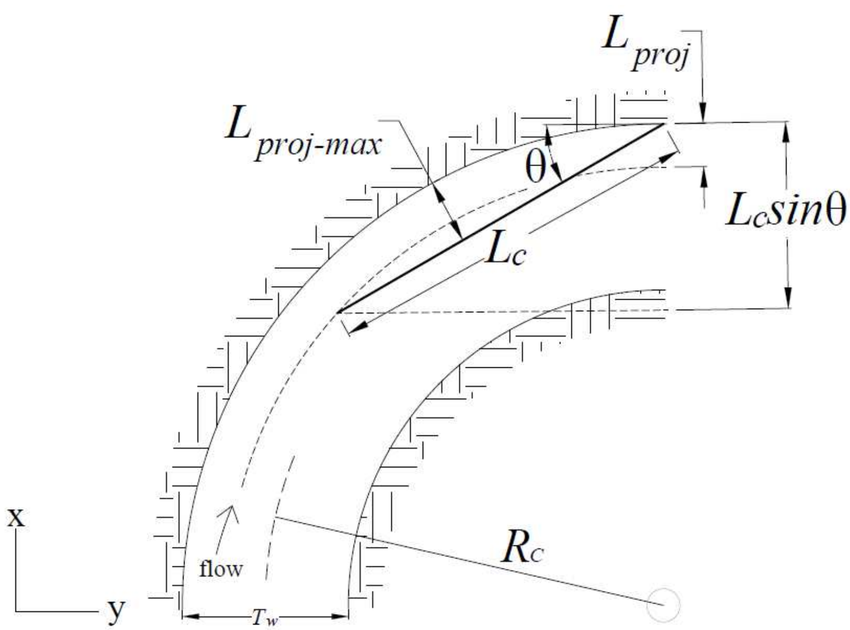

Figure 4: Illustration of the effect of curvature on the projected length of a rock vane (Scurlock et al. 2014)

It is assumed throughout this study that the crest of a rock vane intersects the bank at the elevation of the design water surface, as illustrated in Siefken et al. (2021). The submergence of the vane tip, Δy, usually is related to the crest length and slope of the vane, $\tan\phi$, by the equation:

$$\Delta y = L_c tan\phi \tag{3}$$

It is also useful to consider the area of flow blocked by rock vane or bendway weir structure. The flow blockage is defined as follows:

$A*$ = percentage of baseline cross-sectional flow area blocked by structure, computed using Equation 4.

$$A^* = \frac{A_{structure}}{A_{flow}} \tag{4}$$

Here, A_{flow} is taken as the baseline area of flow before the installation of structures at a cross-section perpendicular to the direction of flow located at the root of the structure. The area of the structure, $A_{structure}$, is determined by projecting the structure onto the cross-section perpendicular to the flow direction, as shown in Figure 5.

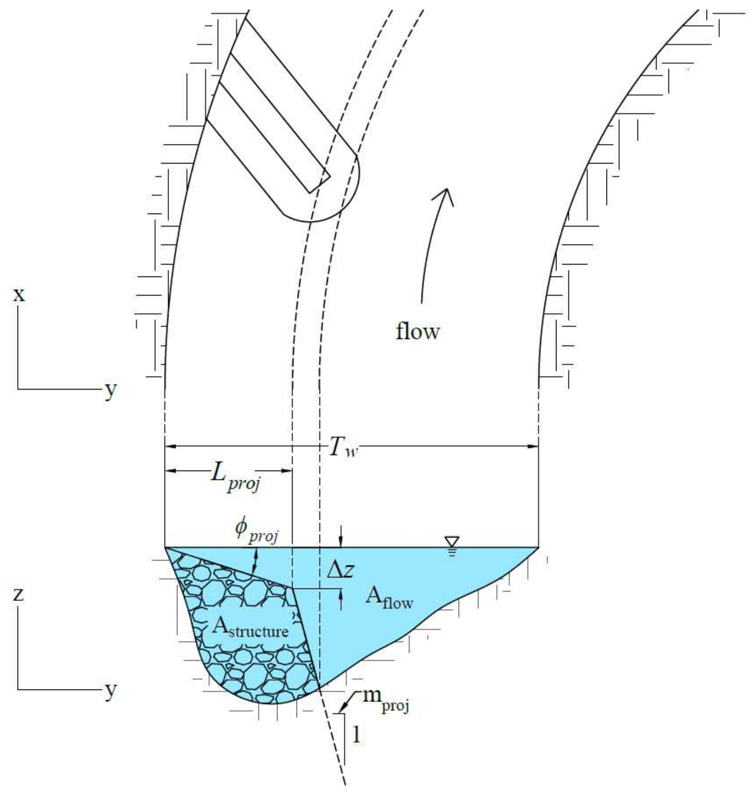

Figure 5: Projection of a structure onto a perpendicular cross-section (Siefken 2019)

The projection results in a projected toe slope (m_{proj}H:1V) that is steeper than the toe slope of the installed structure and a projected crest slope of rock vanes ($\tan\phi_{proj}$) steeper than the installed crest slope. For an exact projection, the crest and toe slopes would vary slightly along the structure, but the variation is small enough to disregard for practical calculations. The mean projected crest slope can simply be computed by dividing the projected length by the tip submergence:

$$\tan(\phi_{proj}) = \frac{L_{proj}}{\Delta y} \tag{5}$$

Because the area blocked under the toe of the structure is usually small compared to the area blocked under the crest, the projected toe slope can be satisfactorily approximated as:

$$m_{proj} \approx m * \sin\theta \tag{6}$$

2.3 Design Guidelines for Rock-Vane Configurations

The leading design guidelines for RV configurations are available in Siefken et al. (2021). They indicate the following dimensions enable configurations to perform as required:

- Upstream angles ranging from 45° to 85° to the outer bank.
- Selection of crest slope is a balance between hydraulic performance and volume of rock required for construction. Decreasing the RV's crest slope reduces velocity along the outer bank.
- Optimal projected crest length ranges from 0.2 to 0.3 times the channel top width (bank-full flow).
- Optimal spacing was 0.75 times the channel top width. Reducing spacing below 0.5 times the top width produces no further reductions in outer bank velocity.
- For RVs installed at small planform angles in tightly curved bends it is recommended to use Equation 1 to compute the projected length.
- Equation 8 gives preliminary estimates of reductions in flow velocities near the outer bank.

The geometric design of RV configurations is primarily concerned with determining vane length, spacing, and planform angle. This review notes that Siefken et al. (2021) do not mention a recommended value of RV height (at the crest tip) relative to the bank-full depth of flow.

Table 1 summarizes nine different sets of geometric design guidelines proposed in the literature, including the guidelines suggested by Siefken et al. (2021). Though these guidelines provide the designer with generally acceptable ranges of geometric parameters, the guidelines prior to Siefken et al. (2021) are largely anecdotal (Thornton et al. 2016) and lack laboratory or numerical verification. Case studies reporting field experience are cited in several design guidelines, but little comparative testing of designs seems to have been done.

Table 1. Summary of various design guidelines for vanes

Source	Length min	Length max	Length Type	Spacing min	Spacing max	θ min	θ max	Crest slope min	Crest slope max
WSDOT (2017)	$T_w/3$		Projected	$4L_{proj}$		50°		10%	
NRCS (2013)	Length based on designed thalweg location, not to exceed $T_w/3$		Crest	Line from DS structure tip, parallel to bank tangent at tie-in, to intersection of US bank		20°	30°	5%	8%
NRCS (2010)	$T_w/10$	$0.35T_w$	Crest, but called effective length	Flow direction analysis		50°	80°	3%	10%
NRCS (2009)	Must cross thalweg, dependent upon horizontal angle, not to exceed baseflow $T_w/2$		Crest	$4L_c$	$5L_c$	50°	80°	0%	n/a
NRCS (2007)	$T_w/10$	$T_w/4$	Projected	$4L_{proj}$	$5L_{proj}$	<20°	45°	20%	
NRCS (2005)	Must cross thalweg, dependent upon horizontal angle, not to exceed $T_w/3$		Crest	Line from DS structure tip, parallel to bank tangent at tie-in, to intersection of US bank		20°	30°	5%	8%
Johnson et al. (2001)	$T_w/4$	$T_w/3$	Projected	n/a	n/a	20°	30°	n/a	n/a

Maryland (2000)	n/a	$T_w/3$	Projected	$5T_w$	$7T_w$	20°	30°	3%	7%

2.4 Design Guidelines for Bendway Weirs

Regarding BWs, the leading guidelines for configuration design are available in Siefken et al. (2021). They indicate the following dimensions enable configurations to perform as required:

- Upstream angles ranging from 45° to 85° to the outer bank.
- Optimal spacing was 0.75 times the channel top width. Reducing spacing below 0.5 times the top width produces no further reductions in outer bank velocity.
- Optimal projected crest length ranges from 0.2 to 0.3 times the channel top width (bank-full flow).
- Most BW configurations are largely ineffective at protecting the outer bank in comparison to RVs. The optimal BW configuration used a projected crest length of 0.25 times the channel top width and an upstream angle of 70°.

Bendway weir geometric parameters are defined in the same manner as those for rock vanes, as shown in Figure 5. Bendway weirs are distinguished from RVs by their flat crest, which is designed to be submerged at the design flow. As such, the crest of a bendway weir intersects the bank below the elevation of the design water surface, unlike rock vanes which intersect the bank at the design water surface. This review also notes that Siefken et al. (2021) do not mention a recommended value of BW crest height relative to the bank-full depth of flow.

While originally developed as a structure to improve navigation, BWs also have potential to mitigate erosion along the outer bank of a curved channel (Biedenham et al. 1997). Table 2 summarizes existing design guidance for bendway weirs from NCHRP Report 544 (McCullah and Gray 2005), Hydraulic Engineering Circular (HEC) 23 (Lagasse et al. 2009), and Julien and

Duncan (2003). The recommended design values vary considerably from one guide to another, with recommend length ranging from $T_w/10$ to $T_w/2$ and spacing from $1.5L_c$ to $5L_c$. This review observes that minimum crest heights of BW are specified by this guideline.

Table 2. Summary of existing design guidelines for bendway weirs (after Scurlock et al. 2014b). Height is given in terms of hydraulic depth (*D*) or bank full depth (BF)

Source	Length min	Length max	Length Type	Spacing min	Spacing max	θ min	θ max	Height min	Height max
NCHRP 544 (2005)	$T_w/3$	$T_w/2$	crest	$1.5L_c$		70°	80°	$D/2$	D
HEC 23 (2009)	$T_w/10$*	$T_w/3$	crest	$4L_c$	$5L_c$	60°	80°	0.3BF	0.5BF
Julien and Duncan (2003)	case-by-case		N/A	$2L$	$3L$	60°		Max permitting navigation	

*HEC 23 further recommends that the crest be long enough to cross the thalweg

As with RVs, purely geometric design criteria for bendway weirs are limited by their failure to consider the approach velocity of flow in the bend (Baird et al. 2015). Several investigators have attempted to overcome this shortfall with regression equations in the same form as that presented for rock vanes (Equation 7). Scurlock et al. (2012a) created a regression equation based on physical model studies at CSU and Shin et al. (2018) created a similar equation based on a numerical model study. However, neither of these equations has been adopted in an official design guide.

2.5 Failure of Rock Vanes and Bendway Weirs

Few studies evidently have been conducted of RVs or BWs in alluvial beds subject to live-bed conditions of sediment transport.

- Papanicolaou et al. 2018 used a y/H of 0.98 to 2.53 with barb dimensions from WSDOT. The study focused on gravel bed scour development around barbs rather than failure of the barbs themselves. However, scour development was found to be a component in BW and RV failure. Here, and below, Y is bank-full depth of flow, H is the height of a barb's mid-crest elevation, and y is flow depth.
- Study by Cunningham and Lyn (2016) used a y/H of 0.95 to 2.00 and used BW design guidelines from HEC-23. Results of the study did not concentrate on BW failure modes but provided useful insight into components causing failure such as the effect of y/H on scour development was more significant at 1.25 than 2.00.
- Garfield and Ettema (2021) report the findings of clear-water scour experiments on a single BW, within CSU's large outdoor flume. The study used a y/H of 1.25 to 2.00 and assessed two-dimensional numerical modeling supported by flume data. The practical implications of using 2D versus a 3D model were briefly assessed by them. They report that 2D models were found suitable for designing BWs to manage thalweg position, but inadequate for estimating near-bank velocities. Garfield and Ettema (2021) did not primarily focus on BW or RV failure modes but provides useful insight into components affecting failure.

However, abutments in alluvial beds subject to live-bed conditions of sediment transport have been researched extensively due to their importance for waterway bridge stability. Despite overtopping flow occurring with BW, abutments have a similar flow field. Studies from Kwan (1984), Ettema et al. (2010), Jia et al. (2009), and Jamieson et al. (2011) show scour effects of flow field structure from abutment installation which can be attributed to scour effects observed around BW and RV installation.

2.6 Conclusions from Literature Review

The overall conclusions from the review of pertinent literature are as follow:

- Few studies have been conducted regarding modes whereby RVs and BWs fail. Therefore, the live-bed experiments that this thesis conducted, and reports provide useful insights into how RVs and BWs fail; and
- Despite development of numerous design guidelines as seen in Table 1 and Table 2. Little comparative testing has been conducted regarding design guidelines and no design recommendations have been made to prevent the scour-related failure of individual RVs or BWs.

Therefore, the present study sets forth the three objectives stated in Chapter 1.

CHAPTER 3. EXPERIMENT SETUP

3.1 Introduction

This chapter presents the experiment setups used to address the three objectives Chapter 1 describes. The first experiment setup used a straight flume, and the second experiment setup used a curved flume. Details regarding each experiment's flume setup, flow control setup, live-bed setup, BW and RV arrangements, program of experiments, instrumentation, and procedure are covered in the ensuing sections of this chapter.

3.2 The Straight Flume

To address the first two objectives of this thesis, and deliberately illuminate the scour-related failure modes, a series of experiments were conducted using CSU's tiltable, 2-ft-wide flume illustrated in Figure 6. The flume's channel was 60 ft long, 2 ft wide, and 2.5 ft deep. For the present experiments, a useful feature of the flume was the flume's ability to recirculate sediment and, thereby, simulate active live-bed conditions in which the RVs and BWs were to be located. Therefore, a hopper was not required to feed sediment into the flume. This feature of the flume involved a sediment recirculating pump that was capable of recirculating water flow and bed sediment, as the general layout drawing in Figure 7 shows.

Figure 6: Photograph of the straight flume

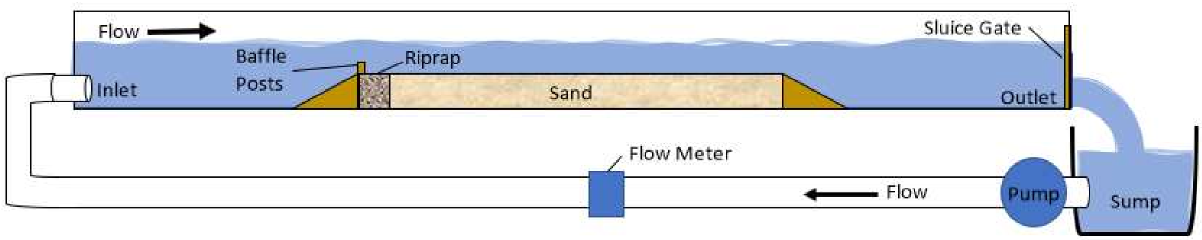

Figure 7: Flow diagram of the straight flume

Illustrations of the experiment configuration formed in the flume's channel are presented in Figure 8, where the length of the 9-in deep, sand, channel bed was 36 ft long, and the slope of the sand bed was adjusted, by means of floor jacks, to be 0.0015 ft/ft to create the active live-bed conditions the experiments needed. The flow depth at the start of the bed was about 6 in (without BWs or RVs).

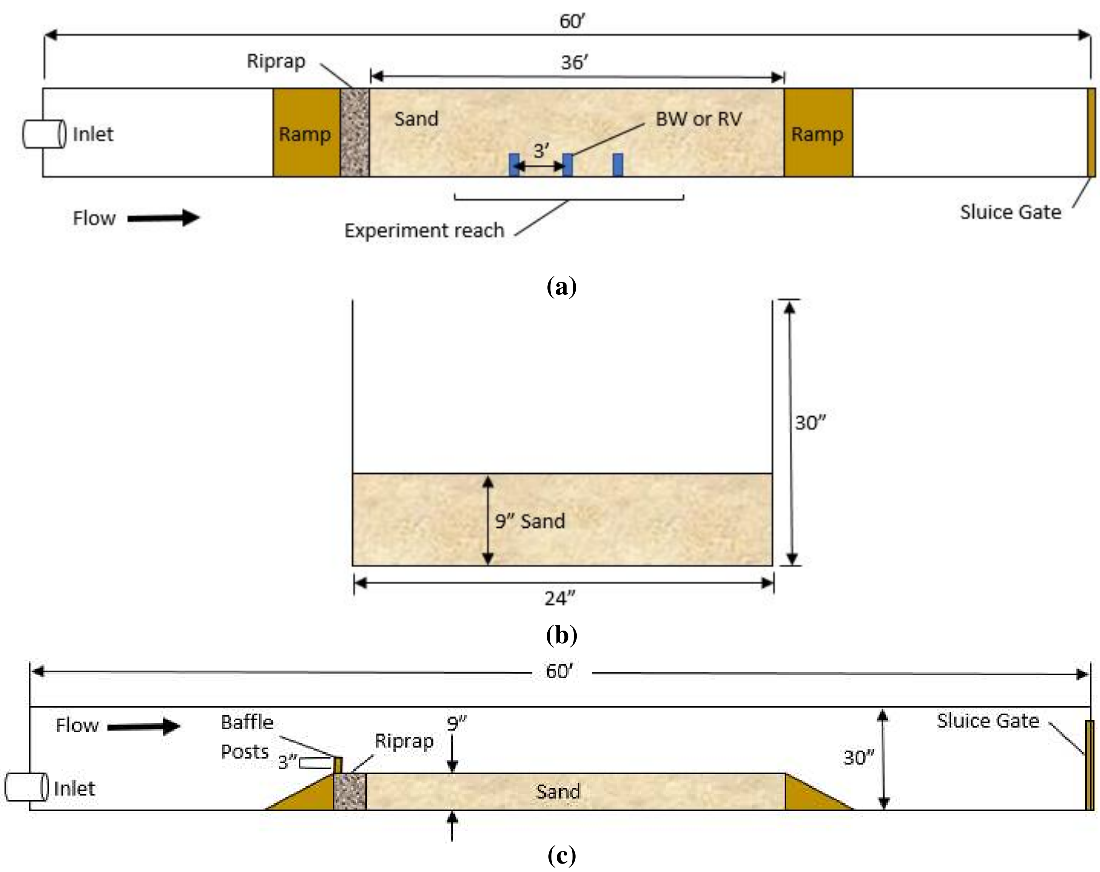

Figure 8: Layout and dimensions of the experiment set-up in the straight flume: (a) plan profile; (b) sand bed cross-section; and (c) longitudinal profile

3.2.1 Flow Control

Wooden ramps were used to form the ends of the 36-ft-long, 2-ft-wide, and 9-in-deep sand bed. At the downstream end of the upstream ramp, 3-in tall, 1-in diameter baffle posts were used to obtain fully developed flow. Riprap was placed immediately downstream of the upstream ramp (see Figure 8) to prevent scour holes from affecting the flow condition. BWs and RVs were placed in the middle third of the channel bed (starting 12 ft from the upstream ramp and ending 12 ft before the downstream ramp). This arrangement provided enough space for the flow to become fully developed (with the aid of the baffle array) in its approach to the BWs or RVs, and it prevent the downstream control from affecting flow depths along the sand bed. Flow depth within the channel was controlled by the vertical sluice gate (Figure 9) at the downstream end of the channel and could be raised and lowered using a ratchet strap mounted above the gate.

Figure 9: The vertical sluice gate used at the downstream end of the straight flume. The strap-controlled flow along the flume

3.2.2 Sediment Size Curve

The sediment used for the experiments was a medium sand, whose median particle diameter, d_{50}, was 0.38 mm, and geometric standard deviation, σ_g, was 0.17 mm; the value of σ_g was determined as

$$\sigma_g = 0.5\left(\frac{d_{84}}{d_{50}} + \frac{d_{50}}{d_{16}}\right)$$

The sand used, therefore, was considered essentially uniform. The sand contained 1-2% by weight of magnetite (black sand), where the specific gravity of magnetite is 5.2 in comparison to sand's 2.65 (Keating & Knight 2008). This concentration was not enough to cause armoring of the bed. The value of shear stress associated with the incipient motion of magnetite was estimated to be τ_c = 0.26 Pa (Julien 2010).

The gradation curve for the sand is given in Figure 12. Consequent to discussions with the USBR, a medium-size sand was selected due to the capacity to develop bedforms, a potential factor contributing to the failure of a BW or RV. The value of shear stress associated with the incipient motion of the sand (d_{50} size) was estimated to be τ_c = 0.23 Pa (Julien 2010). Active sediment transport on the bed was required, and so the mean value of bed shear stress, τ, always exceeded τ_c.

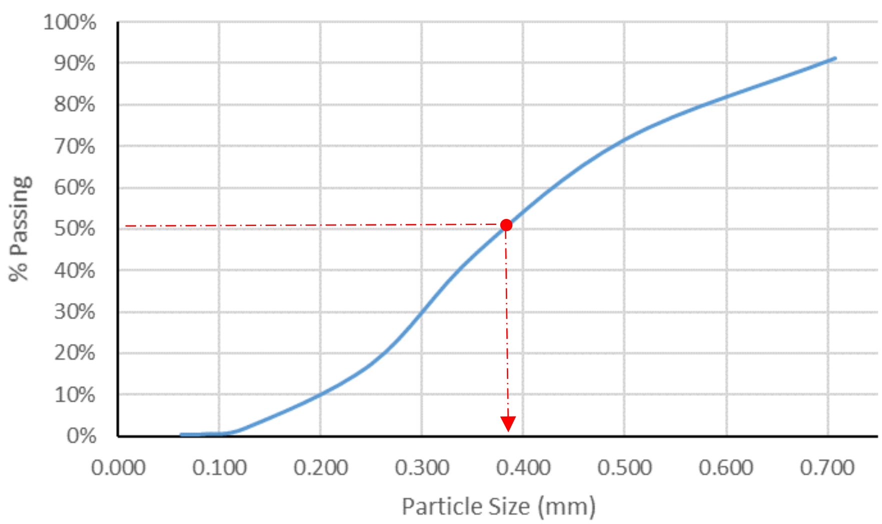

Figure 10: Sediment particle size distribution: (a) the red dot indicates the median particle diameter, d_{50} = 0.38 mm, and geometric standard deviation = 0.17 mm

Additionally, the sediment particle size was selected by prioritizing mixed load conditions (transport of bed particles along the bed and, at times, bed particles projected into suspension within the flow) by obtaining the ratio of shear velocity (u_*) to the fall velocity (ω) to develop Figure 11, which shows a particle size of approximately 0.20 mm to 0.45 mm indeed will provide mixed load conditions (area highlighted in green). If coarser bed-particles had been used (say from

0.45 mm to 0.70+ mm), bedload conditions only would be present in the 2 ft flume (unhighlighted area). The conditions for incipient motion, nor no motion, are indicated by the area highlighted in red.

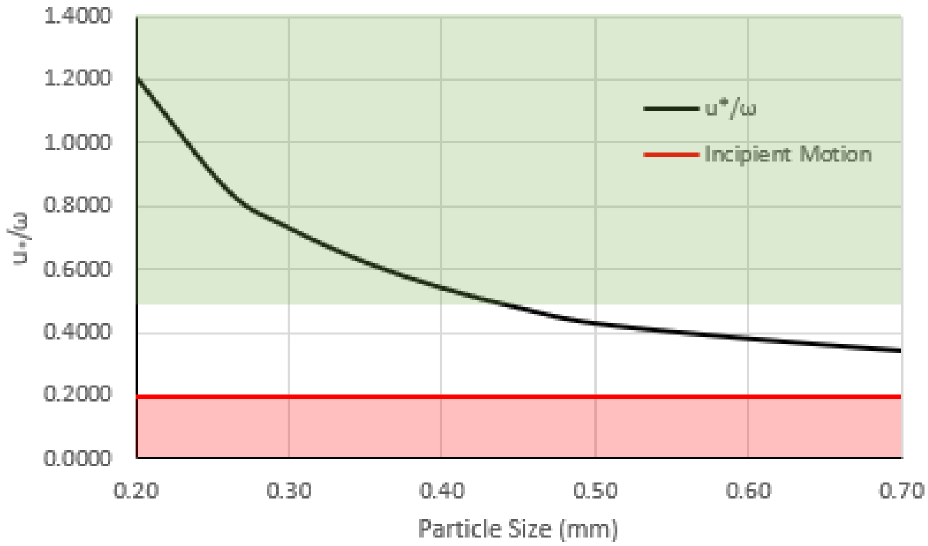

Figure 11: Sediment transport mode for different particle sizes in the 2 ft flume: (a) the green area indicates mixed load conditions; (b) the unhighlighted area indicates bedload conditions; (c) the red line indicates incipient motion of a bed particle seated on the bed; and (d) the red area indicates no motion

The gradation curve relating water flowrate to rate of sediment transport (Figure 12) was generated using the Meyer-Peter Müller (MPM) method (Julien 2010) for a d_{50} of 0.38 mm and quartz sand (specific gravity of 2.65). Though there is some uncertainty associated with this relationship, the uncertainty was checked to see if sediment did not accumulate or erode from the experiment section. This check involved several tests without a BW or RV placed in the experiment reach. Though the reach was relatively short and a slight inaccuracy in the MPM method would not substantially affect the veracity of the experiments, it was found that the rates of sediment transport and the flow rates agreed reasonably, well such that no undue build-up or erosion of sediment occurred in the experiment section.

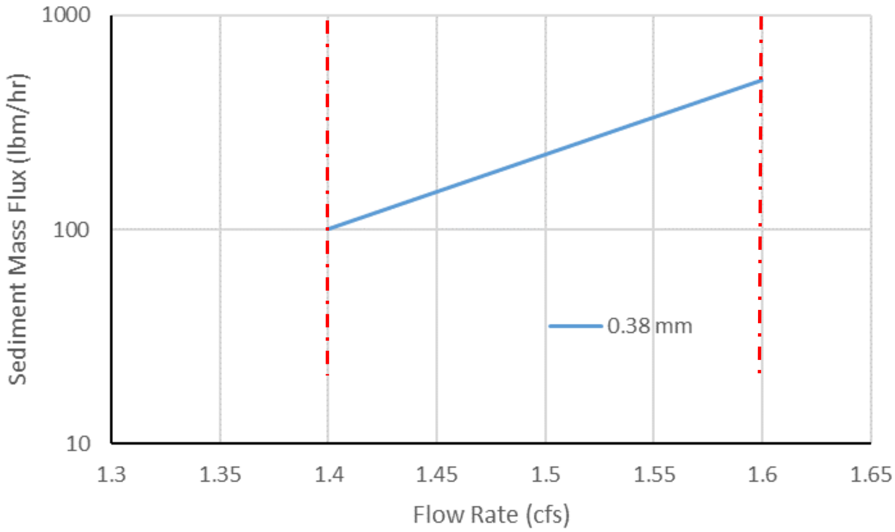

Figure 12: Sediment rating curve used, and checked, for the straight flume. The red lines indicate the flow rates used for experiments. The curve, developed using the MPM method, relates mass rate of sediment transport (lbm/hr) to volumetric flow rate (cfs)

3.2.3 Bendway Weir and Rock Vane Setup

Bendway weirs and rock vanes (BWs and RVs) were constructed along the right side of the middle third of the 36 ft long sand bed, as Figure 8 indicates. An average rock diameter, D_r, of 15 mm and a geometric standard deviation σ_g, of 9 mm, was used to construct both BWs and RVs. The BWs were constructed in accordance with the dimensions in Table 3. Figure 13 and Figure 14 illustrate a constructed BW with dimensions as existed prior to an experiment. Rock vanes were constructed with the dimensions presented in Table 4. Figure 15, Figure 16, and Figure 17 show a constructed RV with dimensions as existed prior to an experiment.

Table 3: Bendway weir dimensions

Crest Height	3.0 in
Crest Width	3.0 in
Crest Length	8.0 in
Side Slopes	1.5H:1V
Spacing (center to center)	3 ft

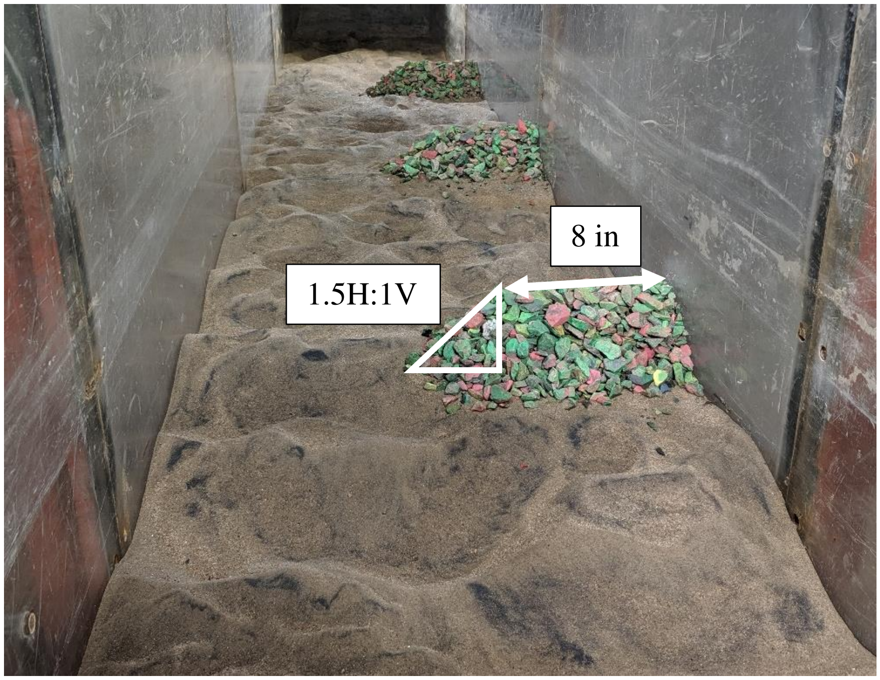

Figure 13: Side profile of a BW placed in the 2ft flume

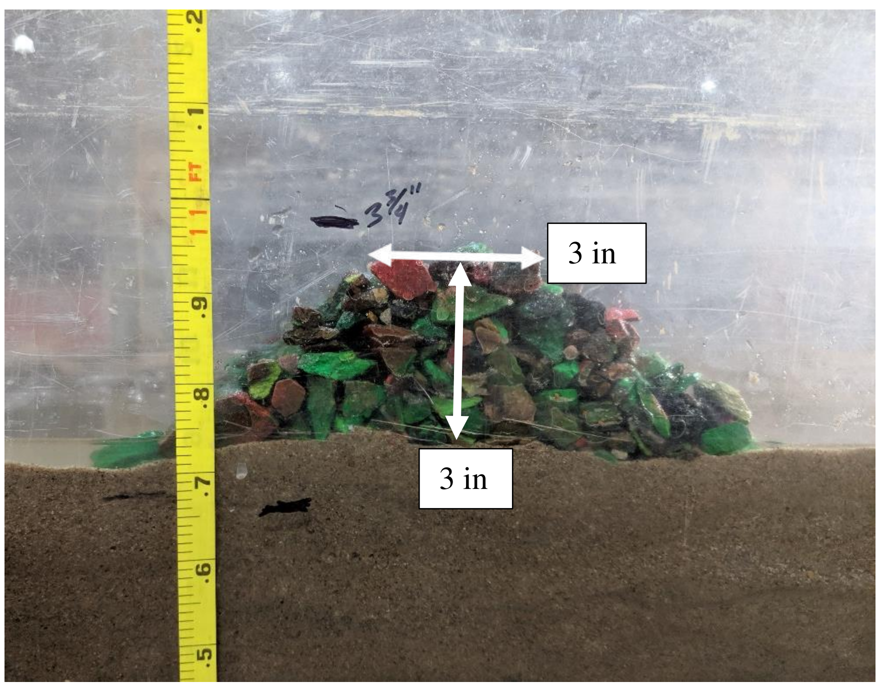

Figure 14: Longitudinal profile of a BW placed in the 2ft flume

Table 4: Rock vane dimensions

Crest Height	6.0 in (top of bank)
Crest Slope	5H:1V (20%)
Crest Width	3.0 in
Crest Length	8.0 in
Side Slopes	1.5H:1V
Spacing (center to center)	3 ft

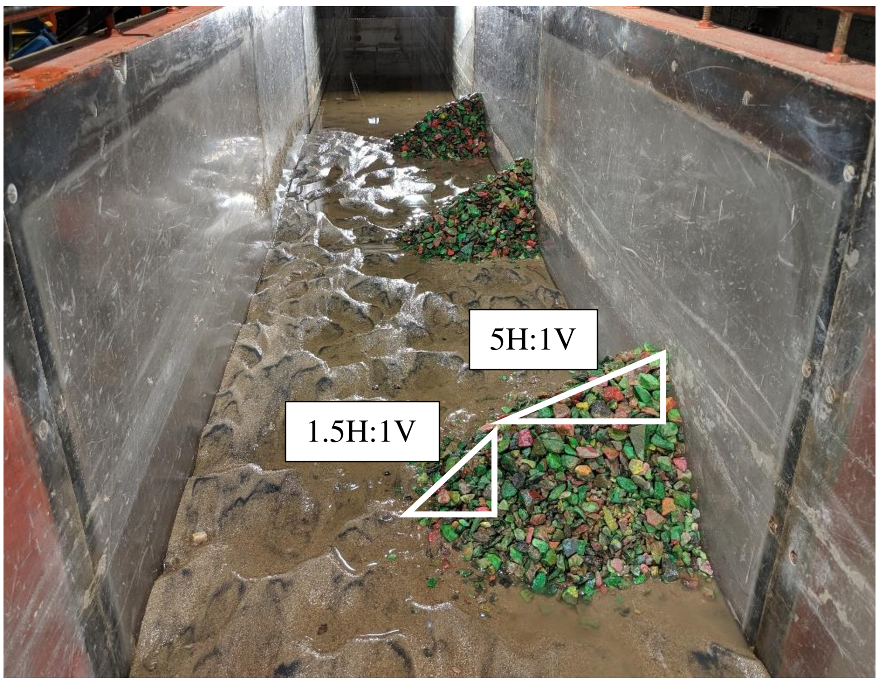

Figure 15: Side profile of a RV placed in the 2 ft flume

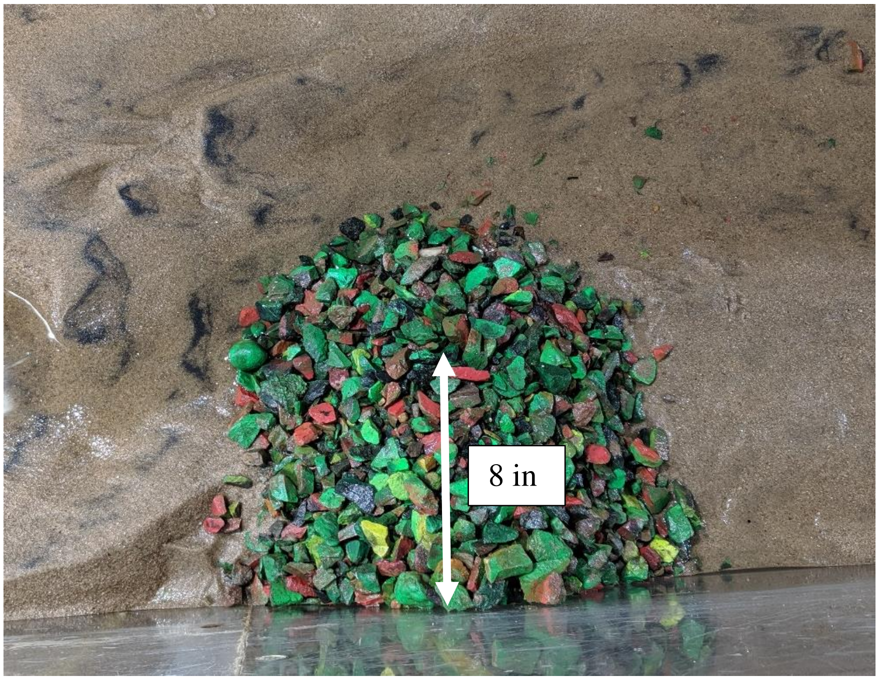

Figure 16: Plan profile of a RV placed in the 2 ft flume

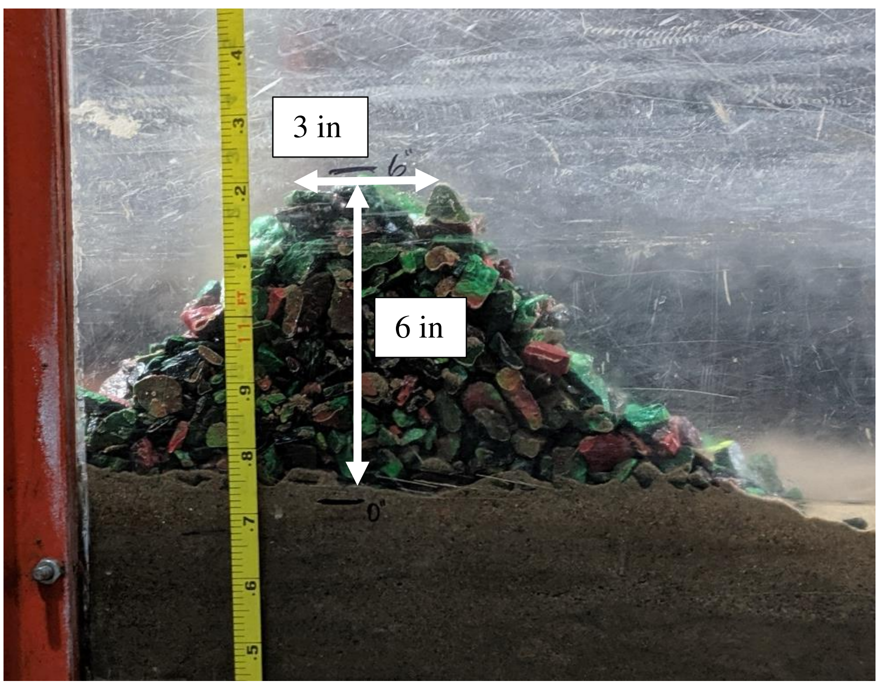

Figure 17: Longitudinal profile of a RV placed in the 2 ft flume

3.2.4 Program of Experiments

The program of experiments was planned to reveal how BWs and RVs failed structurally owing to scour, or bed lowering, at a BW or RV. Accordingly, the experiments were designed to place the BWs and RVs in challenging or severe flow conditions (live-bed conditions), so that the modes whereby these rock structures failed would be very readily observable.

The layout dimensions of the BWs and the RVs followed recommendations given by Siefken et al. (2021), who reported the findings of extensive numerical modeling using FLOW 3D to identify the optimal spacing and other configuration dimensions of BWs and RVs. Additionally, preliminary experiments were conducted using the flume (Figure 6) to obtain preliminary observations regarding the failure of a single BW or RV. These preliminary experiments resulted in the bulk of the straight flume experiments of the straight flume experiments being conducted used three structures to best replicate the flow-field conditions in which such structures are generally installed. It was observed quickly that three structures (BWs or RVs) were needed because each of the three structures could fail in different manners.

Table 5: Program of experiments conducted using the straight, 2-ft-wide flume

Test #	**Rock Structure**	Q (cfs)	y (in)	τ_0/τ_c	y/H	α (Degree)	W (in)	L (in)	**H** (in)	S_0
Preliminary Straight Flume Experiments										
1	BW	1.6	6	9.9	2.0	90	8	8	3	0.0015
2	BW	1.6	6	9.9	2.0	90	8	8	3	0.0015
6	2 BW	1.4	3.75	8.3	1.25	90	8	8	3	0.0015
7	2 BW	1.4	3.75	8.3	1.25	90	3	8	3	0.0015
3	3 BW	1.6	6	9.9	2.0	90	8	8	3	0.0015
4	3 BW	1.6	6	9.9	2.0	90	8	8	3	0.0015
5	3 BW	1.4	3.75	8.3	1.25	90	8	8	3	0.0015
10	3 BW_{Short}	1.6	6	9.9	2.0	90	3	6	3	0.0015
Straight Flume Experiments										
8	3 BW	1.6	6	9.9	2.0	90	3	8	3	0.0015
9	3 BW	1.4	3.75	8.3	1.25	90	3	8	3	0.0015
11	3 BW	1.6	6	9.9	2.0	45	3	8	3	0.0015
13	3 BW	1.4	3.75	8.3	1.25	45	3	8	3	0.0015
12	3 RV	1.6	6	9.9	1.0	90	3	8	6	0.0015
14	3 RV	1.6	6	9.9	1.0	45	3	8	6	0.0015
15	3 RV	1.4	3.75	8.3	0.625	90	3	8	6	0.0015
16	3 RV	1.4	3.75	8.3	0.625	45	3	8	6	0.0015

3.2.5 Instrumentation

The flowrate was monitored using an electromagnetic flow meter connected to a digital display as Figure 18 shows. Figure 18a&b, respectively, show the flow meter and the digital instrument panel indicating the flow rate. The flowrate was controlled using the sediment recirculating pump controls (Figure 18c), where a small dial was adjusted to increase or decrease the flow rate. To maintain sediment recirculation, the 2 ft flume at CSU's hydraulics laboratory operated on a dedicated flow pipe, as Figure 7 indicates.

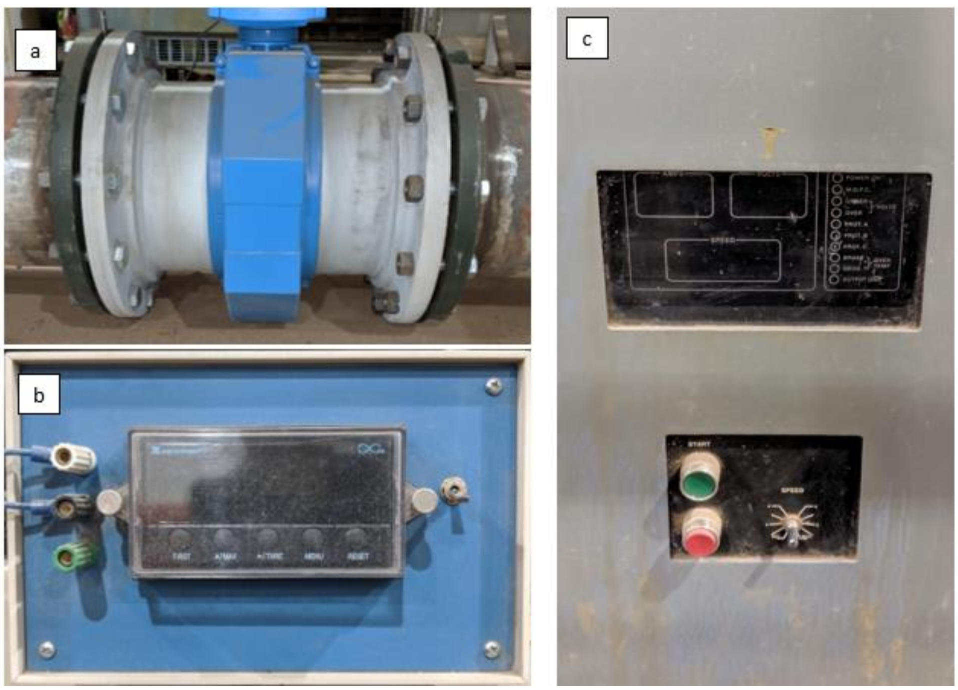

Figure 18: The flow monitoring and pump controls: (a) electromagnetic flow meter located in the flume's return; (b) flow meter display; and (c) pump controls

Tape measures were placed on the walls of the flume to track flow depth during experiments and maintain consistent reference points for initial bed level and structure positioning. Additionally, a portable tape measure was used to confirm the other length dimensions of the BWs and RVs, and to measure depths of scour or bed lowering.

To select the correct sediment, a sieve analysis was completed on multiple sediments. Each sediment was sampled four times to ensure selection of the correct median particle diameter and particle standard deviation for the experiments as described in Section 3.2.2.

For data collection purposes, each experiment was photographed from many angles before and after the experiment. Experiments were also filmed from two different angles for the entire duration of the experiment (3 hours). The angles included a side view and an above view utilizing the data cart (small cart with mobility along the length of the flume) on the 2 ft flume. Table 5 presents a tabulated summary of the experiments conducted using the 2 ft flume.

3.2.6 Procedure

The following procedure was used to perform the live-bed experiments using the 2 ft straight flume:

1. The 36 ft portion between the ramps of the 2 ft flume was checked to contain 9-in of sand. Excess sediment from previous experiments outside of the 36 ft zone was removed or reapplied to the channel bed to ensure the 9-in sediment depth throughout the 36 ft portion. Sediment washed down into the sump was replaced by applying more sediment to the bed.
2. The vertical sluice gate was raised, and the recirculating pump was run at the desired flow condition for approximately 15 – 30 minutes to obtain bedform equilibrium in the channel without the presence of any BWs or RVs.
3. After bedform equilibrium had been reached the vertical sluice gate was closed and the recirculating pump is slowly shutdown to slowly drain the flume and preserve bedforms. Once the flume has been drained, BWs or RVs are constructed in the middle third of the 36 ft section with the dimensions given in Table 5 and using the rock described in Section 3.2.3.

4. When the vertical sluice gate was fully shut, pre-experiment photographs were taken, and the two video cameras began filming. The recirculating pump was turned to the lowest possible setting and the flume was slowly filled to a depth of 1 ft or $y/H = 4.0$.
5. Then the vertical sluice gate was gradually opened, and the flow rate was increased until the target flow rate was reached. Then the vertical sluice gate was adjusted to obtain the target water depth. Then, the flow condition was held for approximately 3 hours to ensure equilibrium with the presence of BWs or RVs. This step entailed observing that the scour regions did not deepen, and additional failure of a BW or RV occurred. It was found that measurements of the scour depth need not be taken over time, as the scour rapidly (within 30 minutes attained an equilibrium depth). As is explained subsequently, rock from the failed slopes of the BWs or RVS essentially acted like scour-prevention aprons and armored the scour zones.
6. After 3 hours, the vertical sluice gate was closed, and the recirculating pump was slowly shutdown to slowly drain the flume and preserve the results. Also, the two video cameras were shut off and post-experiment photographs were taken.

3.3 The Curved Flume

The 4-ft-wide curved flume, especially constructed for this study, was used to check that the BW failure modes also occurred in a curved channel of similar geometry to channel bends in the Middle Rio Grande. The new aspects of the curved flume were the channel's curvature and greater width. The geometric features of the curved flume are described here. The flume had trapezoidal walls built with a side slope of 1.5:1, thereby forming a channel of trapezoidal cross-section. The base of the trapezoidal channel was rectangular to form a bed containing a 10-in-thick layer of sand. A plan-view illustration of the curved flume, indicating its radius of curvature (centerline) and bed width is shown in Figure 19. The radius of curvature was based on bend channel dimensions given by the Bureau of Reclamation. The flume was built within CSU's 20-ft-wide, indoor basin (where the experiments were conducted) and matched the dimensions given in Figure 19.

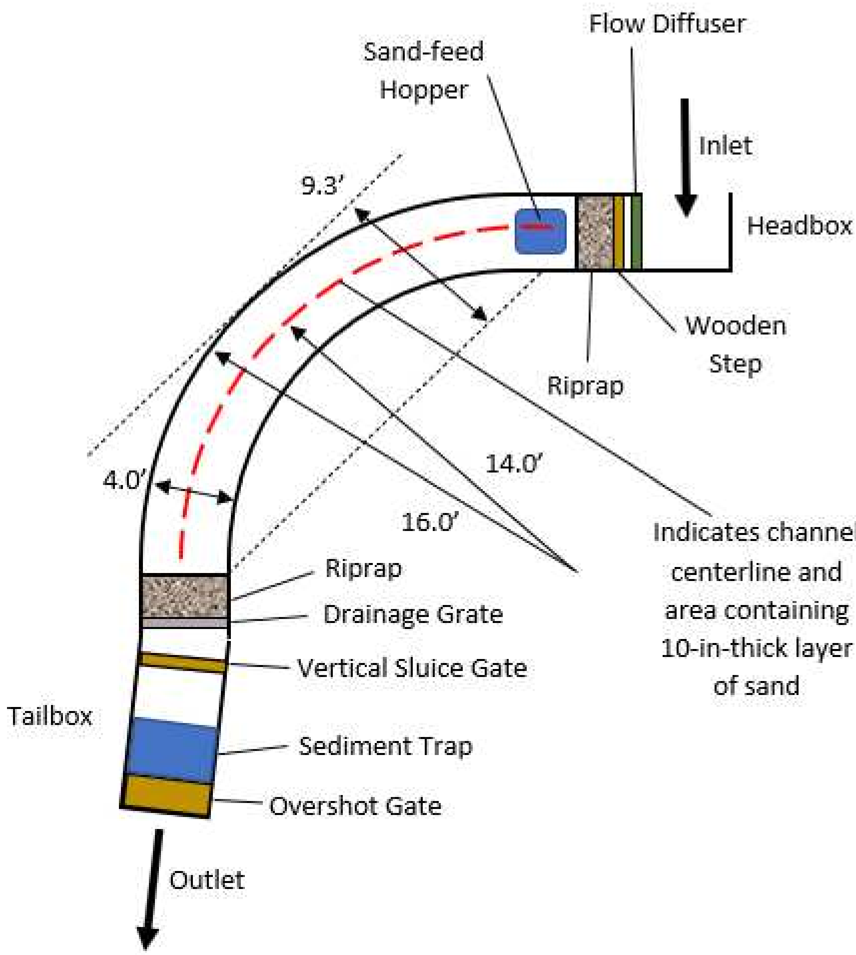

Figure 19: Curved flume dimensions. Note the sand-feed hopper dispensed sand from the upstream side of the hopper.

The curved flume was constructed on a short time frame for temporary use and therefore, an unconventional construction method was used to achieve this. The construction method used built upon pre-existing infrastructure and recycled materials from retired experiment setups.

Moreover, the method of construction was comparatively inexpensive. The remainder of this section details the construction of the curved flume.

Once the flume's position and extent were defined, the lower walls of the flume were constructed using two layers of concrete blocks stacked two-blocks high. The concrete blocks formed the 10-in deep, rectangular portion of the channel bed and support the flume's 1.5H:1V sloped banks, formed using stacked bags filled with sand. Before building the flume's sloped banks, a black matting fabric was used to prevent tearing in the sandbags and pond liner that was draped over the stacked bags and the channel bed. Figure 20 shows the channel's form, comprising of concrete blocks, black matting, and sandbags.

Figure 20: Completed curved flume channel walls without the rubber pond-liner and the Pyramat® cover. This figure shows how the flume's curved channel was built

After the curved walls were completed, wood walled boxes were constructed to form the flume's headbox and tailbox. From the tailbox, flow was directed into the laboratory's main sump (volume of 1 acre-foot) for recirculation back to the headbox. Additionally, at the downstream end of the flume, a wooden sediment trap caught and accumulated suspended particles, and prevented them from entering the laboratory's sump. The sediment trap utilized an overshot gate and a sudden channel expansion (vertical) to decrease the channel velocity to enable settling of the sand particles forming the flume's bed. Once the flume was fully formed and everything was in position, a 50 x 20 ft, 40 mil pond-liner (Figure 21) was fitted over the curved flume walls to prevent leaking during experiments. To hold the pond-liner in position and prevent tearing, rubber clamps and additional sandbags were used. Then, a surface cover formed using green Propex Pyramat® was positioned over the sloping banks of the flume to give the flume's banks a more-or-less uniform texture or surface roughness. The Pyramat® cover was held in position using paracord (a strong rubber chord) anchored by further sandbags. Also, and placed in the rectangular portion of the flume held the Pyramat® cover securely in position.

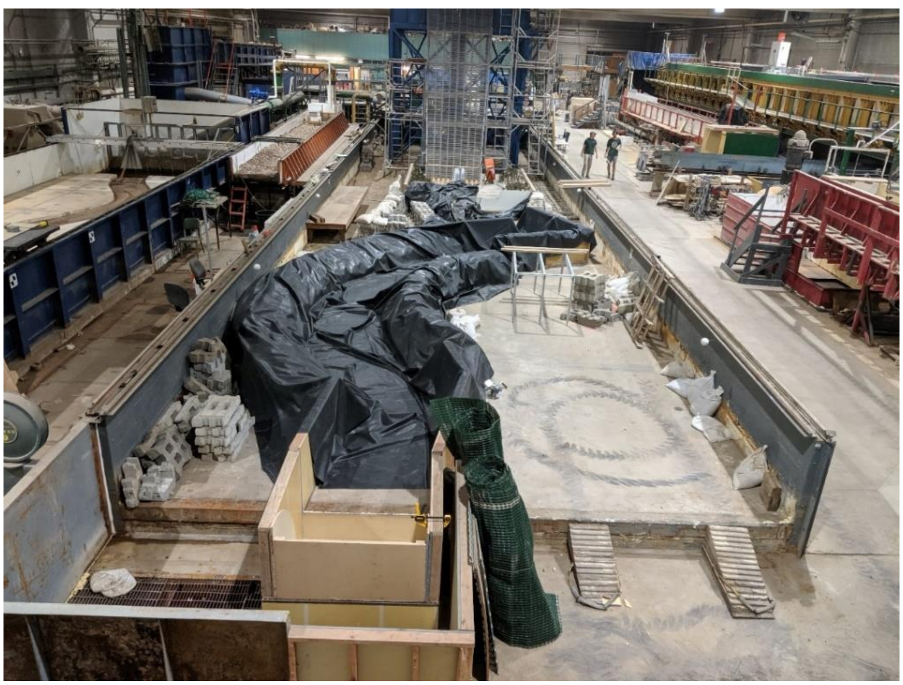

Figure 21: Fitting the thick pond-liner (black) into the flume

Once the Pyramat® had been positioned and fitted to the curved flume, the flume was filled with sand to secure the Pyramat® into position. Paracord anchors were applied after so small adjustments could be made readily. Small concrete blocks were used as temporary anchors hold the Pyramat® in place. Figure 22 shows the initial filling of the flume with the selected sand, which subsequently would create live-bed conditions in flow through the flume. A skid steer (Bobcat) was used to place sand into the flume, and shovels and rakes were used to distribute the sand as needed throughout the flume. After all components of the 4 ft curved flume were completed, the flume was ready to run experiments. Figure 23 is a photograph of the completed flume.

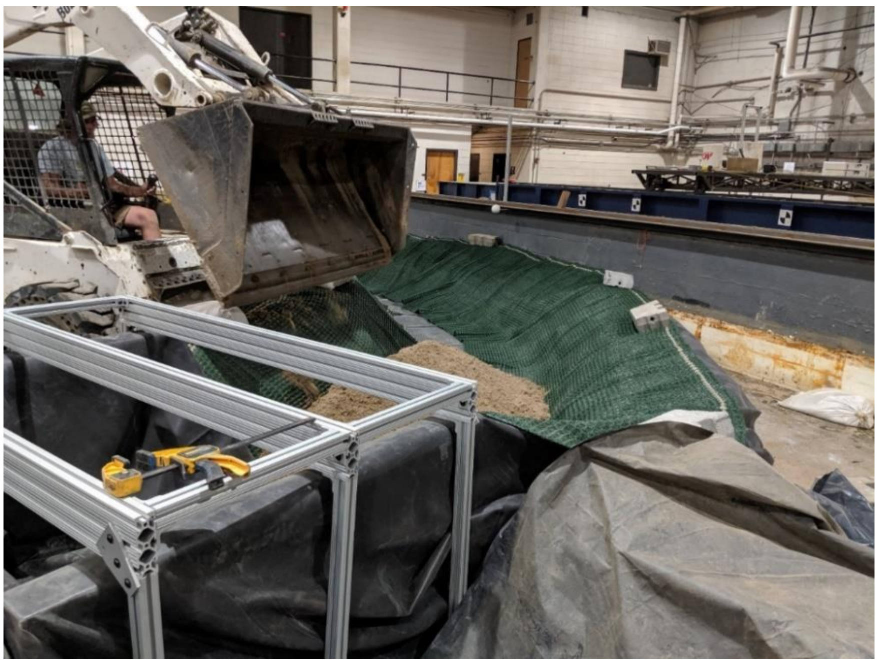

Figure 22: Use of a Bobcat to preliminarily fill the curved flume with the sand forming the flume's bed. Note that the concrete blocks positioned along the top of the sloping wall were temporary anchors, used until the sand had been placed in the curved channel.

Figure 23: A view of the completed curved flume. The view also shows a configuration of BW's placed in the flume.

3.3.1 Flow Control

Water flowrate through the curved flume was controlled using a large pump, the electromagnetic flowrate meter positioned in the pipeline stemming from the pump, and (as a check) a bypass valve was marked to indicate the flowrate. The control for an electronic motor was regulated to produce the necessary flowrate of water flow through the flume.

Water depth for each experiment was controlled within the curved flume using two gates at the downstream end of the flume. A vertical sluice gate (Figure 24) was used to control the water depth during low-flow conditions (flowrate, $Q < 1.0$ cfs). The vertical sluice gate was positioned upstream of the sediment trap to avoid critical flow conditions while filling or draining the flume. The downstream portion of the channel has two sudden expansions; the upstream expansion is located at the downstream end of the sediment bed (Figure 26) and the downstream expansion is located downstream of the vertical sluice gate at the sediment trap (Figure 25). A vertical sluice in this case was easier to seal to prevent leaking, and therefore was more effective than the downstream gate at controlling lower flow conditions due to the small proportion of flow able to pass the gate. Therefore, a vertical sluice gate was better at preventing critical flow conditions during filling and draining of the flume which preserved the bedforms developed from the experiment flow condition. Slow draining of the flume at the end of an experiment was essential for comparing before and after conditions of the bed, and thereby to determine how the BWs failed.

Figure 24: The vertical sluice gate used for the curved flume

The downstream overshot gate (also known as a tilting weir gate shown in Figure 25) was used primarily to control the flow during experiments (Q > 1.0 cfs) and prevent sand from entering the sump. An overshot gate was selected at this section of the flume to create a large enough cross-section of flow to slow flow velocities and enable sand to settle. For example, a vertical sluice gate would be an ineffective choice for this purpose, because a vertical sluice gate releases flow toward the channel bed rather than toward the water surface, the flow released would have high velocity due to head built behind the gate. Whereas an overshot gate maintains flow depth control toward the water surface rather than the channel bed. Then sediment particles at the base of the channel would be able to settle rather than travel into the laboratory sump.

Figure 25: The overshot gate (or sloped weir) used for the curved flume. The gate is positioned immediately downstream of the flume's tailbox.

Riprap was positioned upstream of the two gates at the downstream end of the curved channel (Figure 26). The riprap was used to prevent head-cutting from occurring along the channel bed during the (always slow) filling and draining of the curved flume. Particle size of the riprap was gradually increased in the downstream direction to prevent losses of flume sediment through gaps of larger particles. Finer bedload particles were caught on the upstream portion of riprap and upstream riprap particles are held in place by the transition of particles size in the downstream direction. The largest riprap particles are held in place by a metal grate and helped the flume to drain. Proper flume drainage was crucial for LiDAR data collection, because LiDAR would have been ineffective if water pooled on the bed surface of the curved flume.

Figure 26: Upstream view of riprap and drainage at the downstream end of the flume's curved channel

3.3.2 Sand Size

The sand selected for the straight flume also was selected for the curved flume, thereby maintaining consistency for the desired flow conditions. However, because the curved flume did not have a sediment recirculation system a hopper was used to feed in sand to maintain overall channel-bed equilibrium.

The sand-feed hopper was located at the flume's upstream end, and was used to supply sand into the flow approach to the curved channel. To estimate the necessary rate of sand feed from the hopper (Figure 28), the Meyer-Peter & Müller (MPM) method was used, and the average particle size of sand was the same as used for the selected sand forming the bed of the straight flume. The sand's rating curve (is given in Figure 27). After tuning the hopper to give the estimated rate of sand feed into the straight stretch of flume upstream of the curved channel, a sediment diffuser was fitted to the base of the hopper to spread the sediment across the flume's bed (Figure 29). Tuning entailed estimating the volumes of sand fed into the flume and sand stored in the sediment trap located in flume's tailbox. Several tests showed that the difference in volume trapped was about 4% less than that fed into the flume. This difference is attributed to two causes: sand stored in the point bar formed in the lee of the flume's curved inner bank; and, some sand contained in the flow passed over the overshot gate.

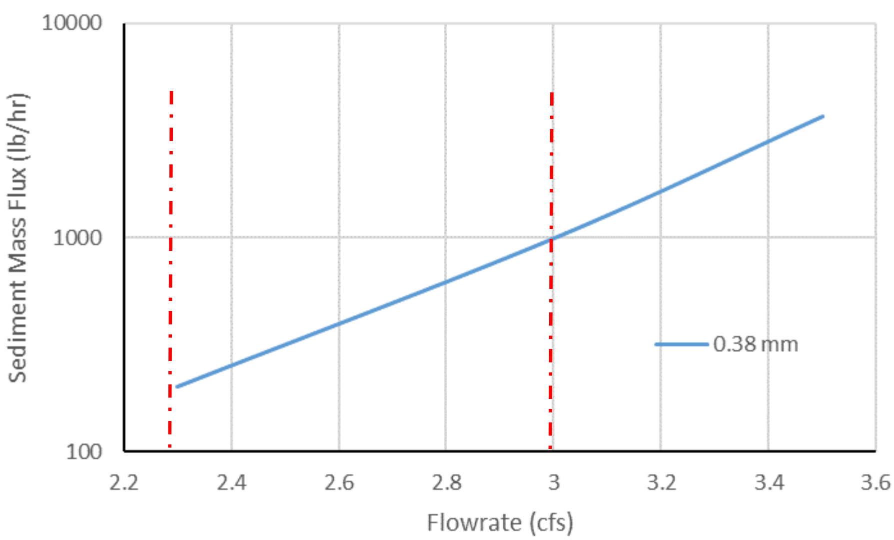

Figure 27: Sediment rating curve used for the curved flume: (a) red lines indicate flowrates used for experiments

Figure 28: The sediment hopper used to feed sand into the approach to the curved flume

Figure 29: Sediment diffuser located at the base of the sand-feed hopper

Also, to ensure sediment equilibrium toward the end of each experiment, five arbitrary points were selected along the channel bed (point 1 being the most upstream and point 5 being the most downstream) and elevation measurements were taken until the channel bed reached equilibrium. Equilibrium conditions took about 30 minutes to develop along the flume's bed (Figure 30). All arbitrary locations showed the same general trend, where changes in bed elevation occurred for approximately 15 minutes then a reduction in changes occurred as the bed elevations approached equilibrium.

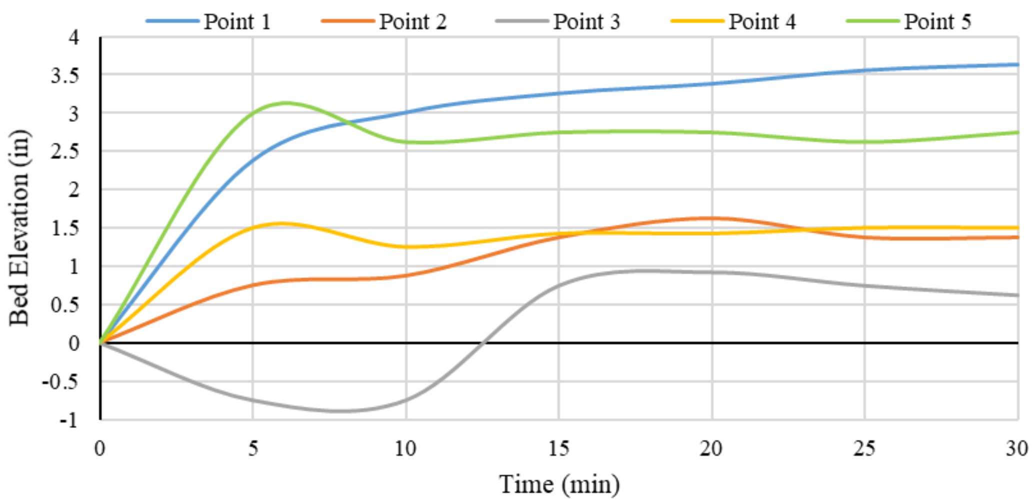

Figure 30: Time to develop equilibrium conditions along the flume's bed. The bed was monitored at five locations (points) along the bed

3.2.3 Program of Experiments

Curved flume experiments were conducted to confirm the occurrence of the failure modes observed for BWs and RVs in the straight flume. Additionally, it was decided to use the experiments to guide further experiments with the curved flume; further experiments are being conducted after the present study. The curved-flume experiments yielded other insights into the BW- and RV-failure modes likely to be noticed in a field situation. The reader may recall that the straight flume was used to deliberately expose BWs and RVs to challenging flow conditions so that the failure modes would be readily apparent.

Table 6: Program of experiments conducted using the Curved Flume

EXPT #	Rock Structure	Q (cfs)	y (in)	τ_0/τ_c	y/H	α (Degrees)	W (in)	L (in)	H (in)	S_0
1a	3BW	3.0	6	9.9	2.0	90	3	8	3	0.0012
2a	4BW	3.0	6	9.9	2.0	90	3	16	3	0.0012
3a	4BW	3.0	6	9.9	2.0	90	3	16	3	0.0012
4a	4BW	2.3	3.75	8.3	1.25	90	3	16	3	0.0012
5a	4BW	2.3	3.75	8.3	1.25	90	3	16	3	0.0012

3.2.4 Data Collection

Water-surface measurements were taken using Massa probes, which used ultrasonic sound waves to determine the water surface elevation (WSE). The Massa probe located on the foot bridge (Figure 31a) was used as a control due to its stationary positioning along the channel. Whereas the mobile Massa probe (Figure 31b) was used to collect data at various points along the channel. The target flow depth for each experiment is presented in Table 8 and flow depth data throughout the duration of the experiments is given in Appendix B. A data station was used so that the Massa probes could communicate with a computer for processing. Processing was completed using a program called NI LabVIEW and results were recorded using Microsoft Excel.

(a)

(b)

Figure 31: Massa probes (ultrasonic sensors) used for collecting bed surface and water-surface elevation (WSE): (a) a stationary Massa probe was used as a control point along the flume; and (b) a mobile Massa probe was used for collecting WSE data at different locations along the flume

LiDAR (TOPCON GLS-2000 3D Laser Scanner) was used to obtain changes in bed topography for before and after experiments. This instrument was positioned at two different locations for each bed scan: a location downstream of the BWs (Figure 32) and on the foot bridge upstream of the BWs. Figure 32 shows the LiDAR instrument collecting bed topography data at the downstream location (1 of 4 scans conducted per experiment). LiDAR data were transferred to a computer for processing with an SD card. A program called MAGNET collage was used to process the data and generate a point cloud corresponding to the CSU Hydraulics Laboratory's coordinate system. Point clouds were transferred to another program called Autodesk Recap for point cloud management (removing excess data, colorizing, and scaling of channel bed data points based on elevation).

Figure 32: A LiDAR instrument scanned the channel bed after a completed experiment

3.2.5 Curved Flume Procedure

The following procedure was used to perform live-bed experiments with the 4 ft wide, curved flume:

1. The sediment within the flume was leveled and made even with the base of the trapezoidal portion of the flume. Excess sediment from previous experiments caught in the downstream sediment trap was removed and reapplied to the bed for leveling. The sediment hopper is also refilled with dry sand.

2. The vertical sluice gate and overshot gate were opened, and the pump was turned on to achieve the desired flow rate. The vertical sluice gate and overshot gate were adjusted to achieve the desired water depth, and the sediment hopper was turned onto the proper sediment feed rate for the flow condition. The flume was run for approximately 2 hours to achieve bedform equilibrium without the presence of BWs. The flow depth was monitored recorded throughout the experiment at 5 points using the two Massa probes.
3. After bedform equilibrium had been reached the vertical sluice gate was closed and the overshot gate was left at that current condition for achieving equilibrium with BWs present. The pump and hopper were turned off and the flume was slowly drained due to the closed vertical sluice gate. Thus, equilibrium bedforms are preserved and the experiment can continue.
4. After the flume was drained the BWs were constructed with the dimensions given in Table 8 and using a median rock diameter of 15 mm and geometric standard deviation σ_g, of 8.9 mm. After construction of BW, a LiDAR scans were taken to record the initial bed condition without the impact of a BW flow field nor impact of scour on BW presence and stability. Then, the vertical sluice gate was checked to be fully shut, and the pre-experiment photographs were taken.
5. The pump was turned on to the lowest possible setting enabling the flume to slowly fill up to approximately a depth equivalent to y/H = 4.0 (deeper than used for an experiment) to preserve the current bed conditions and integrity of BWs. Then, the vertical sluice gate was slowly opened, and the pump was turned up to the desired flow rate. Once the desired flow rate had been achieved and the vertical sluice gate had been fully opened, the overshot gate was used to adjust the flow depth

6. The sediment hopper was turned adjusted to its required sediment feed rate for the water-flow condition used, and the flow condition was held for approximately 2 hours until equilibrium was reached with BWs present. The two Massa probes continually monitored and recorded the water depth throughout the duration of the experiment.
7. After equilibrium was reached the vertical sluice gate was closed and the pump and hopper were turned off. Then the flume was left for several hours to drain slowly. Thereafter LiDAR scans were taken to record the bed bathymetry resulting from BW presence.

CHAPTER 4. EXPERIMENT RESULTS

4.1 Introduction

This section presents the main findings from the straight-flume experiments and the curved-flume experiments. Only the main results are presented here. Observations mentioned are from selected experiments representative of the main findings. Appendix A documents all the experiments. As mentioned above, the curved-flume experiments were done to verify that the failure mechanisms observed for the straight flume also occurred for a curved channel.

Preliminary experiments were done using the straight flume. The purpose of these experiments was to identify tentatively the likely modes whereby BWs and RVs failed in the live-bed conditions. Subsequently, eight detailed straight-flume experiments were conducted to identify and document the failure mechanisms for BWs and RVs arranged in configurations of three structures (see Table 5). A result from the preliminary experiments was that series of three BWs or RVs were needed for each experiment, because each of the BWs or RVs in a series of such structures experienced difference flow conditions.

The experiments involving an individual or a series of BWs or RVs used the configuration dimensions recommended from Siefken et al. (2021). These dimensions pertained particularly to structure length and width. Additionally, the experiments represent field applications typical of conditions anticipated in actual channel bends, especially bends like those along the Middle Rio Grande. The failure mechanisms observed were found to be sufficiently basic and repeatable that they likely would apply to curved channels differing in geometry to the geometry of the curved channel used for the present study and differing in bed sediment size. However, further confirmation work is needed in this regard.

4.2 Preliminary Results

The first two preliminary experiments (Figure 33 and Figure 34) conducted in the straight flume used a single BW with an 8-in-wide-crest, y/H = 2.0, and angled normal to the flume wall, both experiments showed the same failure mechanisms found for the upstream BW and RV. The first two preliminary experiments were conducted with the same flow conditions and BW setup to ensure consistent results between experiments. The following list states the failure mechanisms observed for upstream BW or RV:

- Rock dislodgement due to contraction scour along the crest of the BW thereby, causing a reduction in crest length and crest angle.
- Rock dislodgement from the upstream face of the BW when the trough of a dune reached the toe of the upstream slope, thereby causing the upstream slope to reduce and the crest width of the BW to narrow.

(a) (b)

Figure 33: BW with 8-in-wide crest, y/H = 2.0, and α = 90°, EXPT 1: (a) before; and (b) after

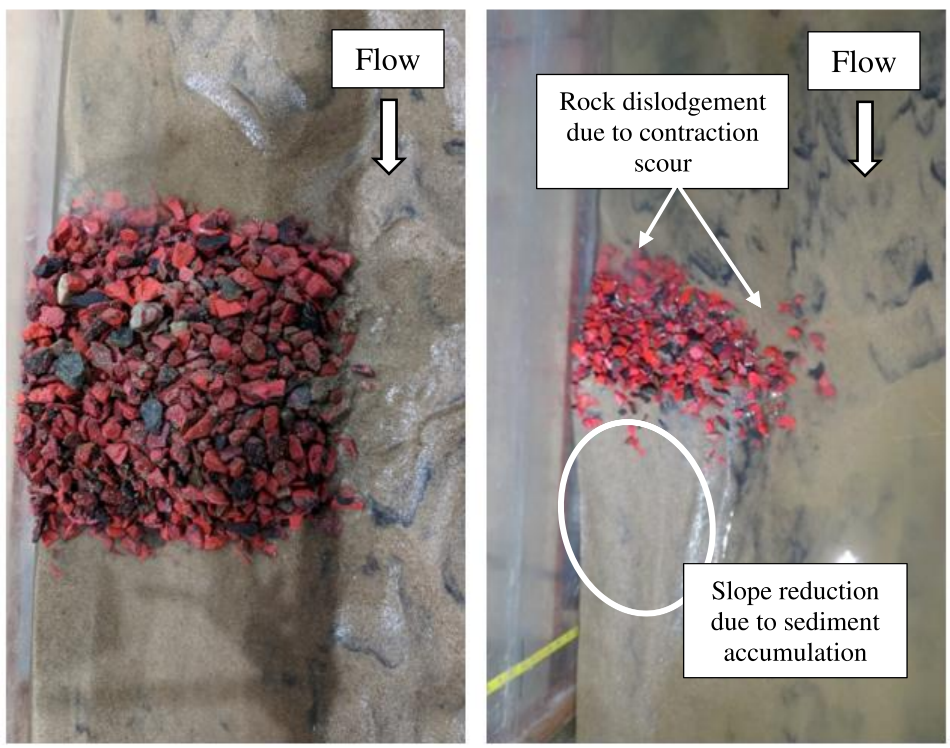

(a) (b)

Figure 34: BW with 8-in-wide crest, y/H = 2.0, and α = 90°, EXPT 2: (a) before; and (b) after

EXPT 5 (Figure 36) used 3 BW with an 8-in-long crest, y/H = 1.25, and angled normal to the flume wall. The upstream BW (BW 1.5) displayed the same failure mechanisms demonstrated by EXPT 1 and EXPT 2. However, EXPT 5 showed the failure mechanisms for the downstream BW (BW 2.5 and 3.5).

- Rock dislodgement due to contraction scour along the toe of the tip of the structures. The dislodgement caused a reduction in crest length for all three BWs.
- Flow from the most upstream BW, impacted the second BW part way along that BW's upstream slope.

Slope reduction occurred along the downstream sides of each structure due to sediment deposition. In some cases, sediment deposition along the downstream side of a structure reduced the slope along the upstream side of the adjacent downstream structure due to a reduction in flow velocity from the reverse eddy current generated by the structure (as Figure 35 depicts).

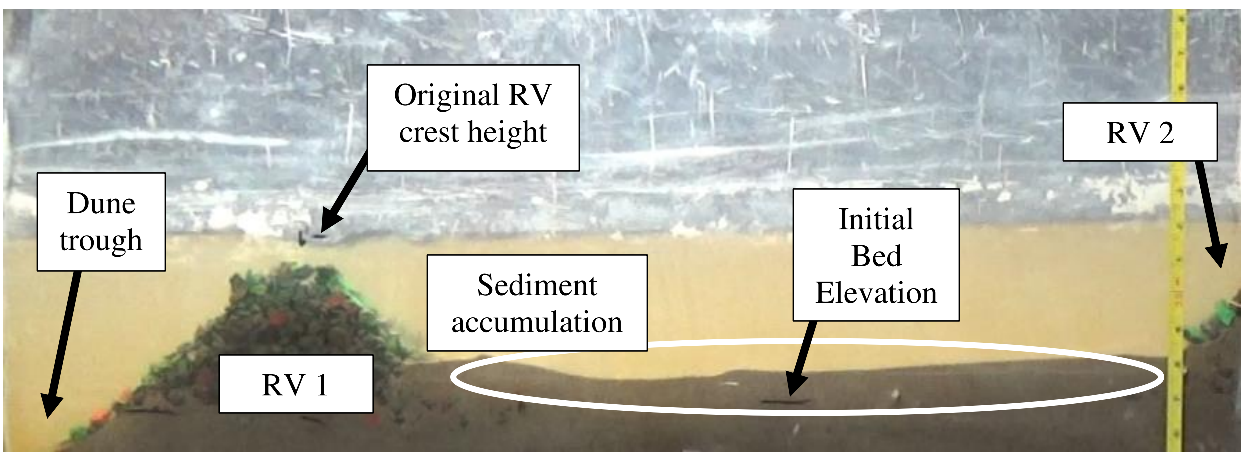

Figure 35: Sediment accumulation between RVs (EXPT 14)

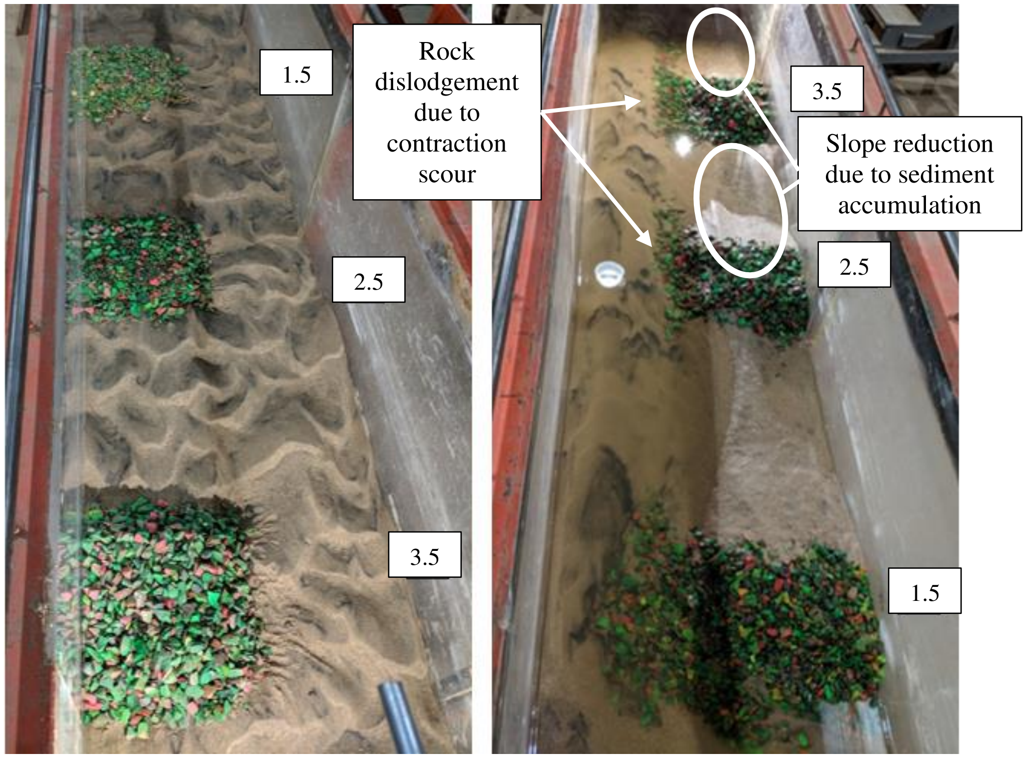

Figure 36: 3BW with 8-in-wide crest, *y/H* = 1.25, and *α* = 90°, EXPT 5: (a) before; and (b) after. The numbers shown (1.5, 2.5, and 3.5) reference the adjacent BWs

For all the preliminary experiments, once contraction scour and sediment accumulation had occurred, the experiments were observed to quickly attained an equilibrium bed bathymetry. This process typically took about 30 minutes in the flume. Further rock dislodgment due to contraction scour was prevented because dislodged rock armored the scour zone in the channel bed. Sediment accumulation along the downstream side of the structure was limited by the structure's crest height, where sediment was unable to deposit because flow velocities of flow passing over the BW no longer were reduced. Sediment deposition also assisted in preventing rock dislodgment by bed sediment filling gaps between the rocks forming the structure. Thus, as the experiment approached equilibrium, the BWs became (in effect) armored bedforms. These mechanisms prevented the further, and complete failure of the BWs; complete failure would entail breaching and collapse of a BW. In most cases, it was found that the BWs failed partially when in the harsh flow conditions imposed by the straight flume; partial failure entailed slope failure and shortening, but not full breaching.

4.3 Straight Flume: Main Results

The main results from the experiments with the straight flume showed essentially the same failure modes as seen during the preliminary experiments. The greatest observed variability occurred between individual BWs in a series of BWs. When comparing failure mechanisms for a BW, it was observed that *y/H* affected the maximum depth of contraction scour at the BW tip (end of crest) and the bed lowering when a dune trough approached the first BW (see Figure 45). The angle, α, of the structure relative to the flume wall impacted sediment deposition patterns and indicated the potential for bank failure that would cause bank scalloping immediately downstream of a BW.

Thee influences of these parameters can be seen when looking at EXPT 9 (Figure 37) and EXPT 11 (Figure 38 and Figure 39). EXPT 9 displayed a greater amount of rock dislodgment due to contraction scour compared to the contraction scour that occurred for EXPT 11; EXPT 9 had a maximum scour depth of 2.33-in, and EXPT 11 had a maximum scour depth of 2.15-in. The effect of α on sediment deposition can be seen when comparing EXPT 9 and 11. EXPT 11 used $\alpha = 45°$, which caused flow streamlines to intrude more between BW 1.11 and 2.11 (i.e., the first and second bendway weirs in EXPT 11). Whereas EXPT 9 used an $\alpha = 90°$, which caused far less intrusion of flow streamlines between BW 1.9 and 2.9 relative to EXPT 11. EXPT 11 also displayed different deposition patterns between the BWs compared to the patterns observed for EXPT 9, which displayed consistent sediment deposition forms between the BWs. Yet, despite the differences observed between the two experiments, the same failure modes mentioned in Section 4.2 occurred for all the experiments involving BWs.

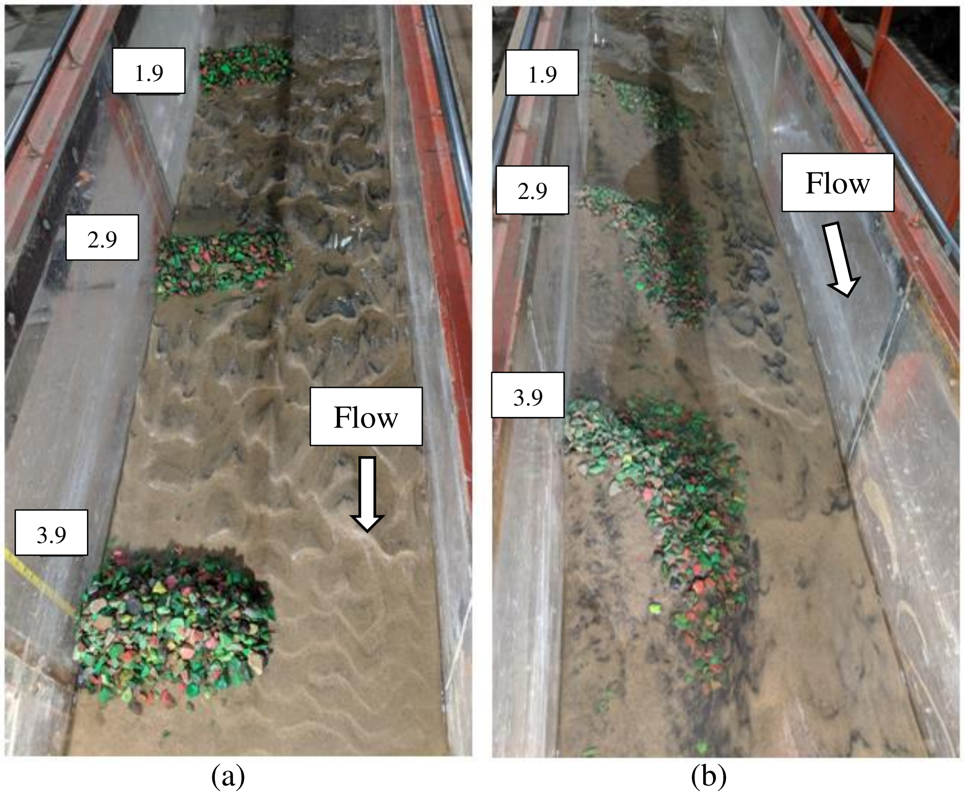

Figure 37: 3BW with 3-in-wide crest, *y/H* = 1.25, and *α* = 90°, EXPT 9: (a) before; and (b) after

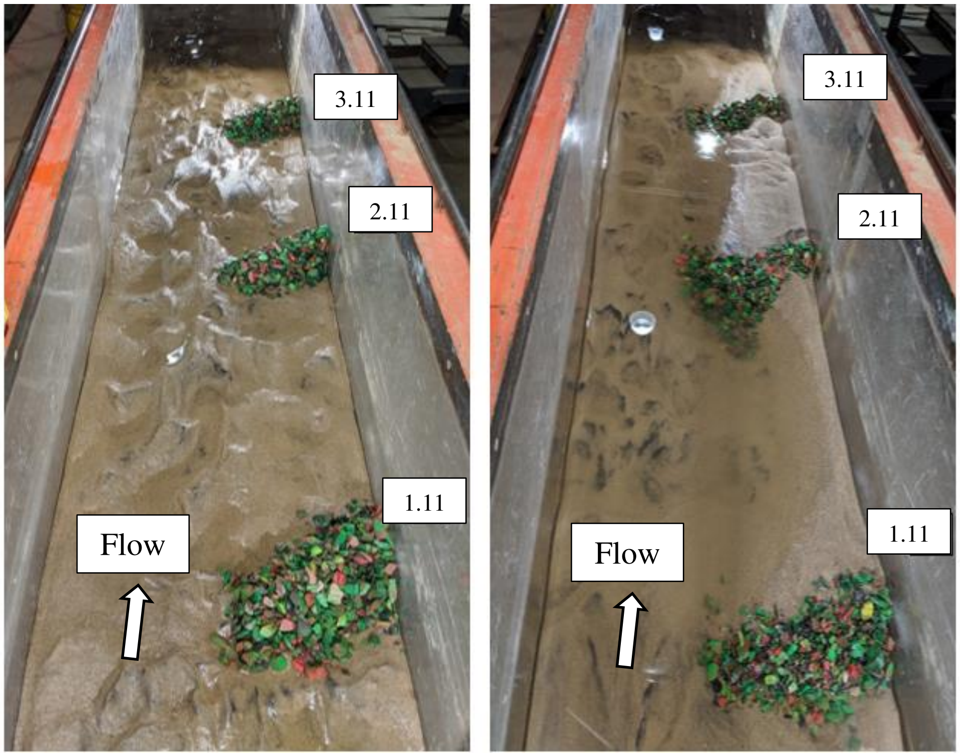

(a) (b)

Figure 38: 3BW with 3-in-wide crest, y/H = 2.0, and α = 45°, EXPT 11: (a) before; and (b) after

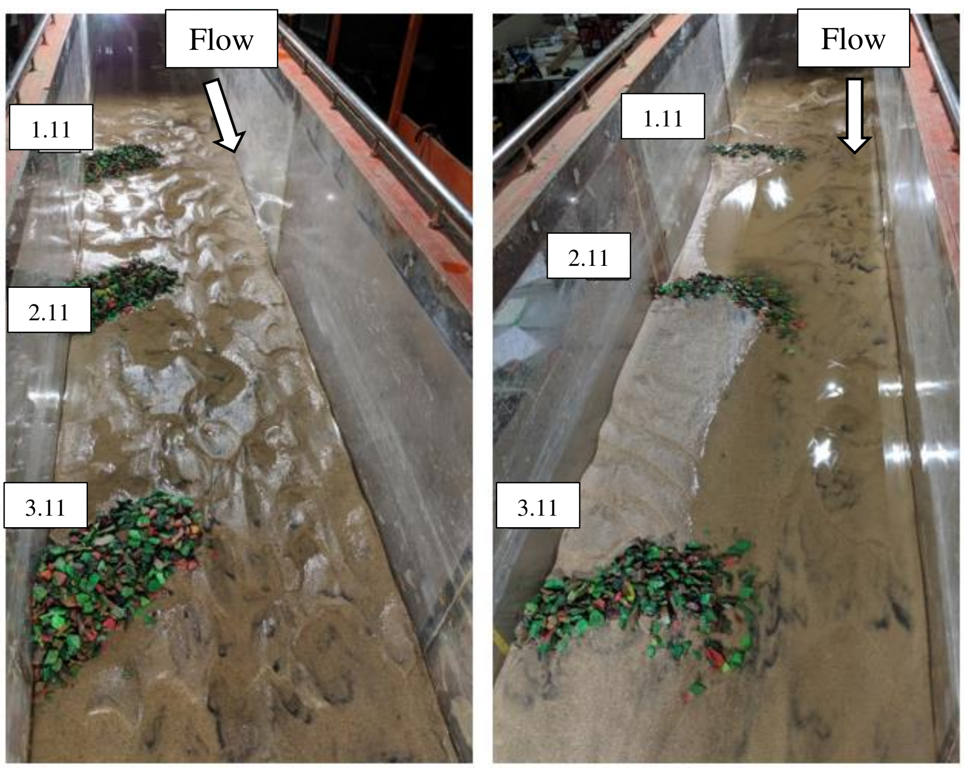

(a) (b)

Figure 39: 3BW with 3-in-wide crest, y/H = 2.0, and α = 45°, EXPT 11: (a) before; and (b) after

The experiments with the three RVs produced the same failure modes as found in the experiments with the three BWs. In all experiments involving the RVs, the upstream RV results were essentially the same as for EXPT 1 and EXPT 2, which involved BWs. The downstream RV displayed similar results to the preliminary findings in EXPT 5. However, the RVs gave more consistency between experiments where changes in parameters such as α and Y/H, made negligible impacts of driving failure mechanisms. For example, when comparing EXPT 12 (Figure 40 and Figure 42) and EXPT 16 (Figure 43 and Figure 44), both experiments showed the same general failure modes. No major differences were noticed between the sets of experiments.

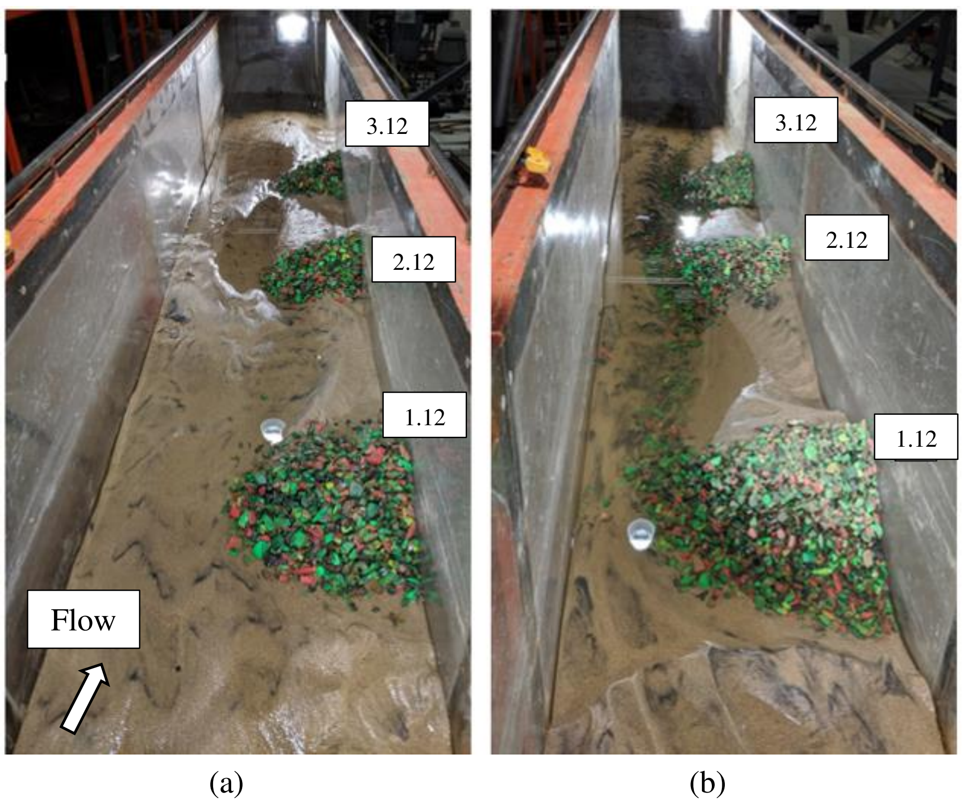

Figure 40: 3RV with 3-in-wide crest, *y/H* = 1.0, and *α* = 90°, EXPT 12: (a) before; and (b) after

Figure 42 provides a more detailed view of the failure mechanism mentioned above. RV 1.12 experienced rock dislodgment due to the presence of a dune trough (Figure 41) along the RV's upstream side, and contraction scour undermining the toe of the RV's tip. Rock dislodged from the dune trough along RV's upstream side reduced the crest height of the structure (Figure 41).

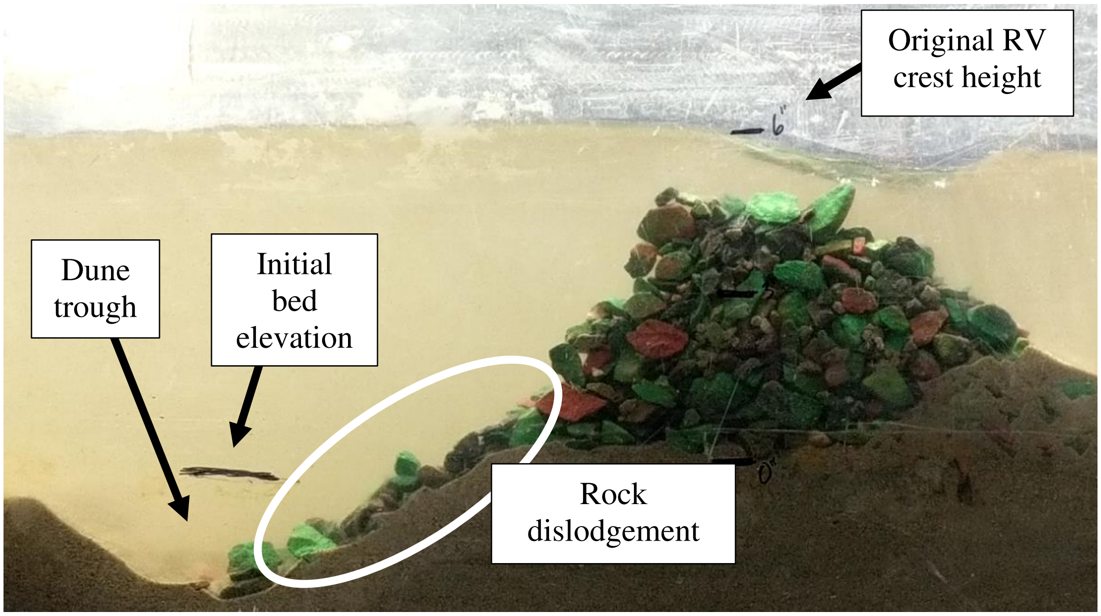

Figure 41: Dune trough along the RV's upstream side.

These failure modes resulted in a reduction in crest length, crest width, and crest height. The downstream RVs (2.12 and 3.12) showed rock dislodgment due to contraction scour along the toe of the RV tips. Dislodged rock was seen along the channel bed for all RVs, and that rock armored the channel bed, thereby preventing further scour from occurring as the experiment approached equilibrium of scour morphology. Slope reductions occurred due to sediment deposition along the downstream side of RV 1.12, along the upstream and downstream side of RV 2.12, and along the downstream side of RV 3.12. Note that the sediment deposition can occur only up to the crest height of the RV.

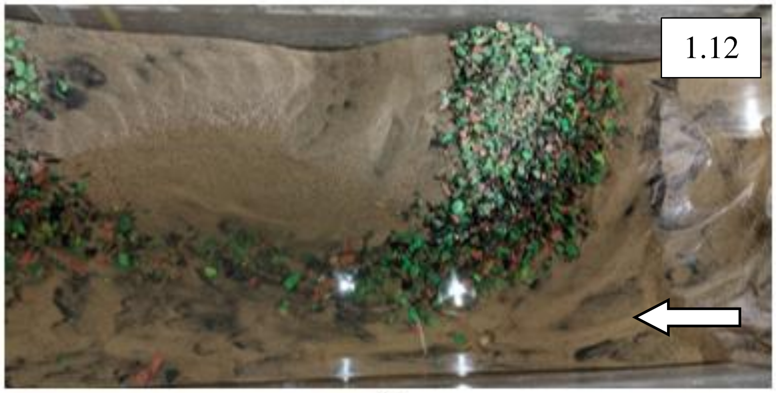

(a)

(b)

(c)

Figure 42: RVs 1 - 3, EXPT 12 (a) upstream RV; (b) middle RV; and (c) downstream RV. The arrow indicates flow direction

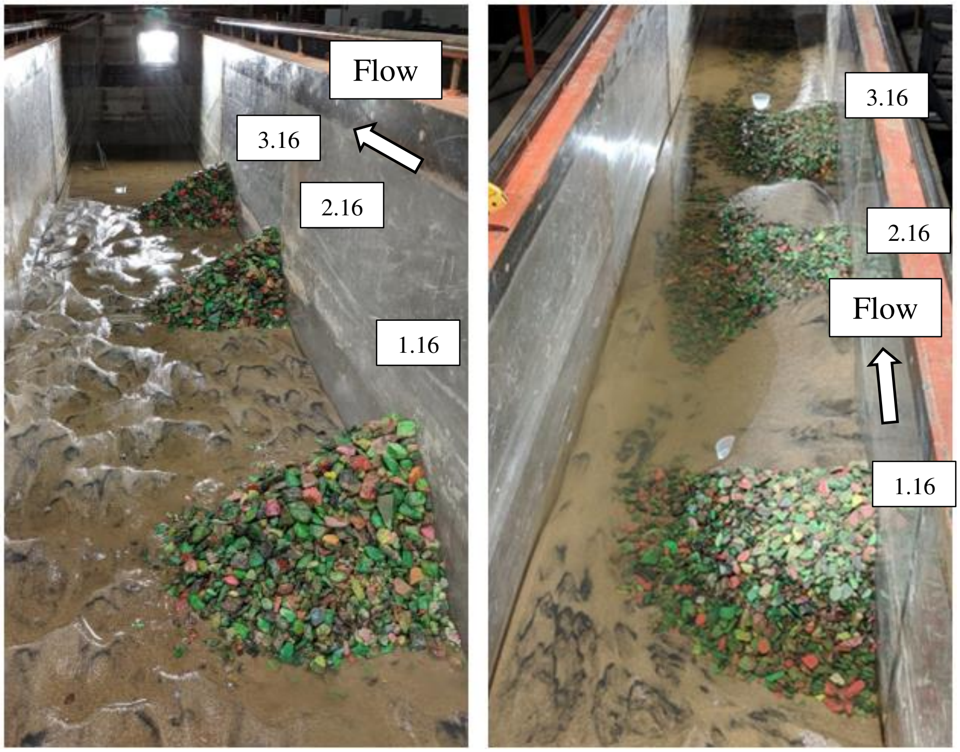

(a) (b)

Figure 43: 3RV with 3-in-wide crest, *y*/*H* = 0.625, and *α* = 45°, EXPT 16: (a) before; and (b) after

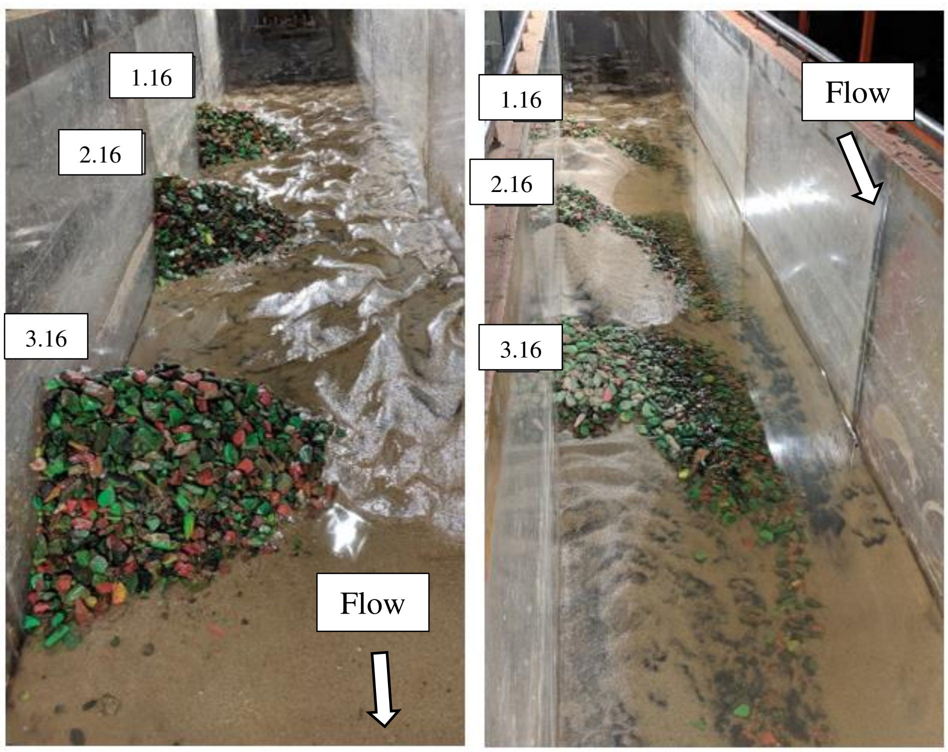

(a) (b)

Figure 44: 3RV with 3-in-wide crest, *y*/*H* = 0.625, and *α* = 45°, EXPT 16: (a) before; and (b) after

Figure 45 shows the maximum depth of contraction scour that occurred for the eight experiments conducted with the straight flume. The experiments show small amounts of variation between scour depths developed for the BWs and RVs. It was noted that the primary difference between experiments regarding maximum scour depth was attributable to the value of *y/H*. The larger value of y/H was associated with more flow passing over the BWs or RVs, thereby reducing contraction flow and the depth of contraction scour. Additionally, the angle of the BWs or RVs (45° or 90°) did not significantly affect the maximum scour depth. Also, the disposition of displaced rock embedded in the sand bed caused some slight variation of scour depth.

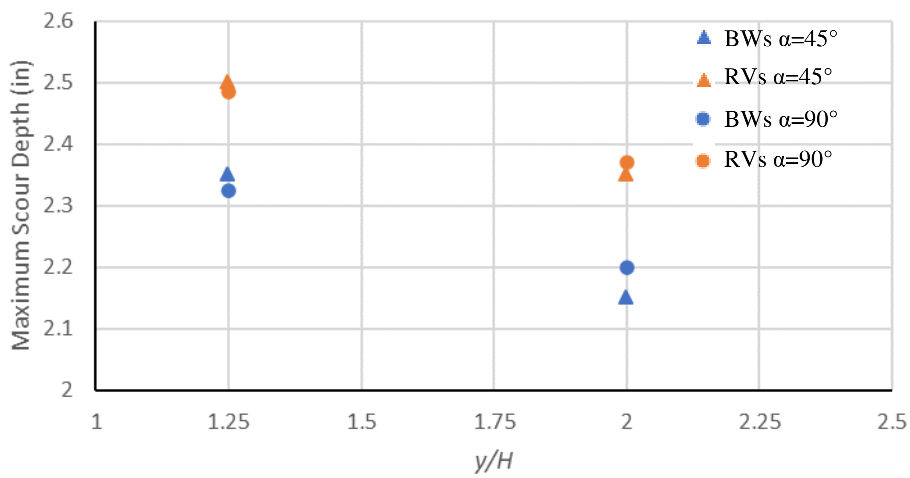

Figure 45: Maximum depth of contraction scour at the BWs and RVs for the straight flume experiments. Note: A triangle indicates α = 45° and a circle indicates α = 90°

As larger dunes occurred for the deeper approach flow, therefore dune troughs were lower in elevation for the deeper flow. This process caused the top layer of rock on the front slope of the first BW or RV to encounter a lower elevation and fail as a rock-layer slide. The lower troughs caused lower bed elevations at the front slope, but those elevations fared into the contraction scour at the tip of the BW or RV, making it difficult to assign a maximum depth of scour or lowering at the front face of the first BW or RV.

4.4 Curved Flume; Main Results

The curved-flume experiments were conducted to verify that the failure-modes observed in the straight flume indeed occurred in a curved flume (or channel). In this regard, EXPTs 3a and 4a were selected as being representative of the findings from the curved flume. Both these experiments used four BWs installed normal to the bank and used the same dimensions for each BW as in the straight flume (see Table 8A); it was found that three BWs were inadequate to represent a configuration of BWs, and in later experiments (still on-going) the number of BWs was increased to six. The main differences between EXPT 3a and 4a were the value of Y/H used for the two experiments varied as did the flowrate: EXPT 3a had $y/H = 2.0$, and EXPT 4a had $y/H = 1.25$.

Immediately a concern as the transverse slope of the bed of the curved channel, and therefore the variable nature of structure height, H. It was decided that H would refer to the structure's (BW or RV) height at the crest tip of the BW or RV. Also, the value of y was taken to be the average depth of flow in the straight transitional portion at the entrance to the curved channel. In this manner, the values of y/H were continued from the values used for the straight flume.

EXPT 3a showed the same failure modes found in straight flume experiments but were less evident than that observed in the straight flume experiments. Rock dislodgment occurred along the upstream side and the tip for BW 1.3a; here, 1.3a refers to the first BW in the series of three BWs used in EXPT 3. For the three downstream BWs (2.3a, 3.3a, and 4.3a), rock dislodgment from the crest tip was due to contraction scour, which occurred at the tips of the BWs. However, rock dislodgment due to contraction scour for EXPT 3a occurred but the contraction scour was not as deep compared to the depths of experiments conducted in the straight flume (Figure 47).

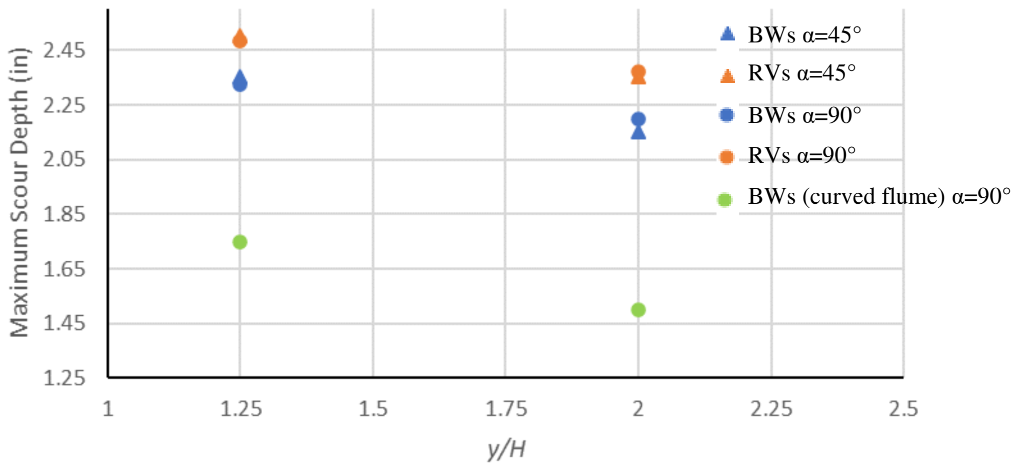

Figure 46: Maximum depth of contraction scour at the BWs and RVs for the straight and curved flume experiments. Note: a triangle indicates α = 45°, and a circle indicates α = 90°

Sediment deposition reduced the rear slope of BW 1.3a and caused reductions in slope for the downstream BWs. However, sediment deposition was not the cause of reduced upstream slope for BW 1.3a or the slope reductions at the tips of the BWs. As the experiment approached equilibrium in terms of thalweg bathymetry, rock gaps on the sideslopes of the BWs (though only the downstream slope of BW 1.3a) were filled with deposited sediment but not to the same extent as the experiments conducted using the straight flume.

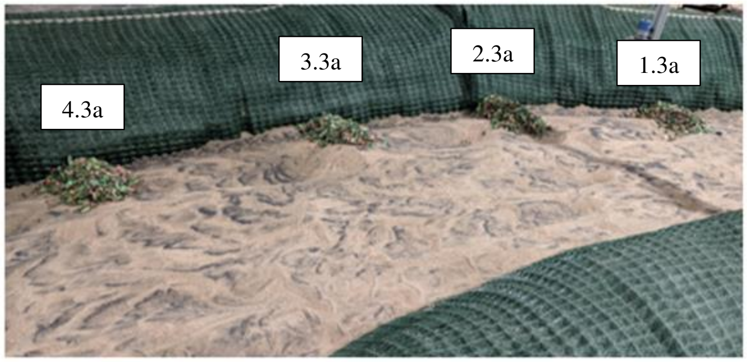

(a)

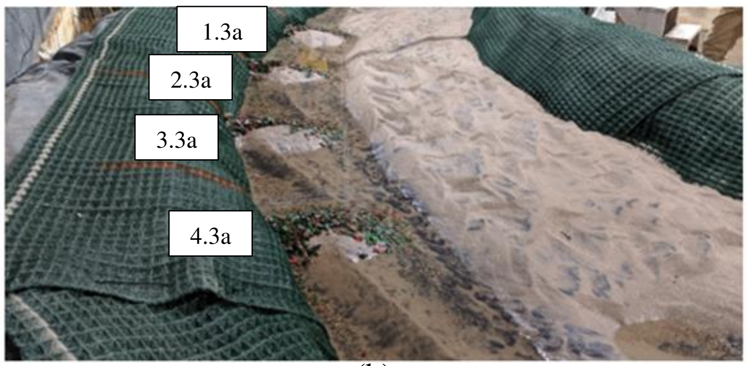

(b)

Figure 47: 4BW with 3-in-wide crest, *y/H* = 2.0 and *α* = 90°, EXPT 3a: (a) before; and (b) after

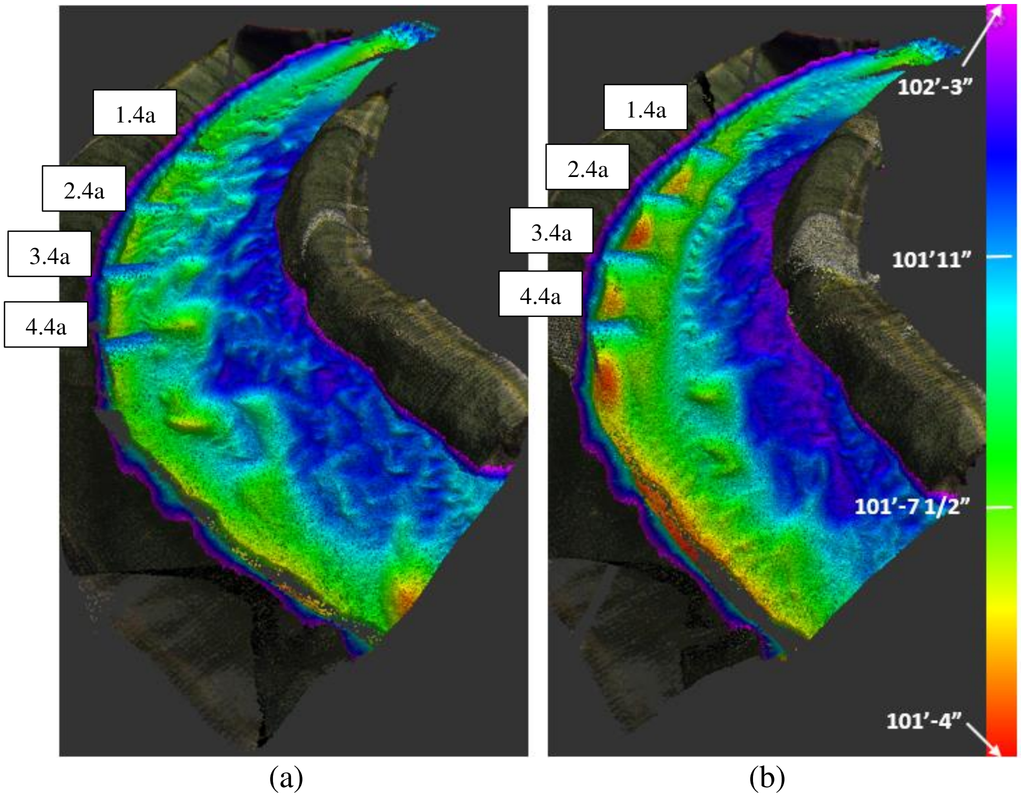

Figure 48: LiDAR scan of EXPT 3a: (a) before; and (b) after. The LiDAR scans show how the BWs did not cause the deepest (red) parts of the channel to move away from the channel's outer bank

EXPT 4a demonstrated an outcome like that of EXPT 3a. However, the modes of failure were more evident in EXPT 4a. Rock dislodgement from the BW occurred due to contraction scour around the tip of BW 1.4a. For the three, downstream BWs, rock dislodgement due to contraction scour primarily occurred along the tips of the BWs. Rock dislodgement led sloughed rock to armor of the channel bed to prevent further scour from occurring as the experiment approached equilibrium in terms of constancy of overall bathymetry. For EXPT 4a, sediment deposition was more substantial when compared to EXPT 3a, because the downstream slopes for all the BWs in EXPT 4a were more reduced (flatter) than for the BWs in EXPT 3a. Consequently, sediment deposition in the gaps between rocks also was more significant in EXPT 4a as the experiment approached equilibrium of the bed's overall bathymetry.

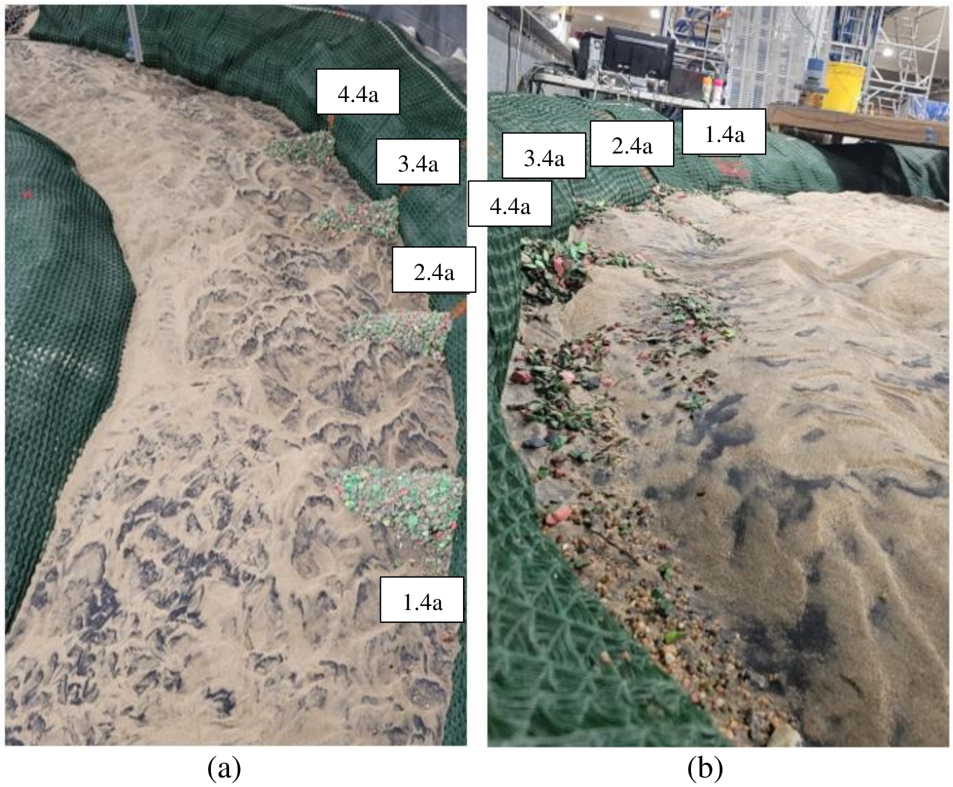

Figure 49: 4BW with 3-in-wide crest, *y/H* = 1.25, and *α* = 90°, EXPT 4a: (a) before; and (b) after

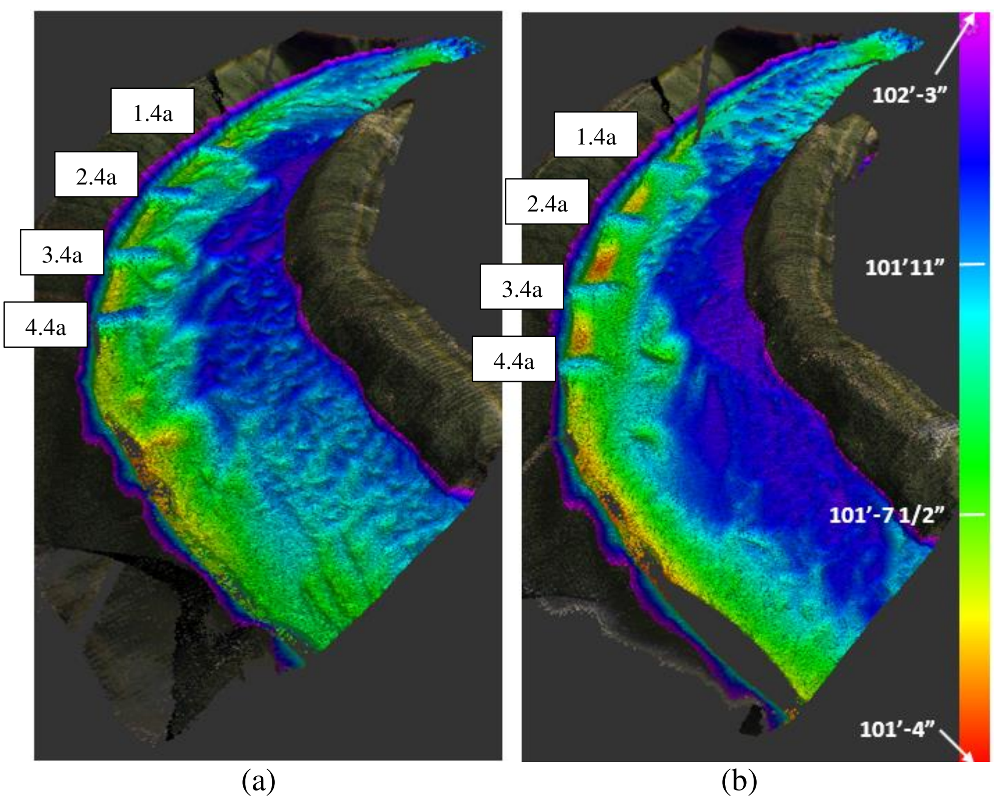

Figure 50: LiDAR scan of EXPT 4a: (a) before; and (b) after

4.4 BW and RV Design Recommendations

The findings from the straight flume and the curved flume led to design recommendations that sought to mitigate the effects that the observed failure modes would exert on BW performance. The following design recommendations, for individual BWs and RVs, resulted from the experiments:

- Increasing the volume of the structure particularly along the upstream side and toe of the structure. The upstream side as well as the toe of the structures is to be increased by $2d_{50}$. The additional volume of rock will become dislodged and armor the surrounding bed thereby, preventing further scour from occurring around the BW or RV. Illustrations of the design recommendation being applied to BW and RV are shown in Figure 52 and Figure 53.
- Based on results from the scour-related, failure tests using the straight flume and (thus far) with the curved flume, the recommended dimensions are:

  Increases length of crest by $2d_{100}$ (d_{100} is the diameter of the largest rock used in building a BW or RV) allowing for

  i. The slide-failure of the top layer of rock forming the end of a BW or RV.
  ii. The flattening of the slope of the failed end of the BW or RV. A crossflow causes the end slope to be flatter than the angle of repose of the rock forming the BW or RV.

  Increase width of crest by d_{100}, allowing for

  i. The slide failure of the top layer of rock forming the upstream slope of a BW or RV. Note that minimal velocities of crossflow cause the failed rock to reside at the angle of repose of the rock.

- The elevations to be considered define some of the geometric parameters for BWs and RVs. Note that Siefken et al. (2021) (and prior studies) does not account for variable values of H. Therefore, the need to consider elevations, though some approximations are needed.

  The parameters use reference elevations taken in the straight-channel segment (sometimes called the "cross-over sub-reach") at the entrance of the curved channel. Reference elevations are needed because flow depth and water-surface slope may vary around the curved portion of the channel. It is presumed that water-surface elevations at the start of the curved channel are about the same as at the entrance of the curved channel. Also, the crest of a BW is horizontal, whereas the crest of an RV slopes up to the bank-full elevation. Further, the sideslopes of the newly constructed BW or RV are at angle.

  Figure 51 shows the pertinent elevations.

  i. The bank-full-flow elevation is EL (Bank Full), and the commensurate bank-full depth of flow is Y.
  ii. The elevation of the tip of the crest of the first BW or RV in a configuration of BWs or RVs is EL (Crest Tip). It is necessary to specify this elevation to design a BW or RV. Usually (e.g., Siefken et al. 2021), this elevation is set as $(K)Y$ below EL (Bank Full) in the straight approach to the curved bed. The coefficient K may vary, though typically is c. 0.33-0.50, as noted in Chapter 2.
  iii. The elevation of the bed at the tip of the crest of the first BW or RV is EL (Bed at Crest Tip). EL (Crest Tip) – EL (Bed at Crest Tip) ≡ H.
  iv. The elevation of flow depth on the crest tip of the first BW

- The elevations lead to the following flow conditions:

  i. $H \geq Y$, the crest of the rock structure emerges above the bank-full flow elevation.

ii. $H \leq Y$, the crest of the rock structure is submerged below the bank-full flow elevation.

Then,

$0 < \Delta y \leq (Y - H)$, flow goes over and around the rock structure

Or,

$-H \leq \Delta y \leq 0$, flow entirely goes around rock structure

The latter flow conditions are usual for BWs or RVs.

- Figure 52 and Figure 53 give the recommended designs. These figures ensue from Figure 51 and give the recommended layout and dimensions of BWs and RVs. This information stems directly from the flume experiments described in this chapter.
- Figure 52 and Figure 53 give "as-constructed" and "operational" layouts of a BW and a RV.
- RV crest slope is $\theta = \tan^{-1}([Y\text{-}H]/L)$.

  Typically, $\theta \leq 20°$

  And

  $L = L_{proj}/\sin(\alpha°) = (TW/3)/\sin(\alpha°)$

  Where TW = average top width of the bed of the curved channel.

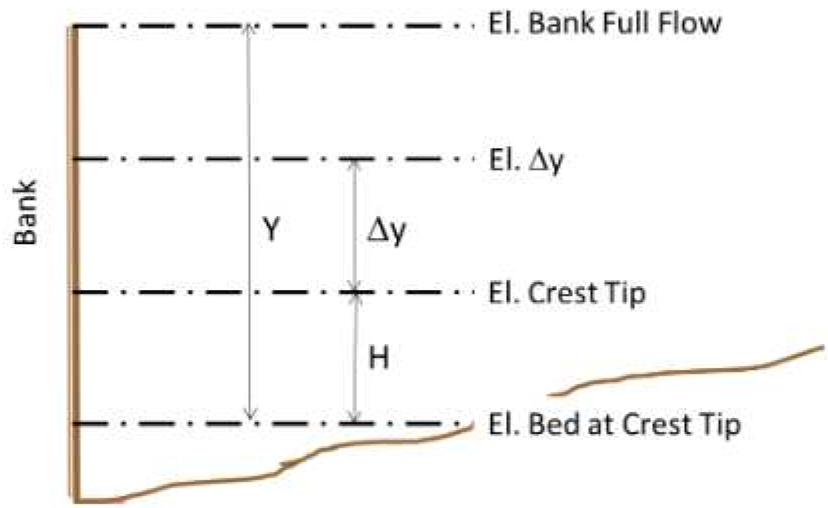

Figure 51: Elevations associated with flow through a curved channel (cross-section). The value of Y is taken at the more-or-less straight approach into the curved channel. The elevation at the crest tip of the BW or RV usually is down about (1/2)*Y* from the elevation of bank-full flow at the approach to the curved channel (Siefken et al. 2021). The elevation of the bed at the crest tip is taken as the average bed elevation in the approach to the curved channel, such that crest height above the bed, *H*, is *Y*/2

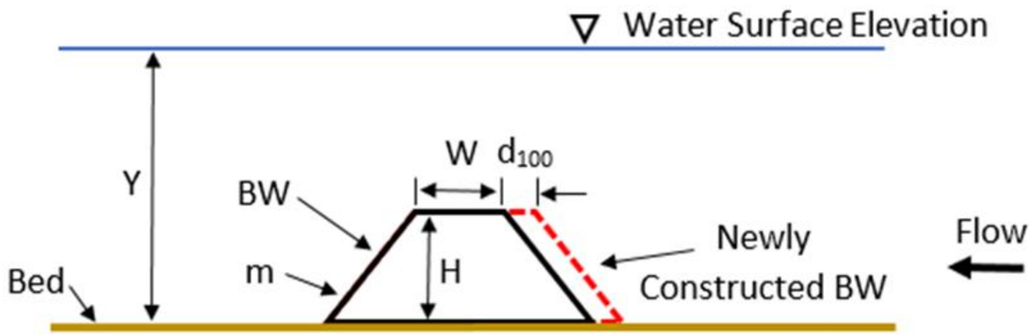

(a)

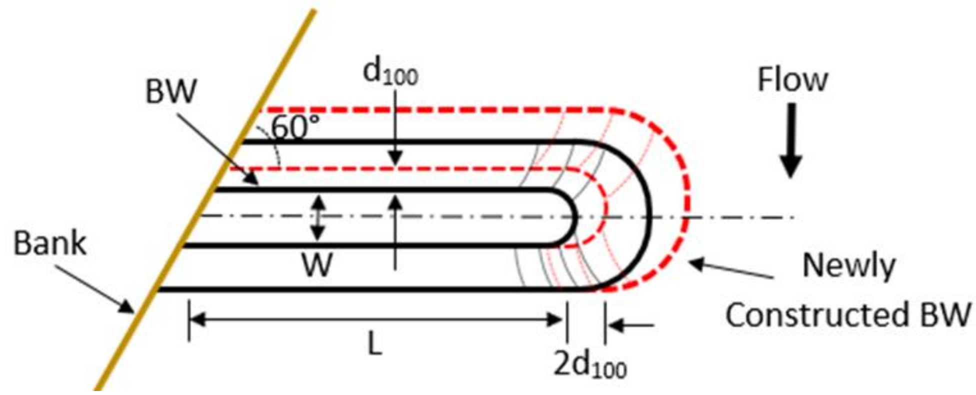

(b)

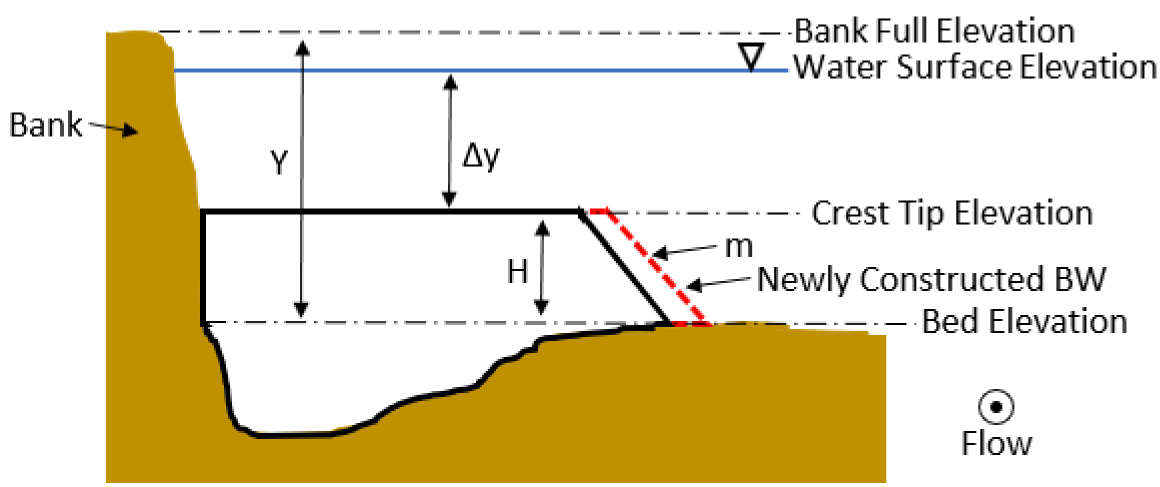

(c)

Figure 52: Design recommendation applied to a BW: (a) cross-section view of the applied design recommendation; (b) plan view of the applied design recommendation; and (c) centerline elevation view of the design recommendation

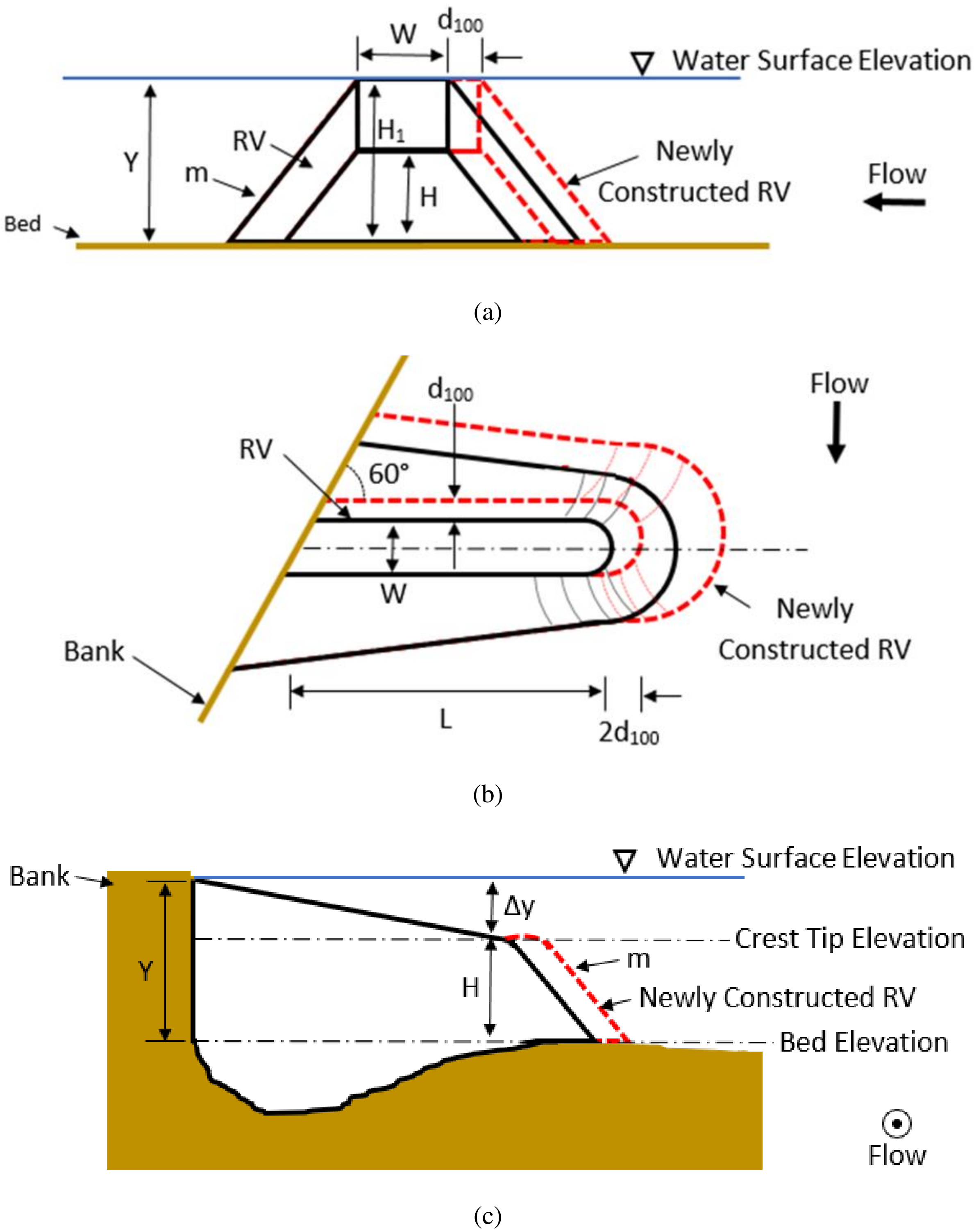

Figure 53: Design recommendation applied to a RV: (a) cross-section view of the applied design recommendation; (b) plan view of the applied design recommendation; and (c) centerline elevation view of the design recommendation

CHAPTER 5. CONCLUSIONS AND RECOMMENDATIONS

This chapter summarizes the overall conclusions from the experiments comprising this thesis.

5.1 Straight Flume Conclusions

The main conclusions drawn from the experiments with the straight flume are as follow:

- The failure mode associated with contraction scour of the bed at the tip of a BW or RV was generally more severe for y/H = 1.25 than when y/H = 2.0. This result occurred because the shallower flow requires proportionately more flow to pass around the BW or RV than for the deeper flow, which has more flow passing directly over the crest of a BW or RV.
- The failure mode associated with the approach of a dune trough lowered the bed level at the upstream sideslope of a BW or RV and led to the failure of that sideslope. This mode was more severe or pronounced when larger dunes occurred. In this sense, the condition y/H = 2.0 was more problematic than when y/H = 1.25, because the former value was associated (observably) with larger dunes.
- The first structure in a series of BW or RV structures typically had rock dislodgement along the upstream sideslope and the tip of the structure, whereas the two downstream structures were primarily affected by contraction scour along the toe with a minority of rock dislodgement occurring along the upstream side. It was difficult to determine how the two modes of rock failure merged, because contraction scour occurred around the tip of a BW or RV and, therefore, merged with the trough of a dune at the upstream side of a BW or RV. Also, the dune's trough itself varied in elevation.
- For BW and RV, sediment accumulation caused slope reductions along the downstream side of the structure and would typically extend to the upstream side of the adjacent

downstream structure. Such accumulation of sediment should not be considered a failure mode, because sediment accumulation reflected a reduction in flow velocity between adjacent BWs or RVs.

- RVs failed in the same modes as observed for BWs. Where the results obtained for the RVs were more prominent for $y/H = 0.625$ ($y/H = 1.25$ for a BW).
- As the experiments approached equilibrium in terms of channel bathymetry remaining overall stable, the BWs and RVs reduced in length and width and slope. However, they did not breach. Further scour around the structures was prevented because dislodged rock armored the bed surrounding the tip of each BW or RV.

5.2 Curved Flume Conclusions

The main conclusions drawn from the experiments with the curved flume (twice as wide as the straight flume) are as follow:

- The failure modes observed in the curved flume verified the modes observed in the straight flume.
- The lateral variation of bed bathymetry requires that a parameter used for the straight channel be re-defined: instead of y/H use $(\Delta y+H)/H$, where Δy is the depth of water above the crest tip of the BW or RV; and H is the height of the crest tip above the local elevation of the bed.
- Failure modes were more severe for $(\Delta y+H)/H = 1.25$ than when $(\Delta y+H)/H = 2.0$ for the curved flume experiments.
- Rock dislodgement was primarily caused by contraction scour. As with the straight flume experiments, the upstream BW was affected by contraction scour along the upstream side

and toe of the structure. The downstream BW were primarily affected by contraction scour along the tips of the structures.

- For BW, sediment accumulation caused slope reductions along the downstream side of the structures, where experiments with $(\Delta y+H)/H = 1.25$ displayed a greater reduction in slope. Slope reduction due to sediment accumulation was less severe for curved flume experiments relative to straight flume experiments. Sediment accumulation around the structures was not considered a failure but showed the structures were functioning properly.
- As the experiments approached equilibrium structures were reduced in size and were less abrupt along the downstream side of the structure. Further scour around the structures was prevented from dislodged rock armoring the surrounding bed.
- Curved flume experiments promoted the ambiguity and complexity of live bed experiments regarding BW failure modes.

5.3 Recommendations for Further Research

The results of this study reveal useful insights into recommendations regarding BW and RV failure modes. However, further research is needed. The ensuing topics indicate some further topics for further research.

1. The influence on BW or RV stability of a gravel bed versus that of a fine sand bed.
2. Experiments including more extensive flow field data: Acoustic-Doppler-Velocimeter (ADV) data collection; and surface patterns of flow via Large-Scale Particle Image Velocimetry (LSPIV) data collection.
3. Experiments conducted following a hydrograph approach.

5.4 Recommendations for Design Guidelines

The results of this study revealed useful insights into prevention of BW and RV failure modes after discussions with the USBR the design recommendations in Figure 52 and Figure 53 were developed. The designs increase the volume of rock forming the structure, particularly along the toe and upstream side of the structure. Where losses in additional volume will armor the surrounding bed to prevent further scour from occurring.

5.5 Limitations

This study focused on the failure of BWs and RVs rather than their performance in managing thalweg alignment. It should be noted that experiment conditions were harsher than field conditions to accelerate the failure process. Also, it should be noted that the experiments did not follow a hydrograph approach, which is being shown to affect the performance of BWs and RVs (Informal Notes 2021). For curved-flume experiments conducted in this study, the BWs were placed normal to the flume wall which caused scour to occur along the outer bank. When the BWs are placed between $\theta = 45^{o}$ and 85^{o}, the structures perform as required. However, since the study was not focusing on BW or RV performance, but rather on their failure, the experiments were able to be used to provide the necessary insight into BW and RV failure.

REFERENCES

Baird, D., Fotherby, L., Klumpp, C., and Sculock, S. M. (2015). *Bank stabilization design guidelines*. Bureau of Reclamation, Denver, CO.

Biedenharn, D. S., Elliott, C. M., and Watson, C. C. (1997). *The WES stream investigation and streambank stabilization handbook*. US Army Engineer Waterways Experiment Station, Vicksburg, MS.

Castro, J., and Sampson, R. (2001). *Design of stream barbs*. Natural Resources Conservation Service, Salina, KS.

Cox, A. L. (2005). *A Study of In-stream Rehabilitation Structures in Sand-bed Channels*. M.S. Thesis, Colorado State University, Department of Civil Engineering, Fort Collins, CO.

Darrow, J. D. (2004). *Effects of Bendway Weir Characteristics on Resulting Flow Conditions.*Thesis, Colorado State University, Fort Collins, CO.

Ettema, R., Nakato, T., and Muste, M. (2010). *Estimation of scour depth at bridge abutments*. NCHRP 24-20, National Cooperative Highway Research Program, National Transportation Board, 436.

Garfield, M. and Ettema R. (2021). *Effect of clearwater scour on the flow field at a single bendway weir: Two-dimensional numerical modeling supported by flume data*. ASCE, Journal of Irrigation and Drainage, Vol. 147 (2).

Heintz, M. L. (2002). *Investigation of bendway weir spacing*. Fort Collins, CO: Colorado State University.

Hogan, A. T. (2019). *Investigating the effects of bend radius of curvature on the flow around bendway weirs*. M.S. Thesis, Colorado State University, Department of Civil Engineering, Fort Collins, CO.

Informal Notes (2021). *Task 6: Scour-effects evaluation for bendway weirs and rock vanes*. Informal Notes T6-46, Bureau of Reclamation, Denver, CO.

Jamieson, E. C., Rennie, C. D., Jacobson, R. B., and Townsend, R. D. (2011). *3-D flow and scour near a submerged wing dike: ADCP measurements on the Missouri River: 3-D FLOW and scour near a submerged wing dike*. Water Resources Research, 47(7). https://doi.org/10.1029/2010WR010043

Jia Y., Scott S., Xu Y., and Wang S. S. Y. (2009). *Numerical study of flow affected by bendway weirs in Victoria Bendway, the Mississippi River*. Journal of Hydraulic Engineering, 135(11), 902–916. https://doi.org/10.1061/(ASCE)0733-9429(2009)135:11(902)

Johnson, P.A., Hey, R.D., Tessier, M., and Rosgen, D.L. (2001). *Use of vanes for control of scour at vertical wall abutments*. Journal of Hydraulic Engineering. 127(9). 772-778.

Julien, P. Y., & Duncan, J. R. (2003). *Optimal design criteria of bendway weirs from numerical simulations and physical model studies.* Colorado State University, Fort Collins, CO.

Julien, P.Y. (2010). *Erosion and sedimentation.* Second Edition, Cambridge University Press, UK.

Julien, P.Y. (2018). *River Mechanics.* Second Edition, Cambridge University Press, UK.

Kasper, K. E. (2005). *Accuracy of HEC-RAS to Calculated flow depths and total energy loss with and without bendway weirs in a meander mend*. M.S. Thesis, Colorado State University, Department of Civil Engineering, Fort Collins, CO.

Keating, K. and Knight, R. (2008). *A Laboratory study of the effect of magnetite on NMR relaxation rates*. Journal of Applied Geophysics, Volume 66, pp. 188-196.

Kinzli, K. (2005). *Effects of bendway weir characteristics on resulting eddy and channel flow conditions*. M.S. Thesis, Colorado State University, Department of Civil Engineering, Fort Collins, CO.

Kwan, T.F. (1984). *Study of abutment scour*. School of Engineering, Report No. 328. The University of Auckland, Auckland, New Zealand.

Lagasse, P.F., Clopper, P.E., Pagan-Ortiz, J.E., Zevenbergen, L.W., Arneson, L.A., Schall, J.D., and Girard, L.G. (2009). *Bridge scour and stream instability countermeasures: experience, selection, and design guidance*. 3rd ed. HEC-23. Federal Highway Administration. FHWA-NHI-09-111.

Lyn, D.A. and Cunningham, R. (2010). *A laboratory study of bendway weirs as a bank erosion countermeasure*. Purdue e-Pubs. JTRP Technical Reports. FHWA/IN/JTRP-2010/24.

Maryland Department of the Environment (2000). *Maryland's waterway construction guidelines*. Water Management Administration, Baltimore, ML.

McCullah, J.A. and Gray, D. (2005). *Environmentally sensitive channel- and bank-protection measures*. NCHRP Report 544, Transportation Research Board, National Academies of Science, Washington, D.C.

NRCS (Natural Resources Conservation Service). (2005). *Design of stream barbs*. Technical Note 23, Version 2.0. Portland, OR: US Dept. of Agriculture.

NRCS (Natural Resources Conservation Service). (2007). *Flow changing techniques*. Part 65: National engineering handbook. Technical Supplement 14H. NRCS, Washington, D.C.

NRCS (Natural Resources Conservation Service). (2009). *Streambank and shoreline protection*. Chap. 16 in Wisconsin supplement engineering field handbook. NRCS, Washington, D.C.

NRCS (Natural Resources Conservation Service). (2010). *Design of stream barbs for low gradient streams*. Minnesota Technical Note No. 8. NRCS, Washington, D.C.

NRCS (Natural Resources Conservation Service). (2013). *Kansas engineering technical note No. KS-1 (Revision 1)*. NRCS, Washington, D.C.

Schmidt, P. G. (2005). *Effects of bendway weir field geometric characteristics on channel flow conditions*. M.S. Thesis, Colorado State University, Department of Civil Engineering, Fort Collins, CO.

Scurlock, S., M., Baird, C., D., Cox, L., A., & Thornton, I., C. (2012). *Bendway weir design - Rio Grande Physical Model. Bureau of Reclamation*, Denver, CO.

Scurlock, S. M., Cox, A. L., Thornton, C. I., & Abt, S. R. (2014). *Calibration and validation of a numerical model forevaluation of transverse in-stream structure research.* Bureau of Reclamation, Denver, CO.

Scurlock, S. M., Thornton, C. I., & Abt, S. R. (2014). *Evaluation of bendway-weir structures within the native topography channel.* Denver, CO: Bureau of Reclamation.

Shin, K., Ettema, R., & Thornton, C. I. (2018). *Native channel topography and rock-weir structure channel-maintenance techniques.* Colorado State University, Fort Collins, CO.

Siefken, S. A. (2019). *Computational fluid dynamics models of Rio Grande bends fitted with rock vanes or bendway weirs*. M.S. thesis, Dept. of Civil and Environmental Engineering, Colorado State University.

Siefken, S.A. (2021). *Optimal configuration of rock vanes and bendway weirs for river bends: Numerical-Model Insights*. ASCE, Journal of Hydraulic Engineering, 147(5).

Papanicolaou, A. N., Bressan, F., Fox, J., Kramer C., & Kjos L. (2018). *Role of structure submergence on scour evolution in gravel bed rivers: Application to slope-crested* *structures*. ASCE, Journal of Hydraulic Engineering, 144(2), 03117008. https://doi.org/10.1061/(ASCE)HY.1943-7900.0001411

Thornton, C. I., James, M., & Shin, K. (2016). *Testing of instream vane structures within the native-topography channel*. Colorado State University, Fort Collins, CO.

Walker, K. G. (2009). *Comparison of a generalized trapezoidal hydraulic model to a native topography patterned bed Surface model of the Rio Grande*. M.S. Thesis, Colorado State University, Department of Civil and Environmental Engineering, Fort Collins, CO.

Welch, S., and Wright, S. (2005). *Design of stream barbs*. USDA Natural Resources Conservation Service, Salina, KS.

WSDOT (Washington State Department of Transportation). (2017). *Hydraulics manual*. Washington, DC: WSDOT.

APPENDIX A. EXPERIMENT RESULTS

Table 7: Straight Flume Qualitative Experiments

Test #	**Structure**	**Q** (cfs)	**y** (in)	**Shear stress ratio τ_0/τ_c**	***y/H***	**α** (Degrees)	**W** (in)	**L** (in)	**H** (in)	**S_0**
Preliminary Straight Flume Experiments										
1	BW	1.6	6	9.9	2.0	90	8	8	3	0.0015
2	BW	1.6	6	9.9	2.0	90	8	8	3	0.0015
6	2 BW	1.4	3.75	8.3	1.25	90	8	8	3	0.0015
7	2 BW	1.4	3.75	8.3	1.25	90	3	8	3	0.0015
3	3 BW	1.6	6	9.9	2.0	90	8	8	3	0.0015
4	3 BW	1.6	6	9.9	2.0	90	8	8	3	0.0015
5	3 BW	1.4	3.75	8.3	1.25	90	8	8	3	0.0015
10	3 BW_{Short}	1.6	6	9.9	2.0	90	3	6	3	0.0015
Straight Flume Experiments										
8	3 BW	1.6	6	9.9	2.0	90	3	8	3	0.0015
9	3 BW	1.4	3.75	8.3	1.25	90	3	8	3	0.0015
11	3 BW	1.6	6	9.9	2.0	45	3	8	3	0.0015
13	3 BW	1.4	3.75	8.3	1.25	45	3	8	3	0.0015
12	3 RV	1.6	6	9.9	1.0	90	3	8	6	0.0015
14	3 RV	1.6	6	9.9	1.0	45	3	8	6	0.0015
15	3 RV	1.4	3.75	8.3	0.625	90	3	8	6	0.0015
16	3 RV	1.4	3.75	8.3	0.625	45	3	8	6	0.0015

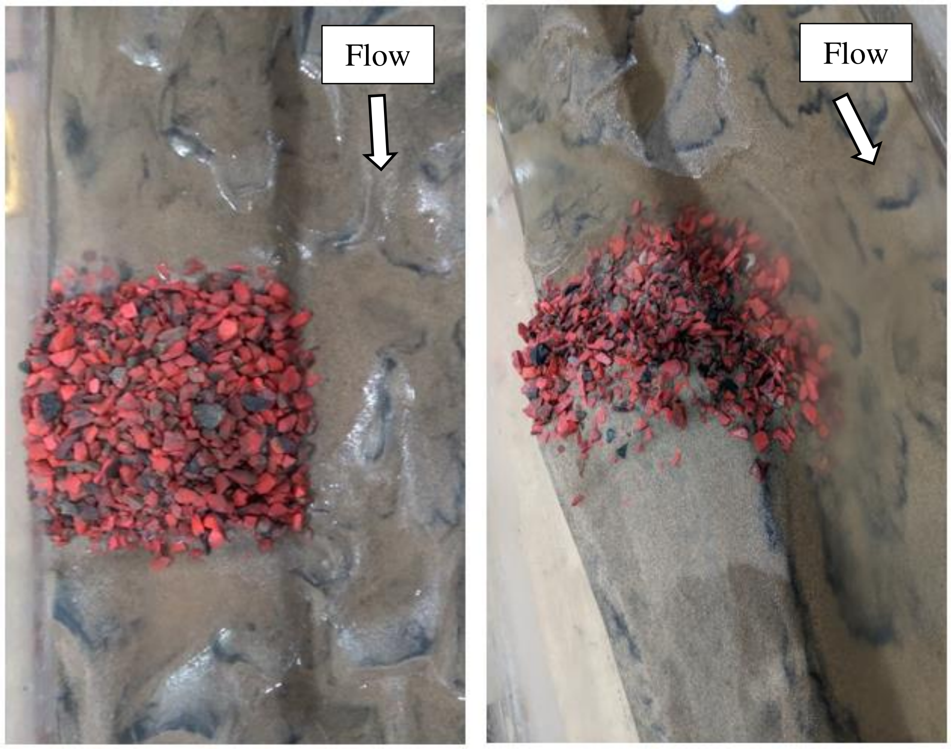

(a) (b)

Figure 54: BW with 8-in-wide crest, *y/H* = 2.0, and α = 90°, EXPT 1: (a) before; and (b) after

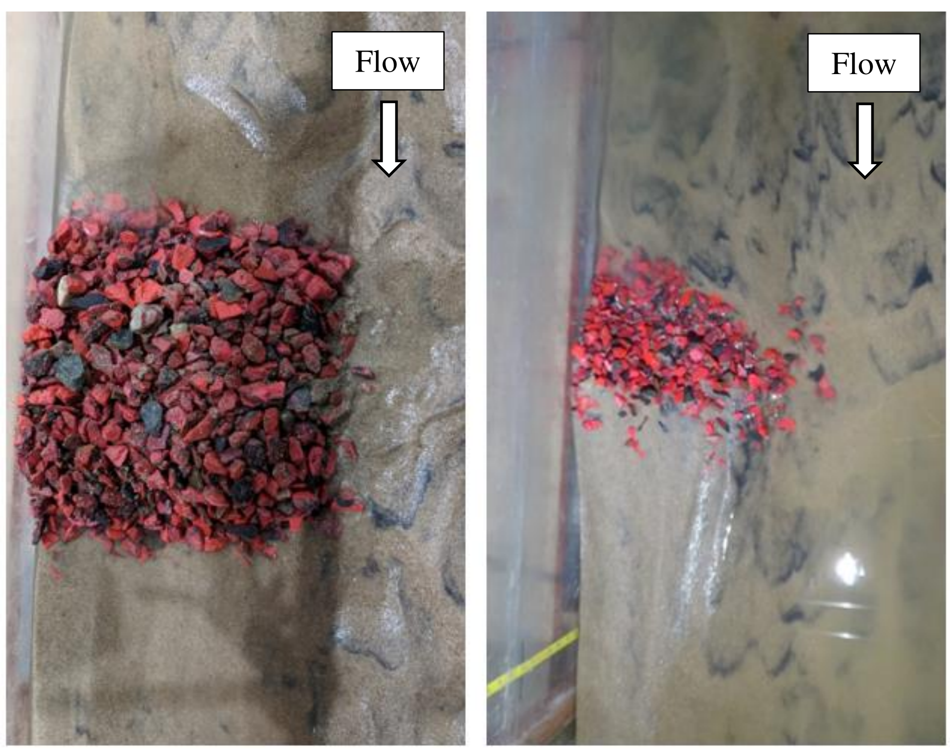

(a) (b)

Figure 55: BW with 8-in-wide crest, *y/H* = 2.0, and α = 90°, EXPT 2: (a) before; and (b) after

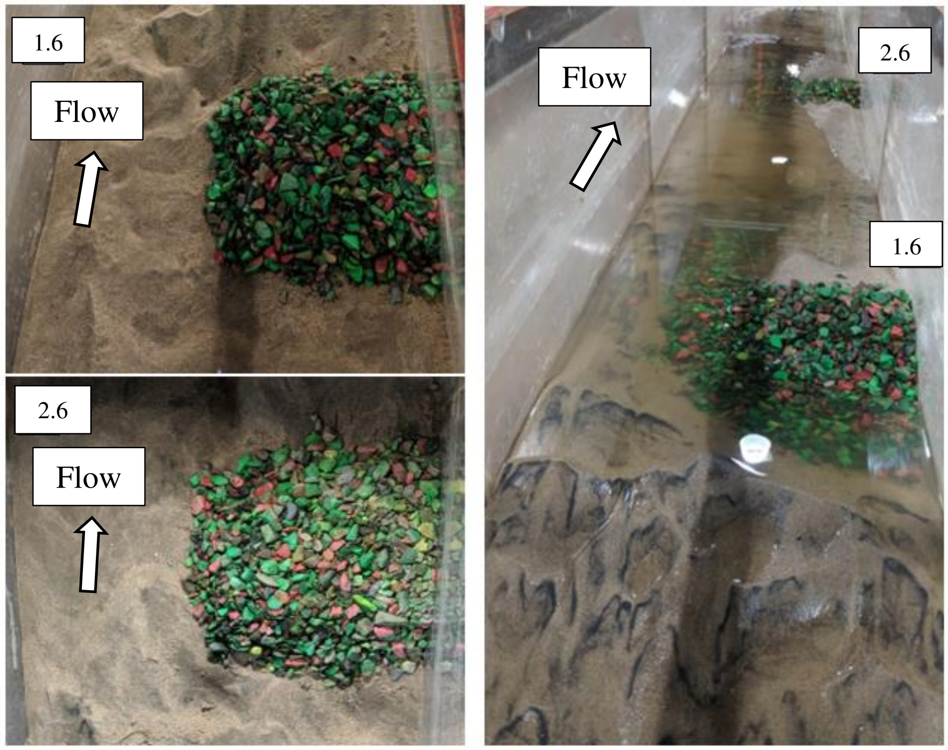

(a) (b)

Figure 56: 2 BW with 8-in-wide crest, *y/H* = 1.25, and α = 90°, EXPT 6: (a) before; and (b) after

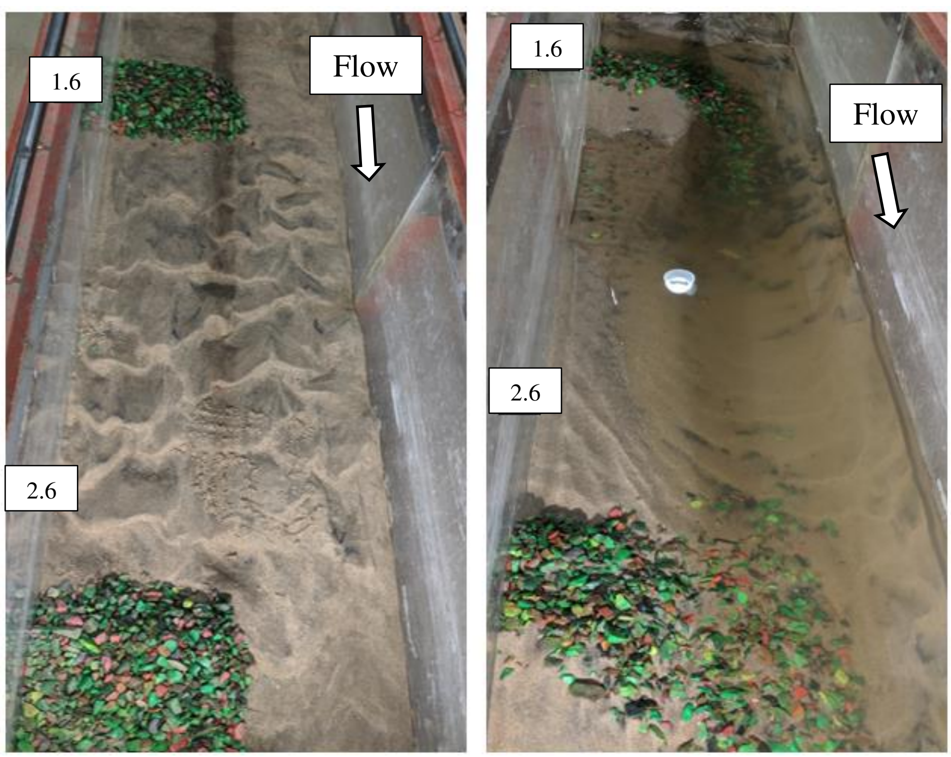

(a) (b)

Figure 57: 2BW with 8-in-wide crest, *y/H* = 1.25, and α = 90°, EXPT 6: (a) before; and (b) after

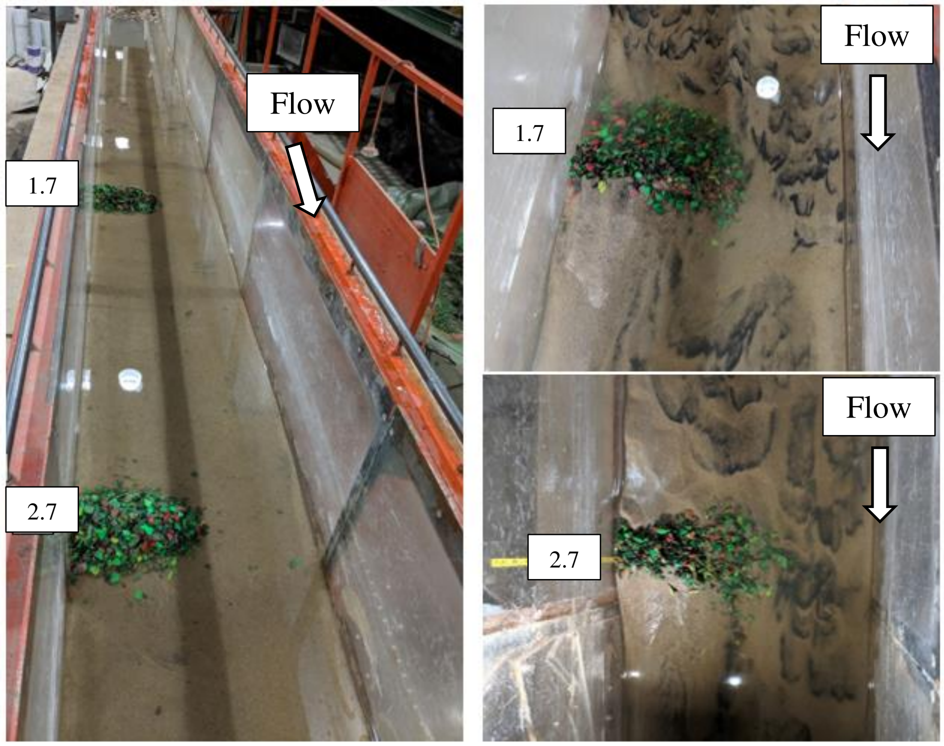

(a) (b)

Figure 58: 2BW with 3-in-wide crest, *y/H* = 1.25, and α = 90°, EXPT 7: (a) before; and (b) after

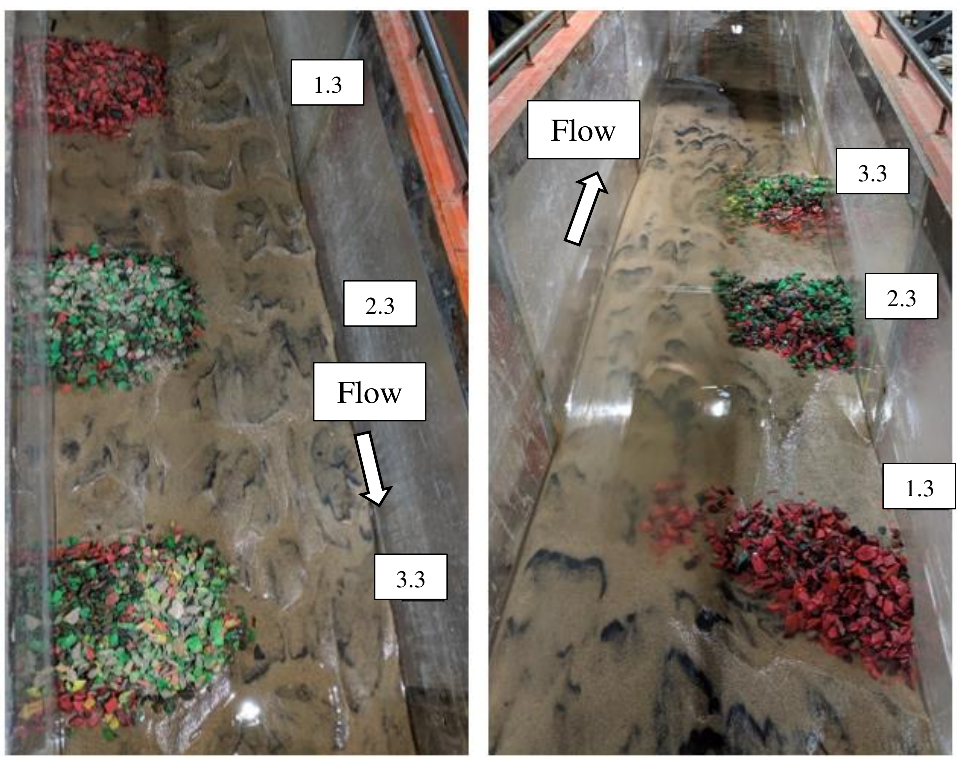

(a) (b)

Figure 59: 3BW with 8-in-wide crest, *y/H* = 2.0, and α = 90°, EXPT 3: (a) before; and (b) after

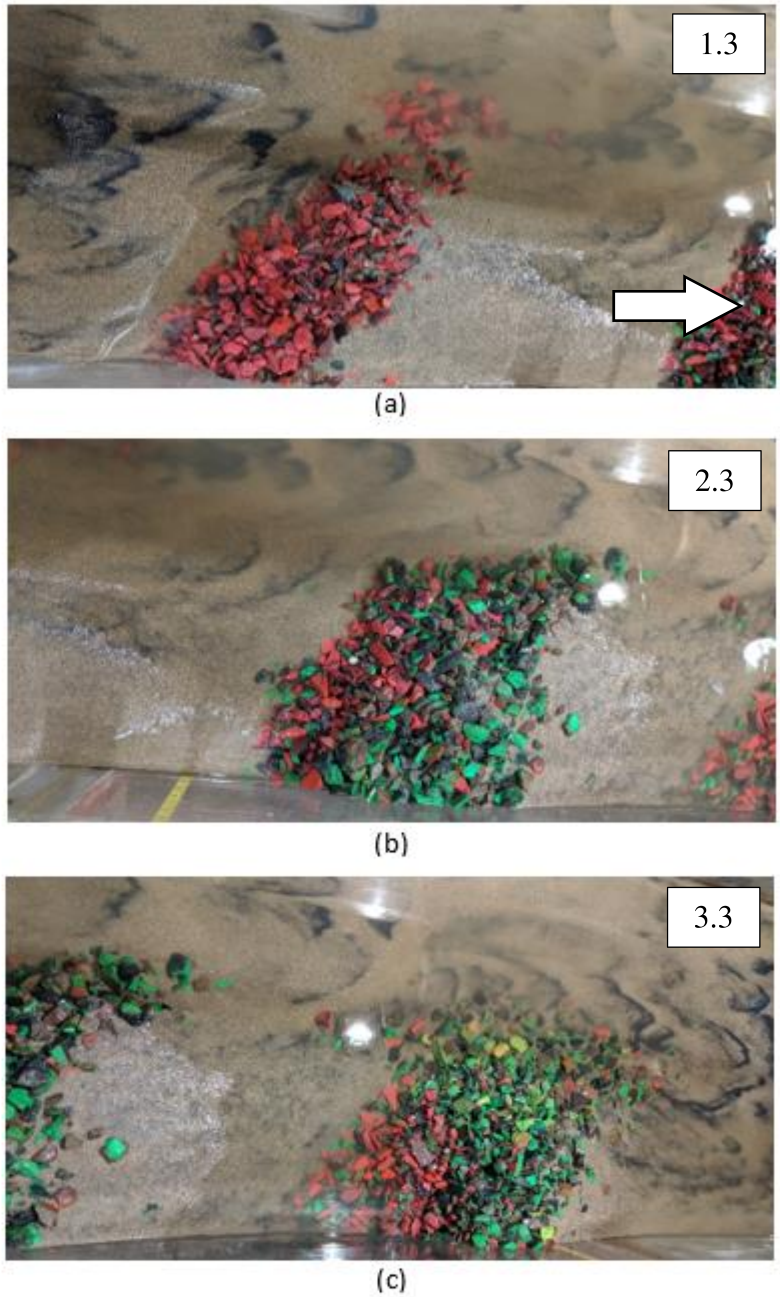

Figure 60: 3BW with 8-in-wide crest, *y/H* = 2.0, and α = 90°, EXPT 3 (a) upstream BW; (b) middle BW; and (c) downstream BW. The arrow indicates flow direction

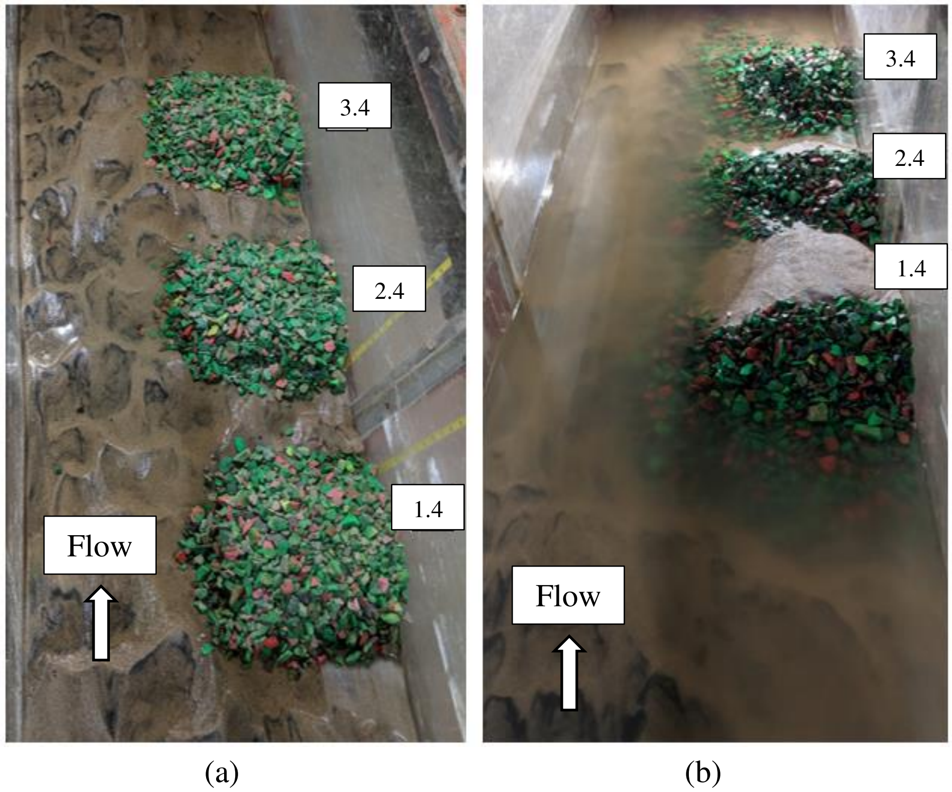

Figure 61: 3BW with 8-in-wide crest, *y/H* = 2.0, and α = 90°, EXPT 4: (a) before; and (b) after

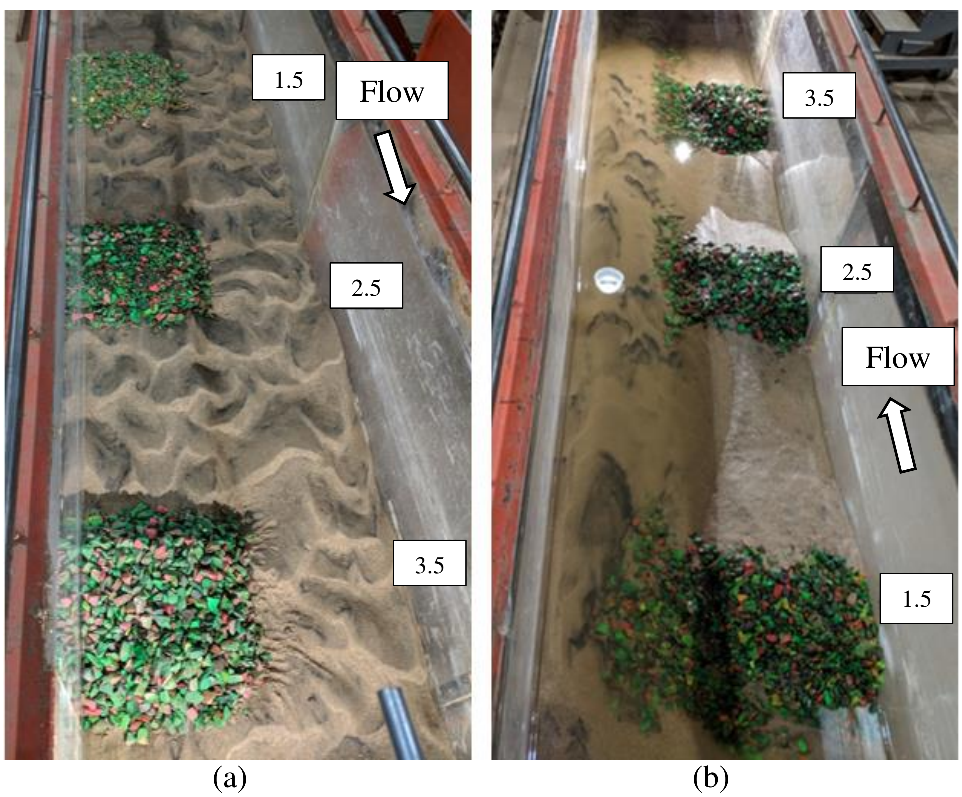

Figure 62: 3BW with 8-in-wide crest, *y/H* = 1.25, and α = 90°, EXPT 5: (a) before; and (b) after

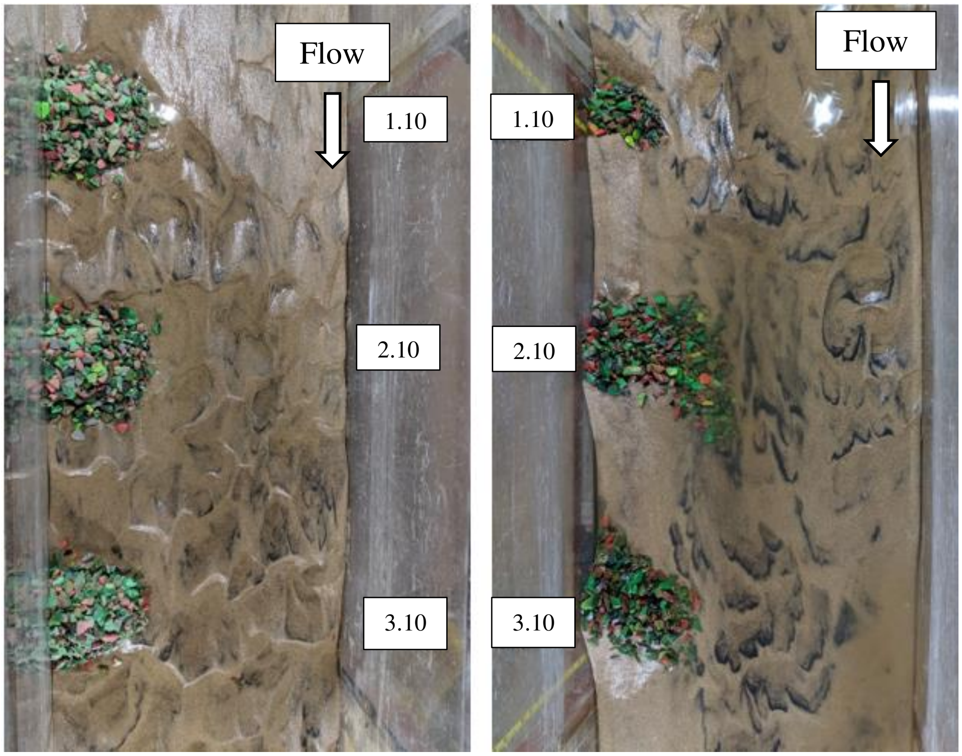

(a) (b)

Figure 63: 3BW$_{Short}$ with 3-in-wide crest, *y/H* = 2.0, and α = 90°, EXPT 10: (a) before; and (b) after

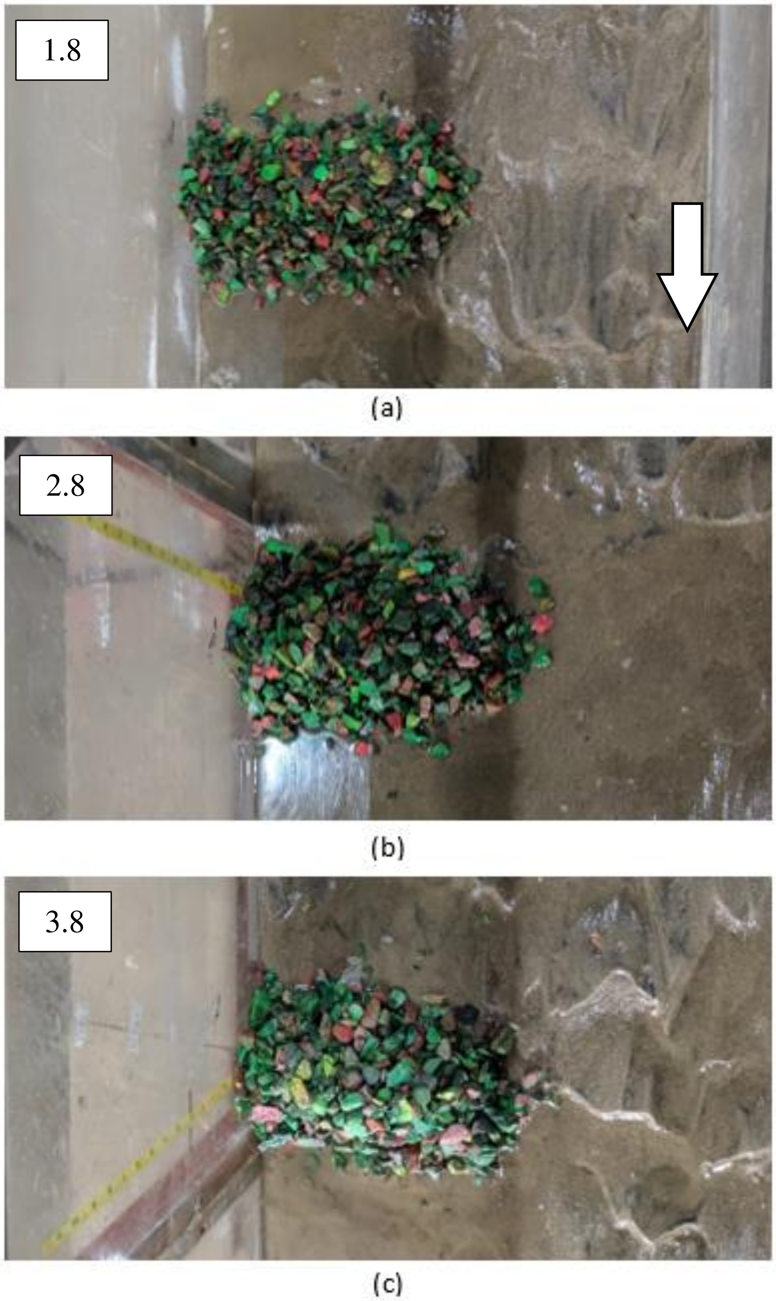

Figure 64: 3BW with 3-in-wide crest, *y/H* = 2.0, and α = 90°, Before EXPT 8 (a) upstream BW; (b) middle BW; and (c) downstream BW. The arrow indicates flow direction

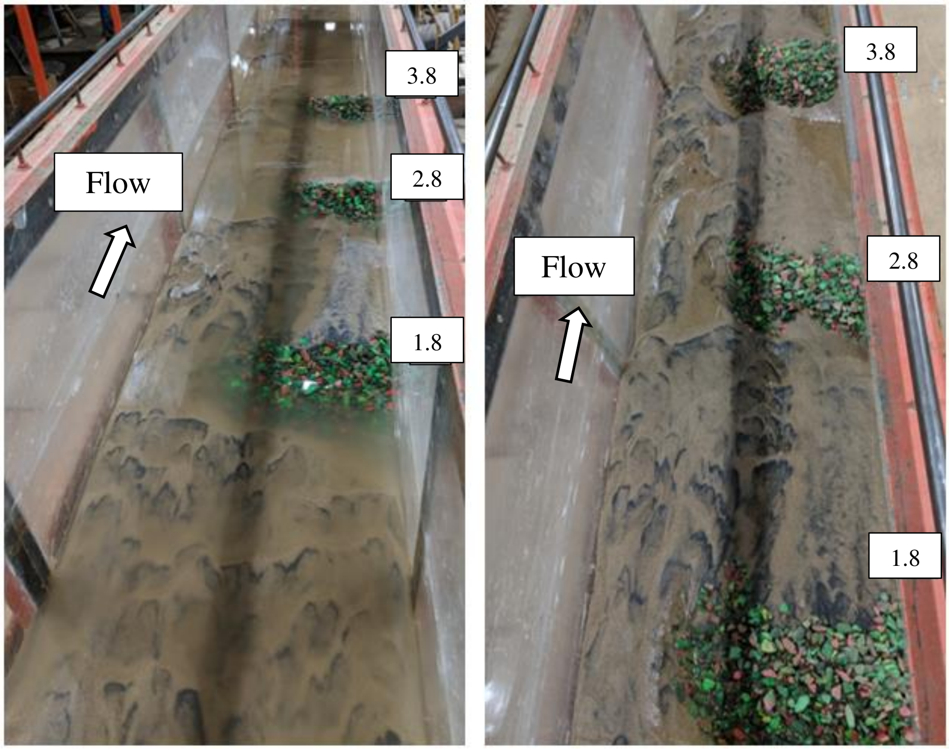

Figure 65: 3 BW with 3-in-wide crest, *y/H* = 2.0, and α = 90°, After EXPT 8

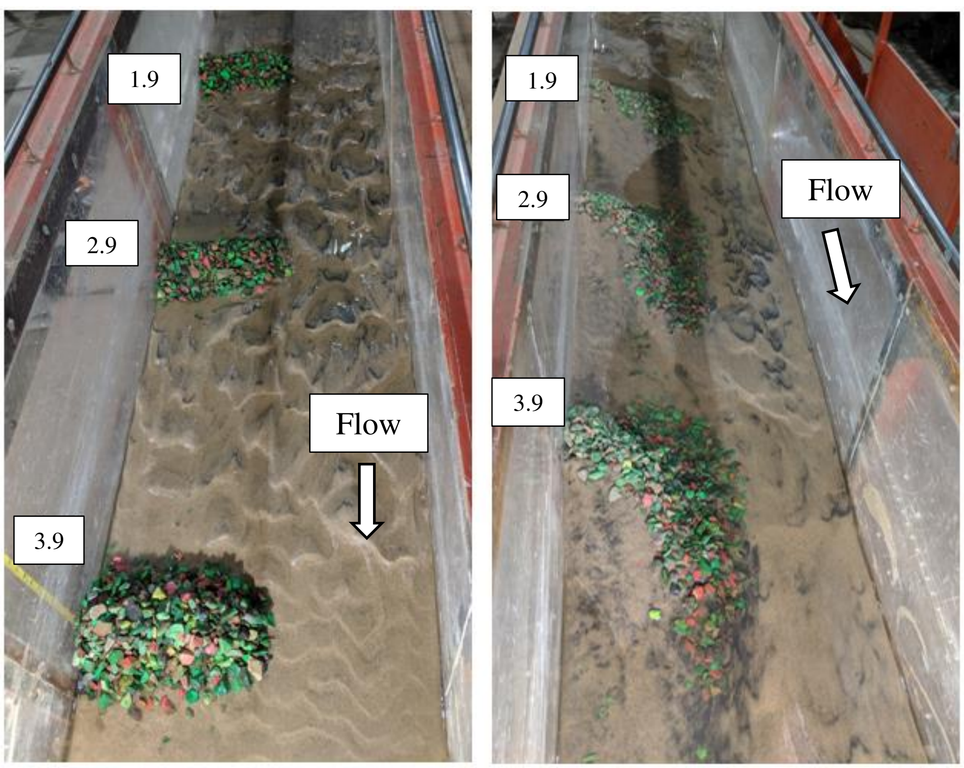

(a) (b)

Figure 66: 3BW with 3-in-wide crest, *y/H* = 1.25, and α = 90°, EXPT 9: (a) before; and (b) after

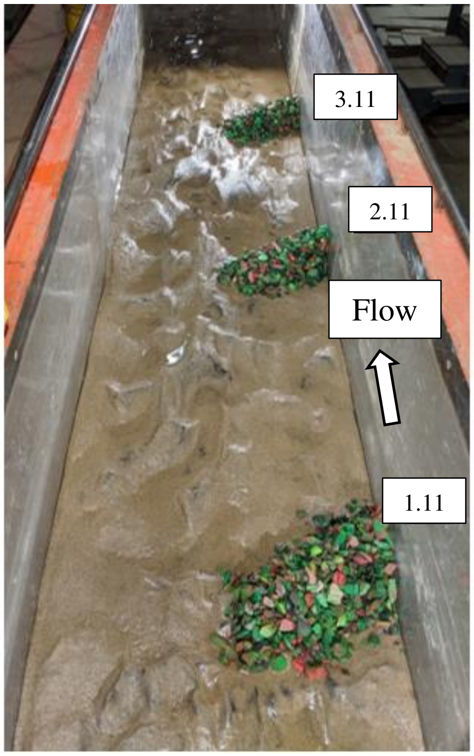

(a)

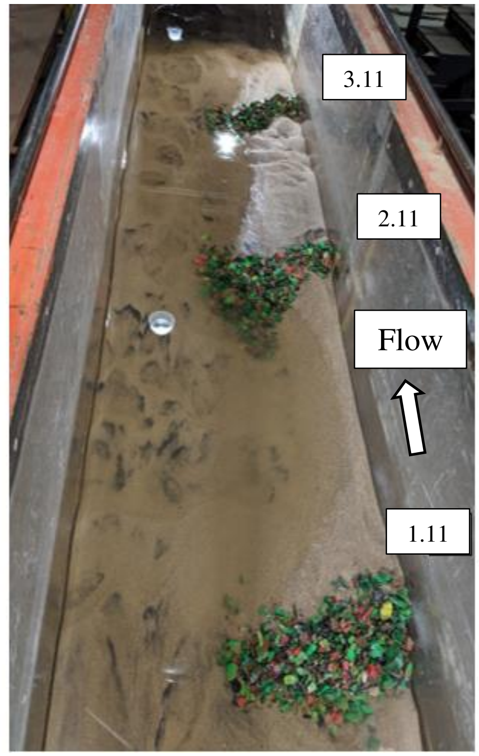

(b)

Figure 67: 3BW with 3-in-wide crest, *y/H* = 2.0, and α = 45°, EXPT 11: (a) before; and (b) after

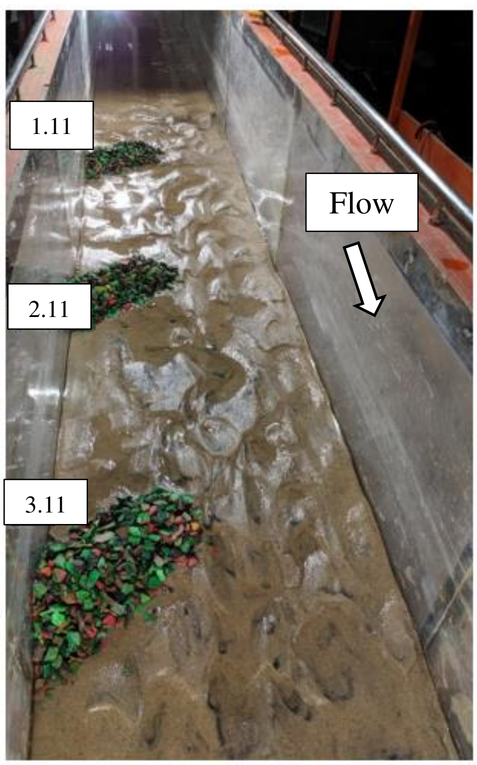

(a)

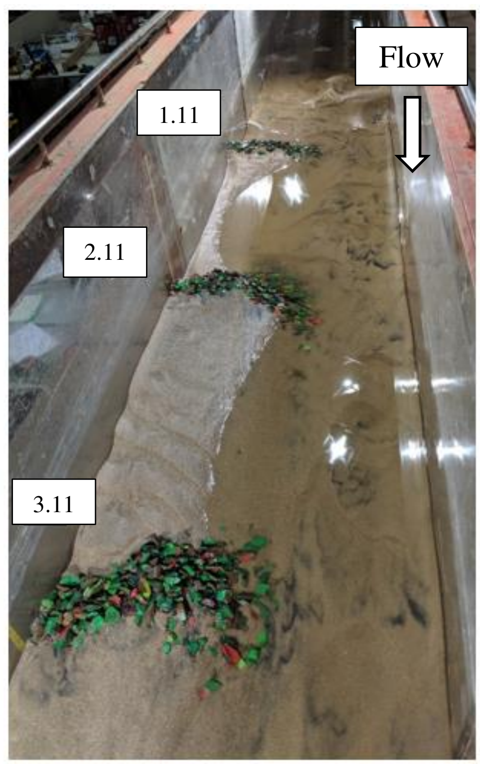

(b)

Figure 68: 3BW with 3-in-wide crest, *y/H* = 2.0, and α = 45°, EXPT 11: (a) before; and (b) after

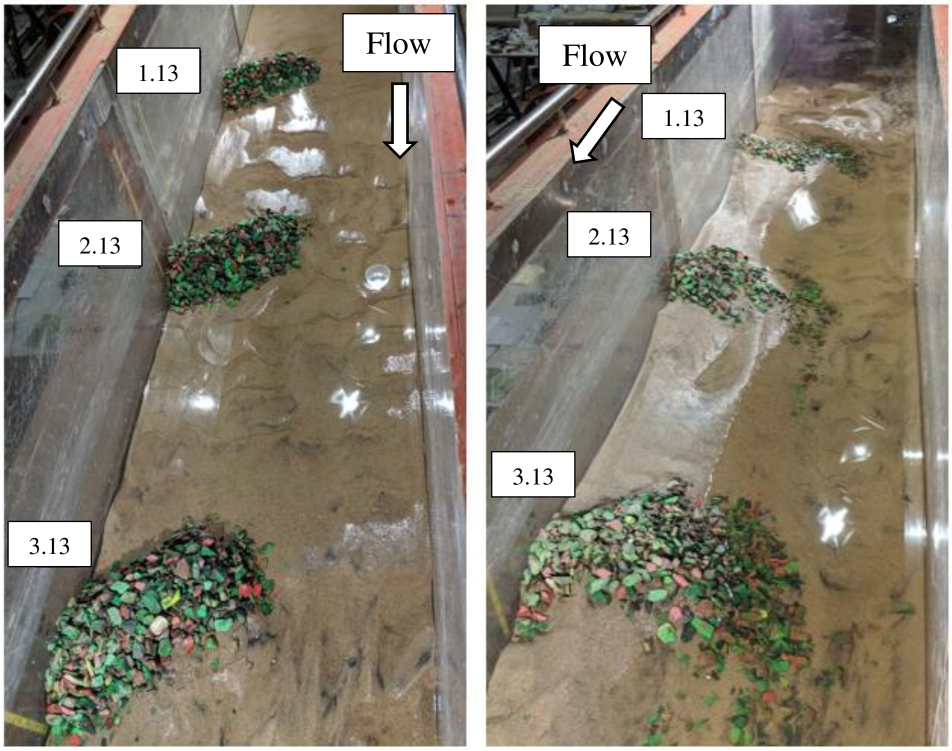

(a) (b)

Figure 69: 3BW with 3-in-wide crest, y/H = 1.25, and α = 45°, EXPT 13: (a) before; and (b) after

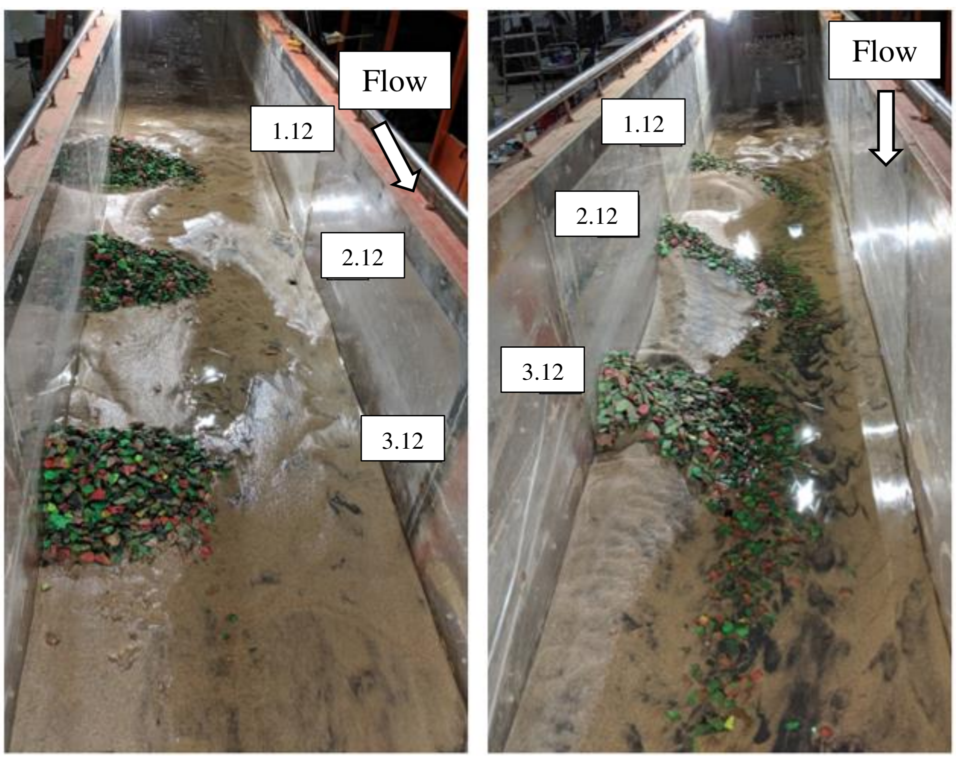

(a) (b)

Figure 70: 3RV with 3-in-wide crest, y/H = 1.0, and α = 90°, EXPT 12: (a) before; and (b) after

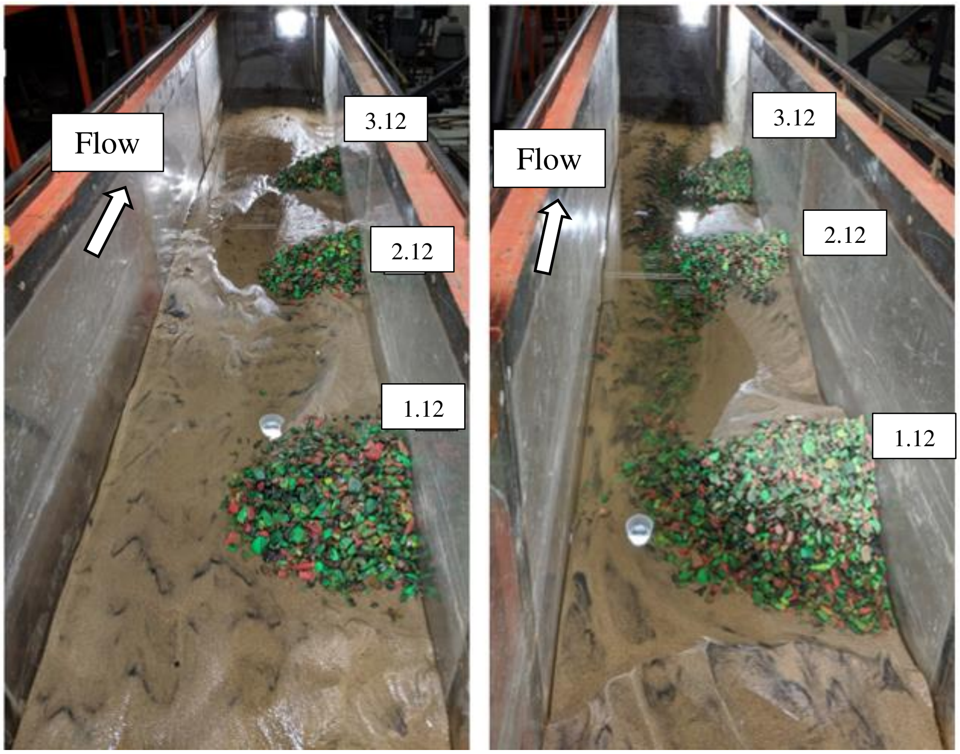

(a) (b)

Figure 71: 3RV with 3-in-wide crest, *y/H* = 1.0, and α = 90°, EXPT 12: (a) before; and (b) after

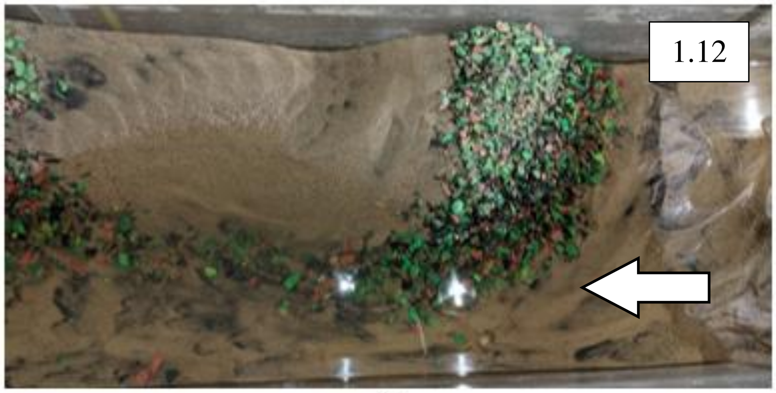

(a)

(b)

(c)

Figure 72: RVs 1 - 3, EXPT 12 (a) upstream RV; (b) middle RV; and (c) downstream RV. The arrow indicates flow direction

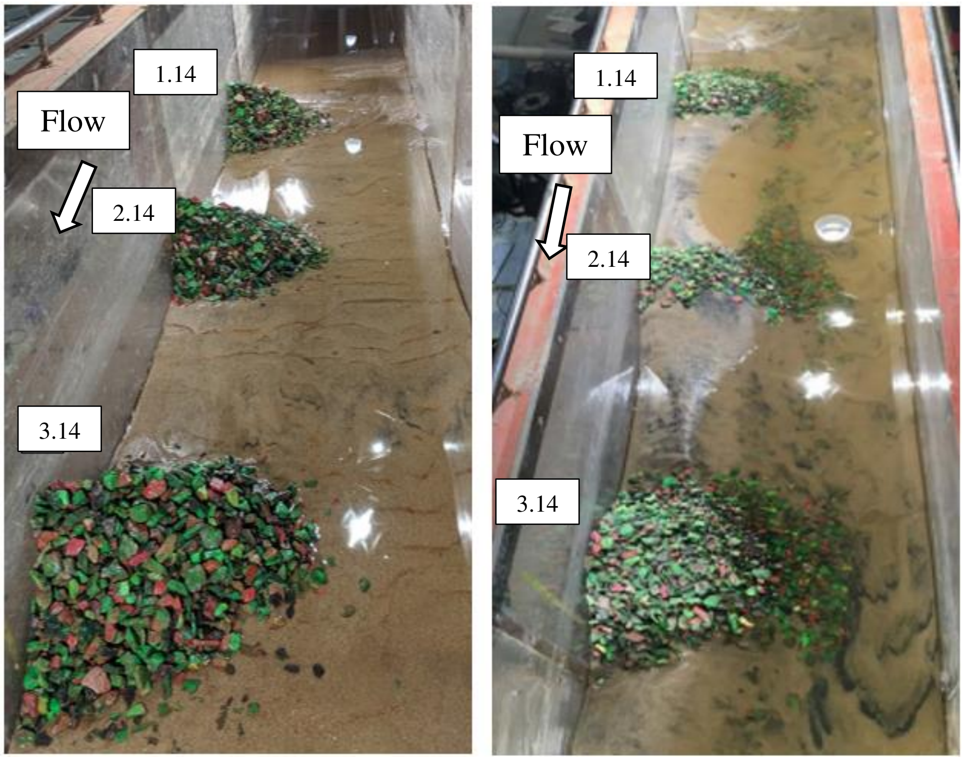

(a) (b)

Figure 73: 3RV with 3-in-wide crest, *y/H* = 1.0, and α = 45°, EXPT 14: (a) before; and (b) after

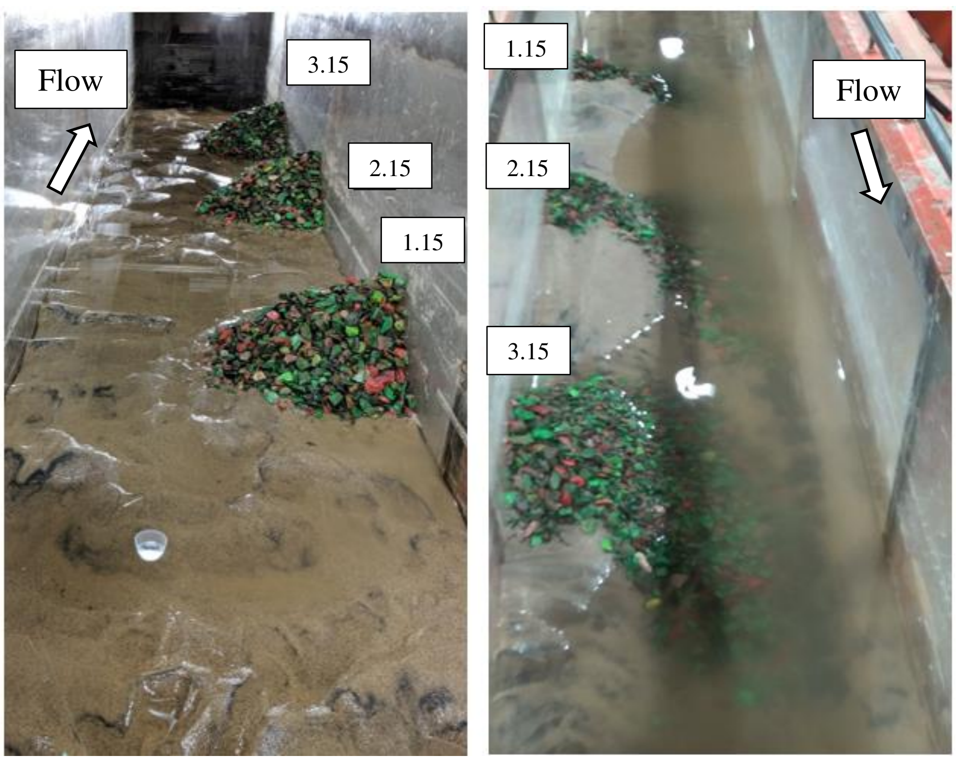

(a) (b)

Figure 74: 3RV with 3-in-wide crest, *y/H* = 0.625, and α = 90°, EXPT 15: (a) before; and (b) after

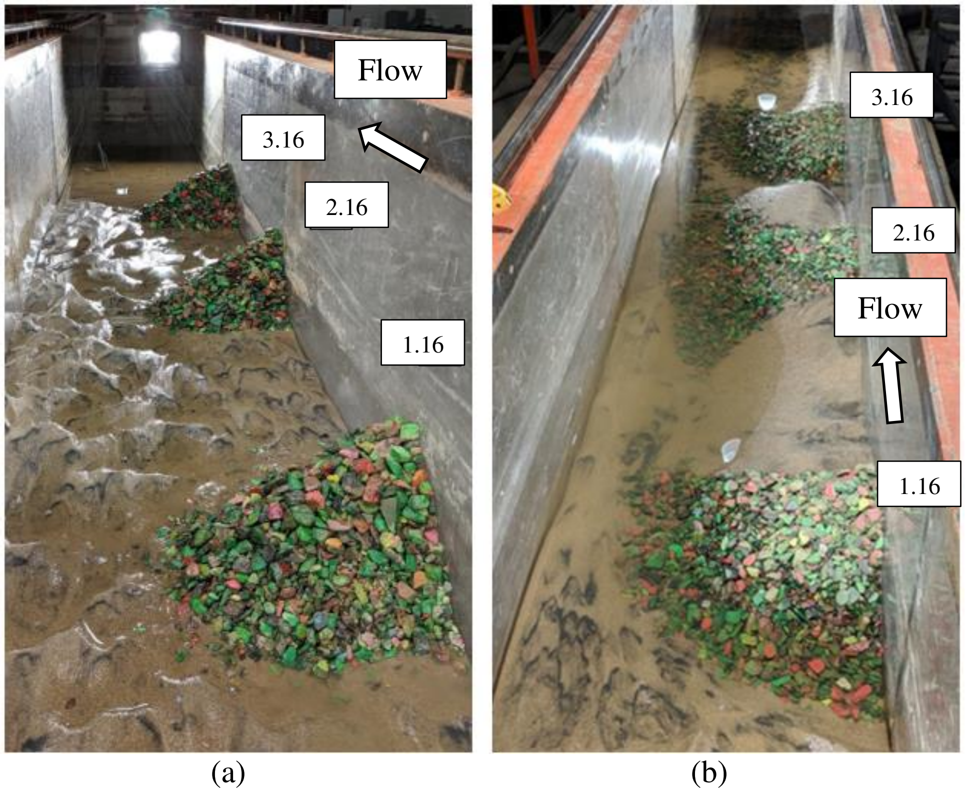

Figure 75: 3RV with 3-in-wide crest, *y/H* = 0.625, and α = 45°, EXPT 16: (a) before; and (b) after

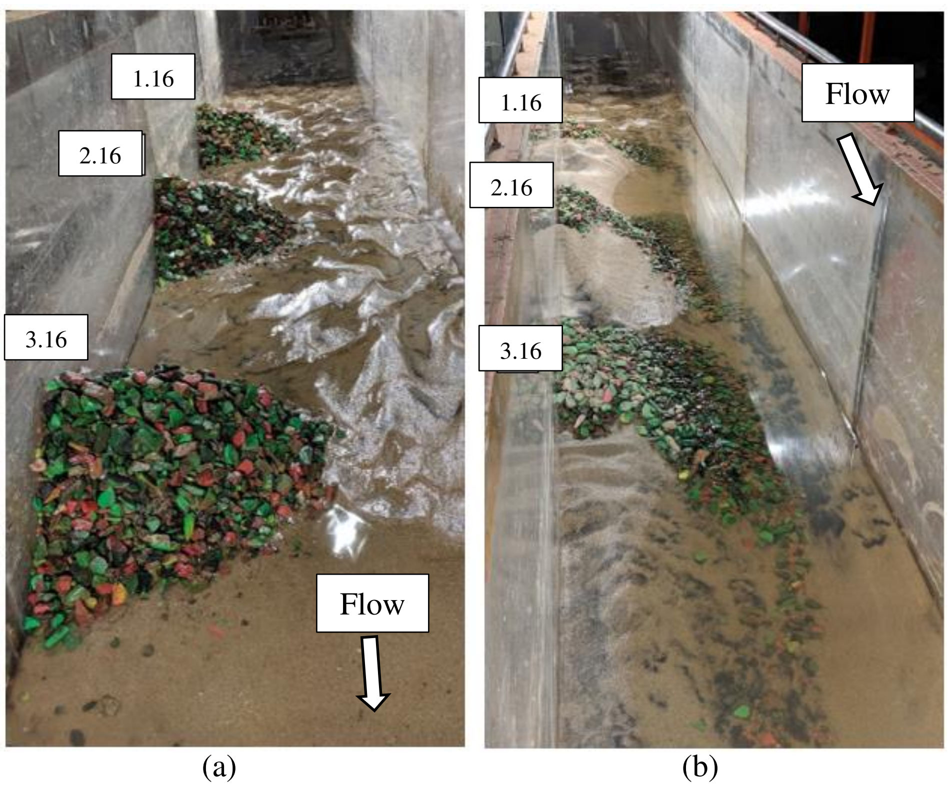

Figure 76: 3RV with 3-in-wide crest, *y/H* = 0.625, and α = 45°, EXPT 16: (a) before; and (b) after

Table 8: Curved Flume Experiments

EXPT #	**Structure**	**Q** (cfs)	**y** (in)	**Shear stress ratio τ_0/τ_c**	***y/H***	**α** (Degrees)	**W** (in)	**L** (in)	**H** (in)	**S_0**
1a	3BW	3.0	6	9.9	2.0	90	3	8	3	0.0012
2a	4BW	3.0	6	9.9	2.0	90	3	16	3	0.0012
3a	4BW	3.0	6	9.9	2.0	90	3	16	3	0.0012
4a	4BW	2.3	3.75	8.3	1.25	90	3	16	3	0.0012
5a	4BW	2.3	3.75	8.3	1.25	90	3	16	3	0.0012

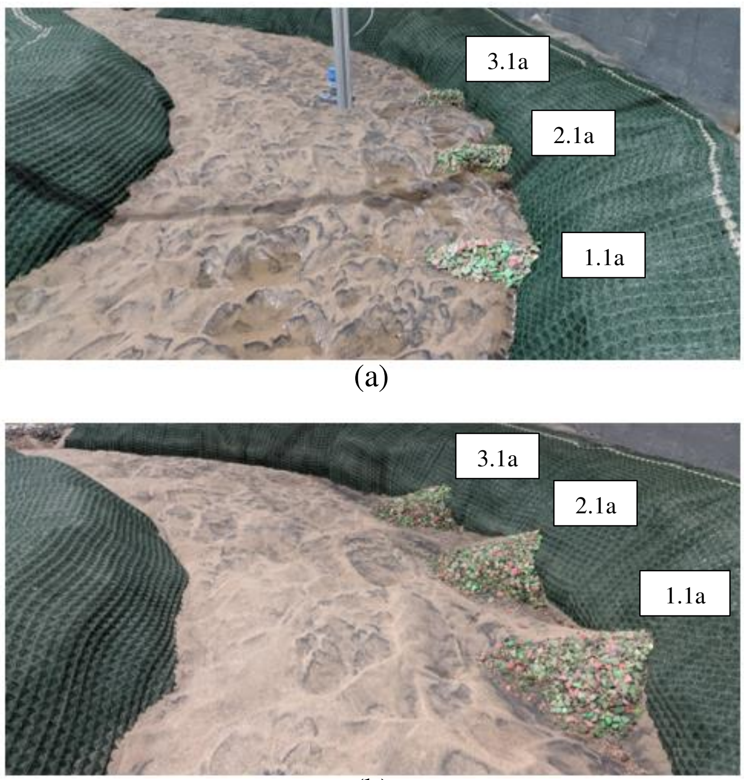

Figure 77: 3BW with 3-in-wide crest, *y/H* = 2.0 and α = 90°, EXPT 1a: (a) before; and (b) after

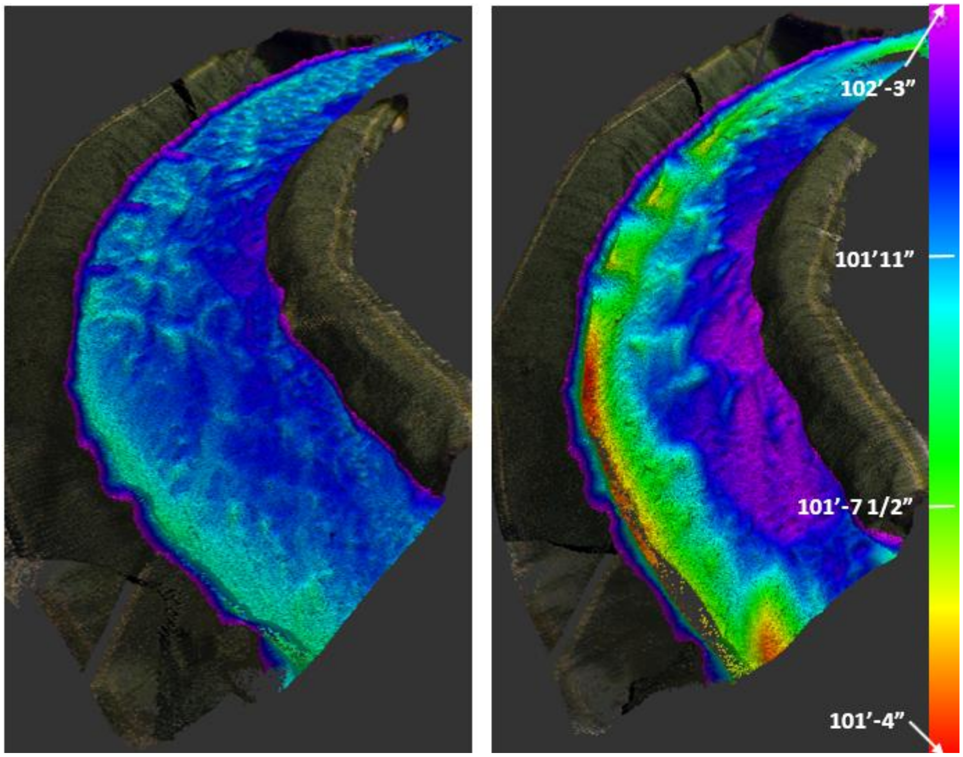

(a) (b)

Figure 78: LiDAR scan of 3BW of EXPT 1a: (a) before; and (b) after

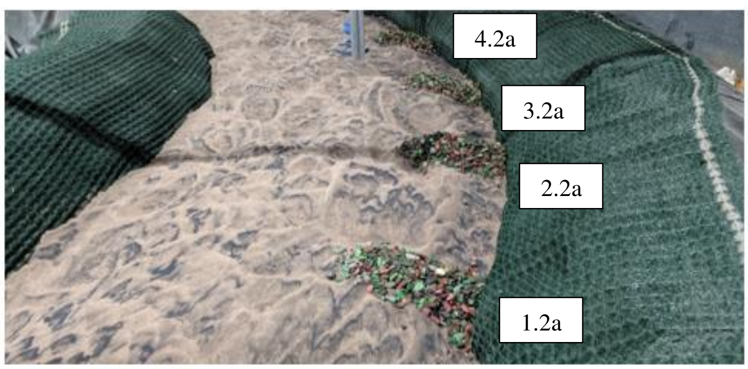

(a)

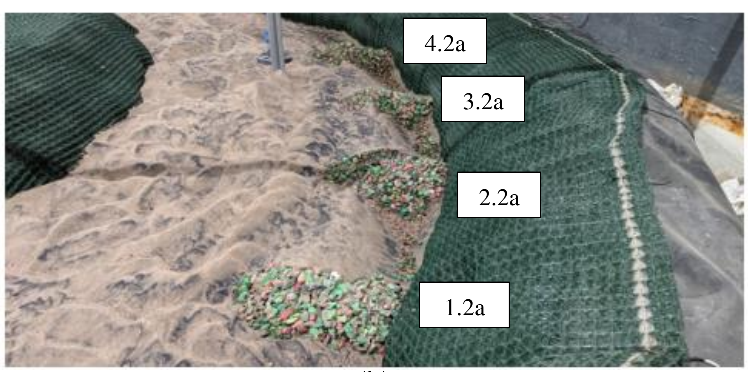

(b)

Figure 79: 4BW with 3-in-wide crest, *y/H* = 2.0, and α = 90°, EXPT 2a: (a) before; and (b) after

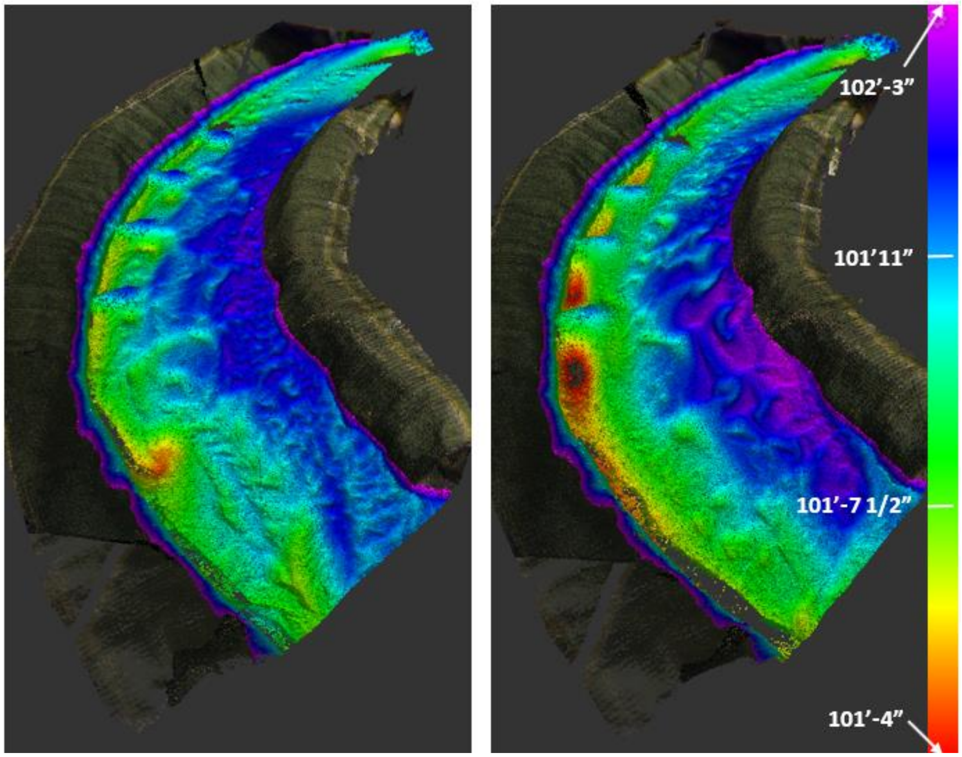

(a) (b)

Figure 80: LiDAR scan of EXPT 2a: (a) before; and (b) after

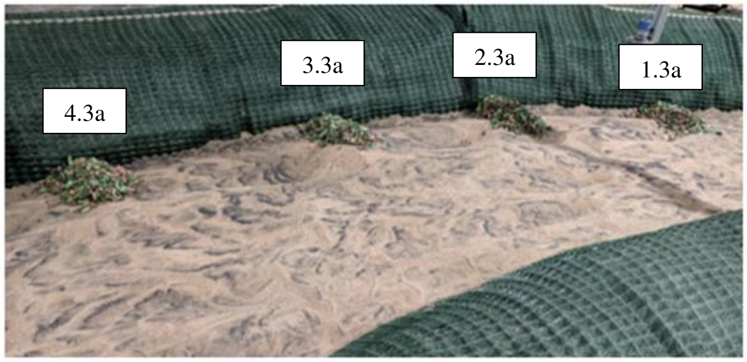

(a)

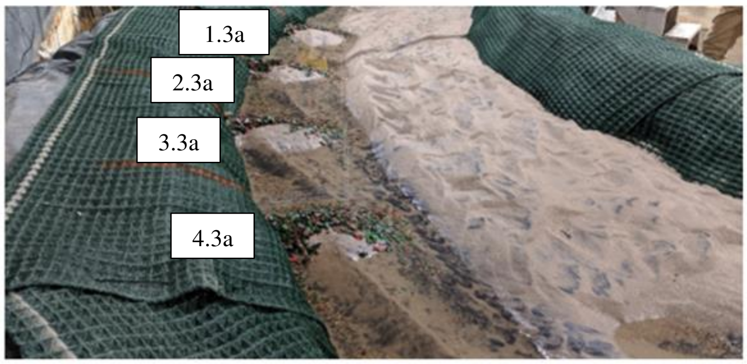

(b)

Figure 81: 4BW with 3-in-wide crest, *y/H* = 2.0 and α = 90°, EXPT 3a: (a) before; and (b) after

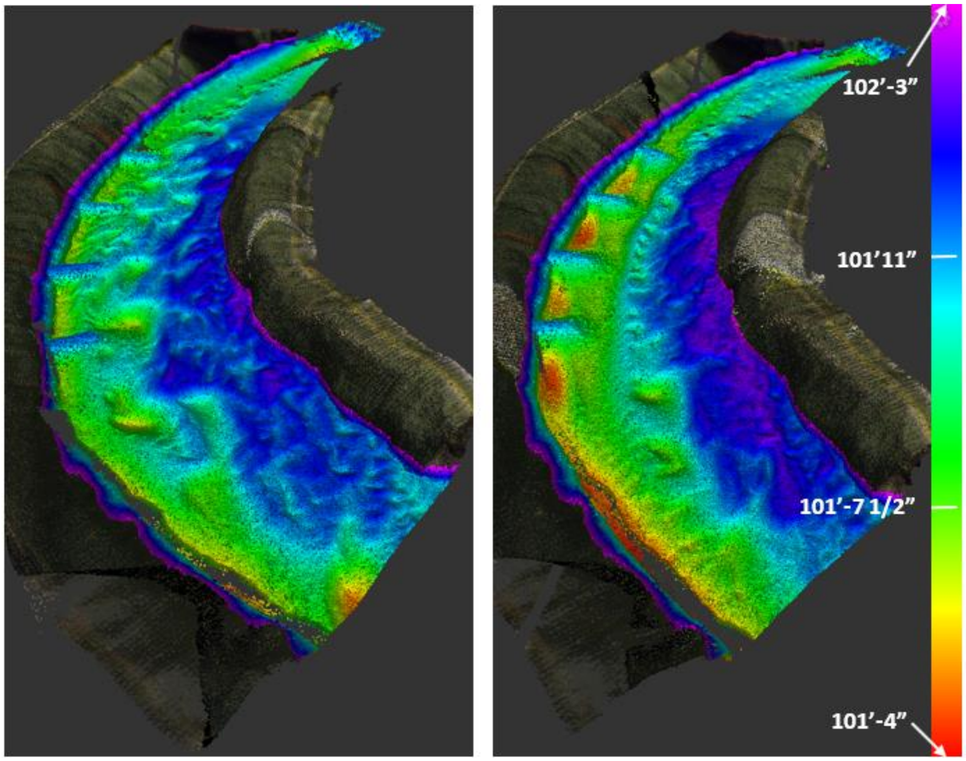

(a) (b)

Figure 82: LiDAR scan of EXPT 3a: (a) before; and (b) after

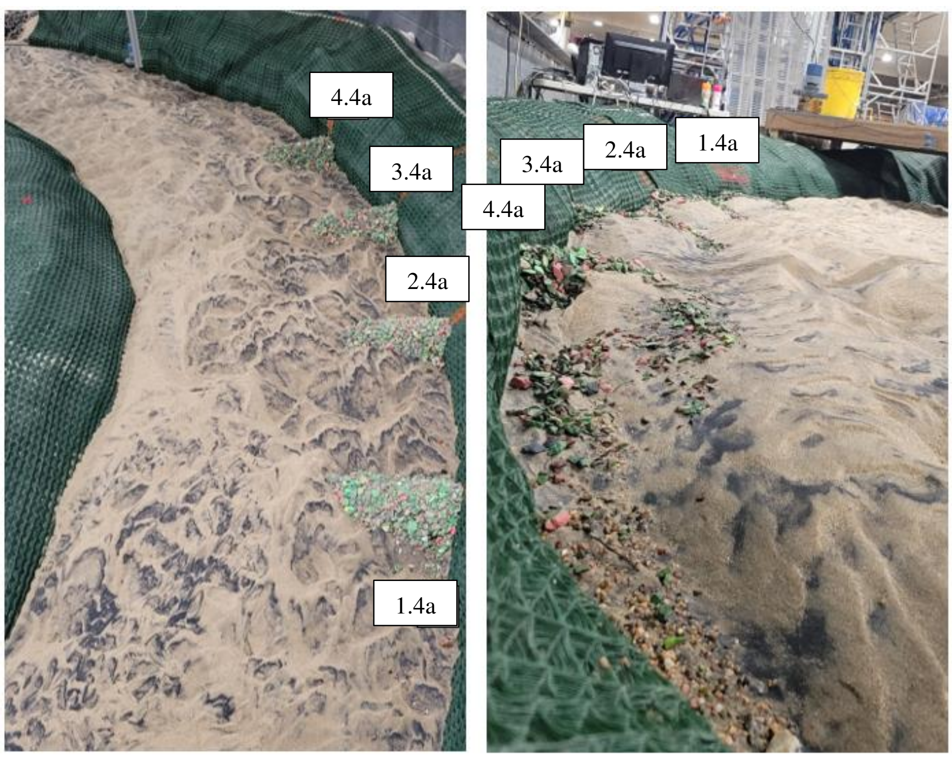

(a) (b)

Figure 83: 4BW with 3-in-wide crest, *y/H* = 1.25, and α = 90°, EXPT 4a: (a) before; and (b) after

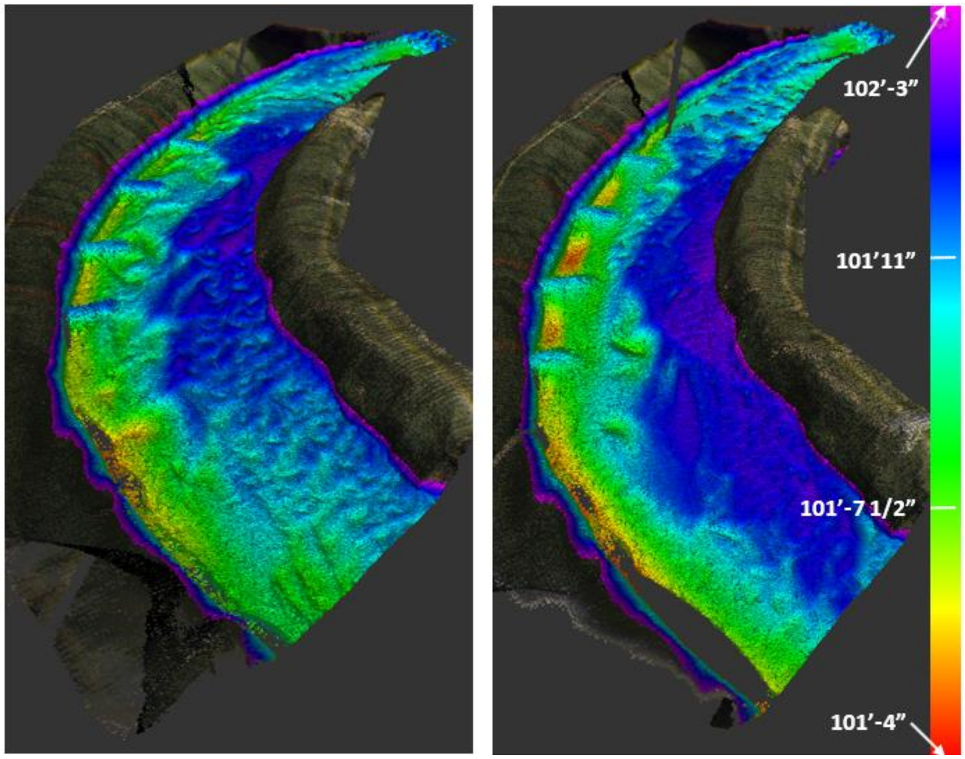

(a) (b)

Figure 84: LiDAR scan of EXPT 4a: (a) before; and (b) after

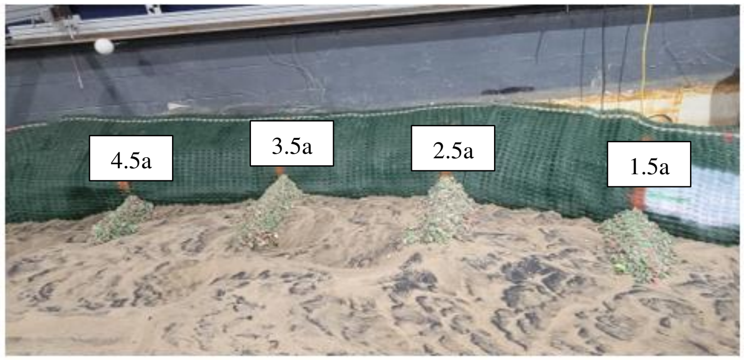

(a)

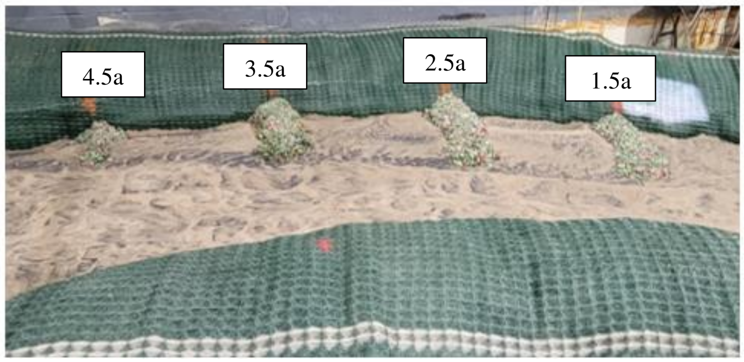

(b)

Figure 85: 4BW with 3-in-wide crest, *y/H* = 1.25, and α = 90°, EXPT 5a: (a) before; and (b) after

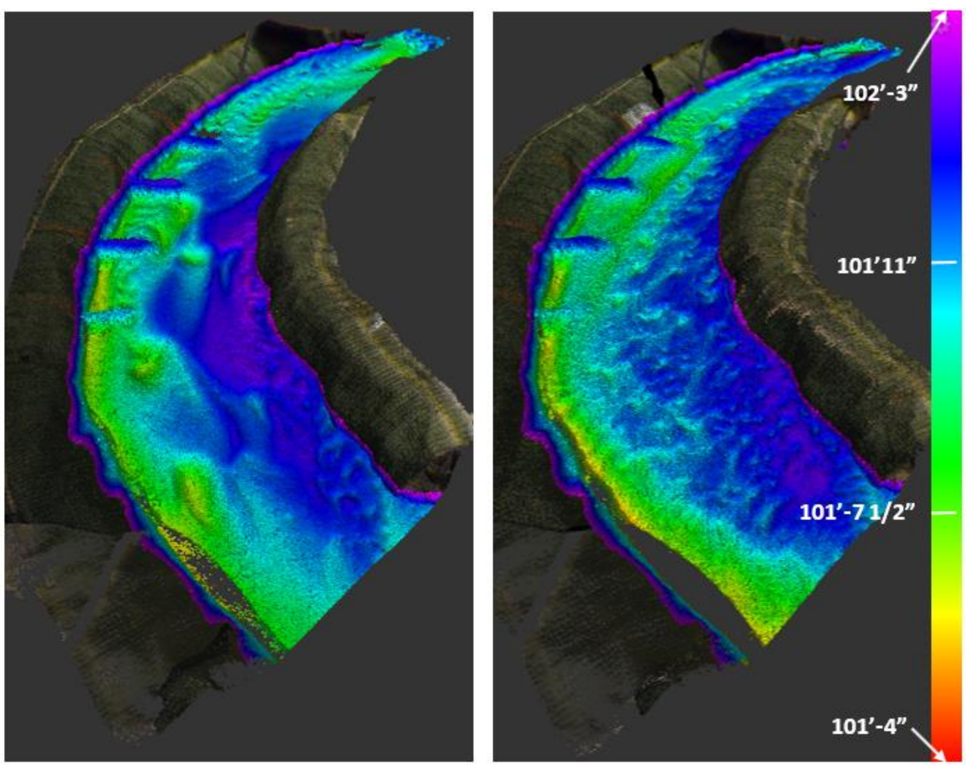

(a) (b)

Figure 86: LiDAR scan of EXPT 5a: (a) before; and (b) after

APPENDIX B. CURVED FLUME MASSA PROBE DATA

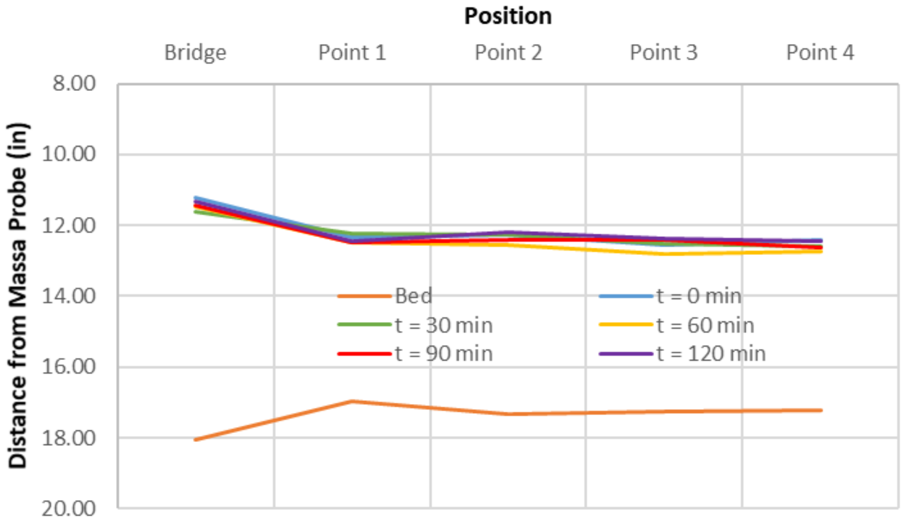

Figure 87: EXPT 01 Raw Massa Probe Data

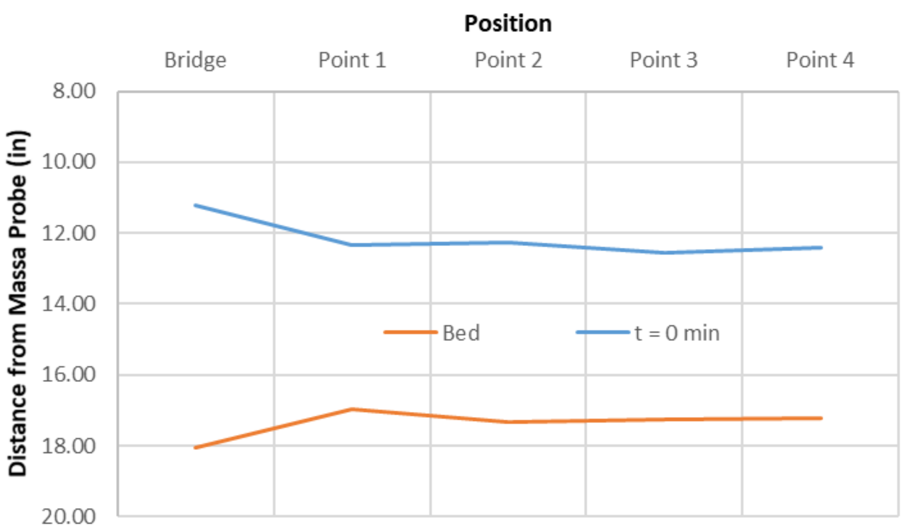

Figure 88: EXPT 01 Initial raw Massa probe data

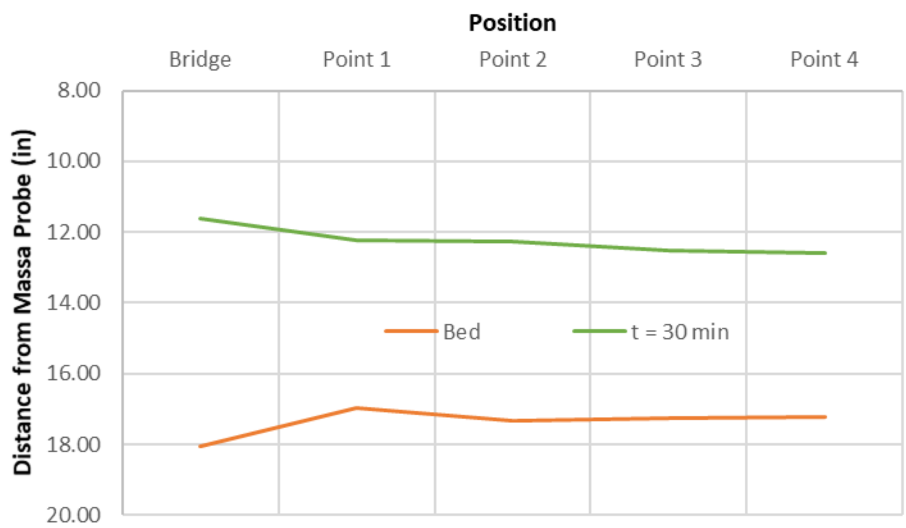

Figure 89: EXPT 01 Raw Massa probe data at 30 minutes

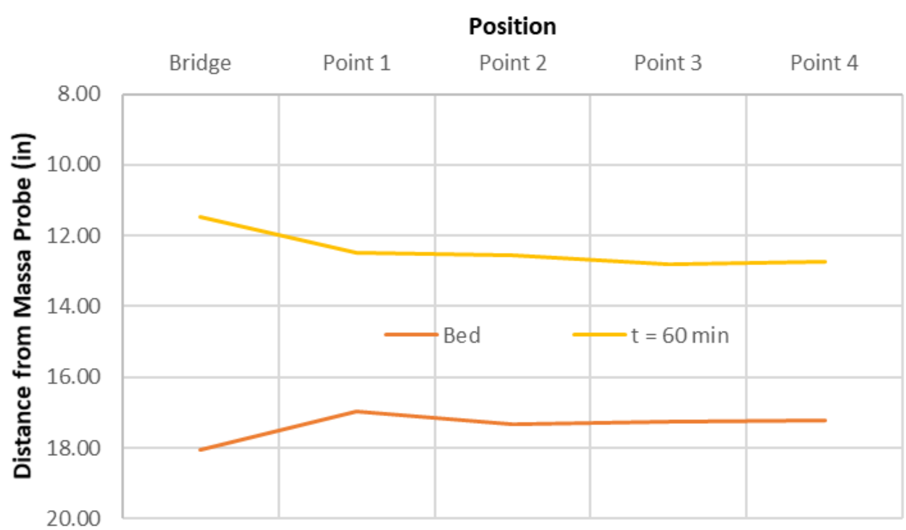

Figure 90: EXPT 01 Raw Massa probe data at 60 minutes

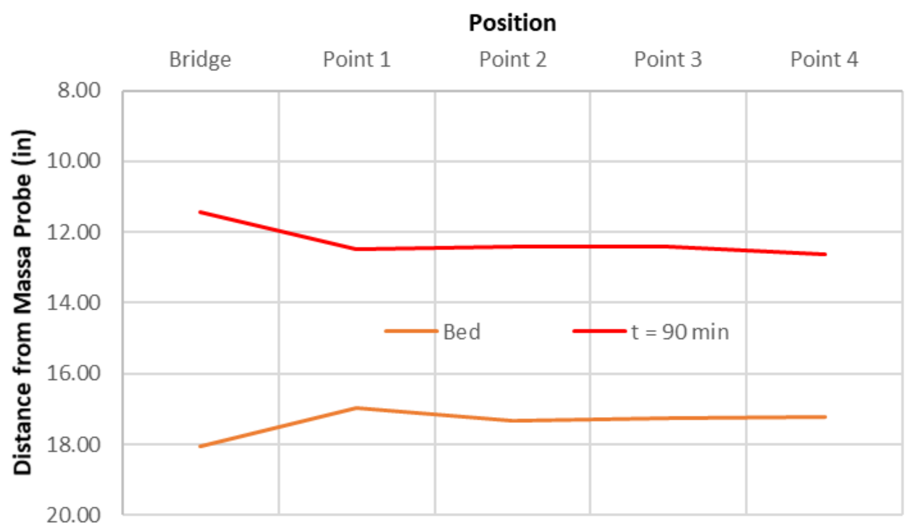

Figure 91: EXPT 01 Raw Massa probe data at 90 minutes

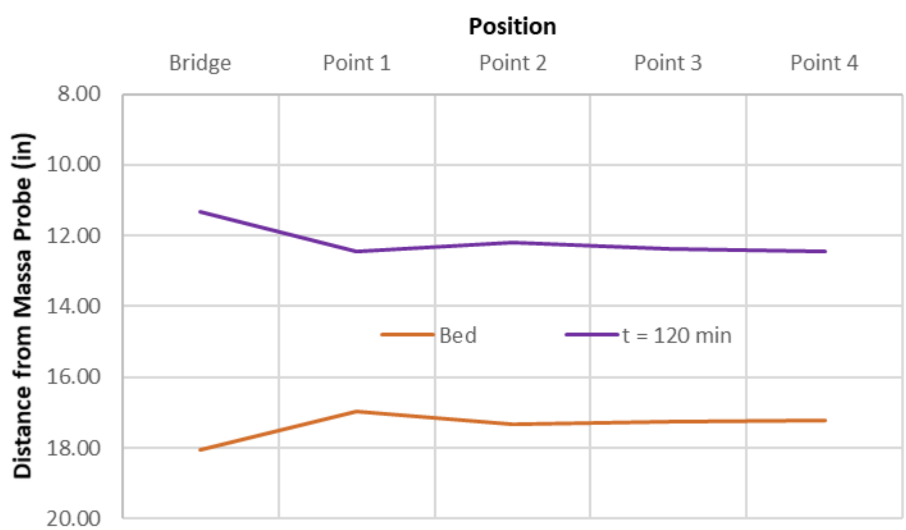

Figure 92: EXPT 01 Raw Massa probe data at 120 minutes

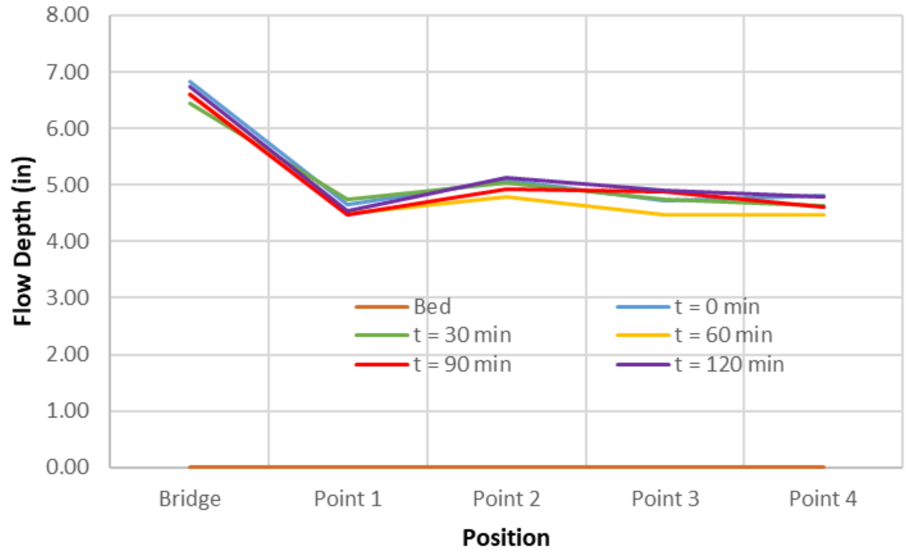

Figure 93: EXPT 01 Flow Depth

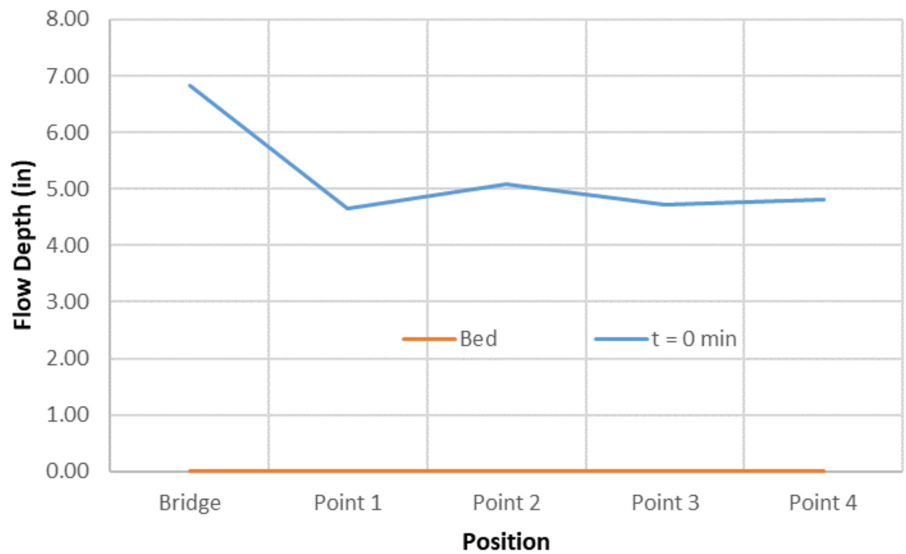

Figure 94: EXPT 01 Initial flow depth

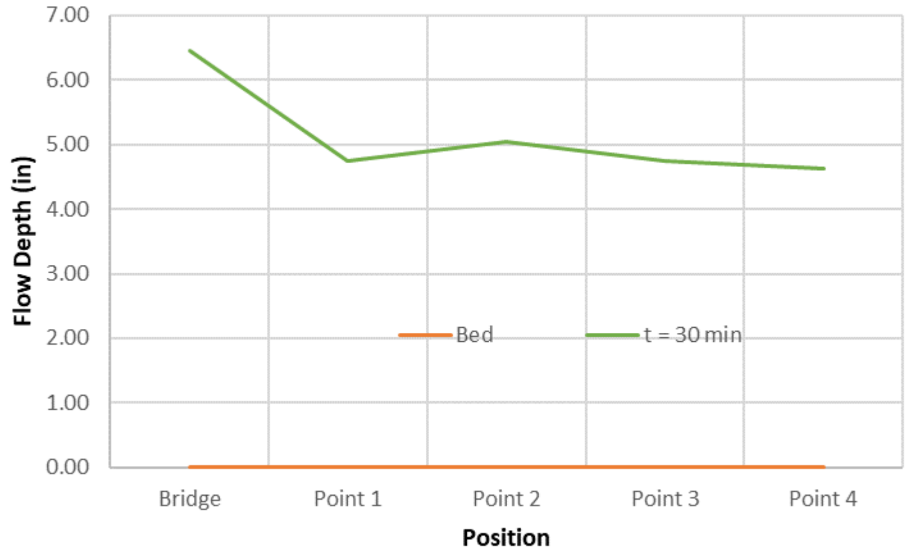

Figure 95: EXPT 01 Flow depth at 30 minutes

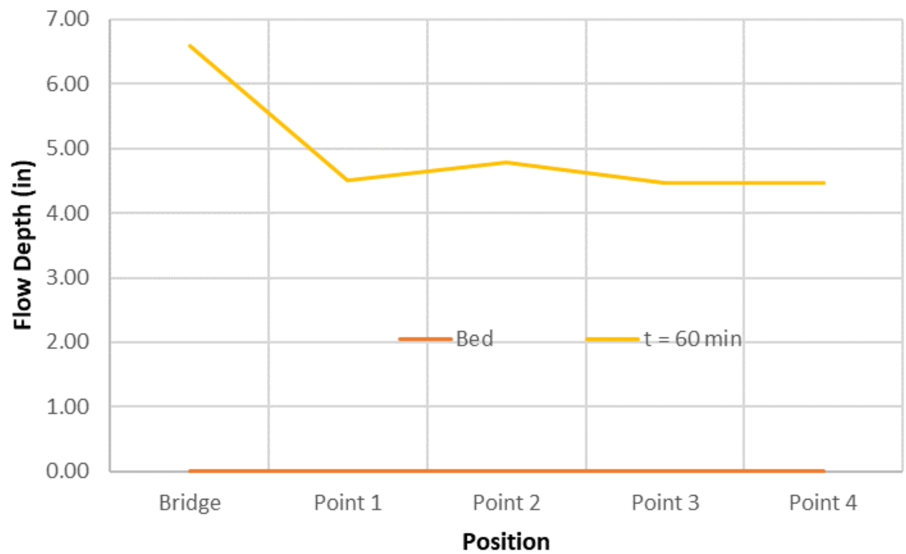

Figure 96: EXPT 01 Flow depth at 60 minutes

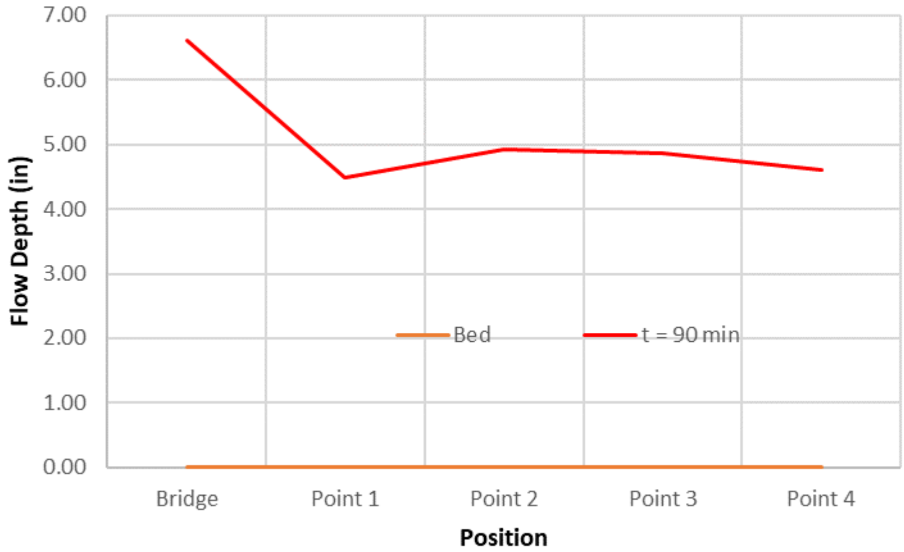

Figure 97: EXPT 01 Flow depth at 90 minutes

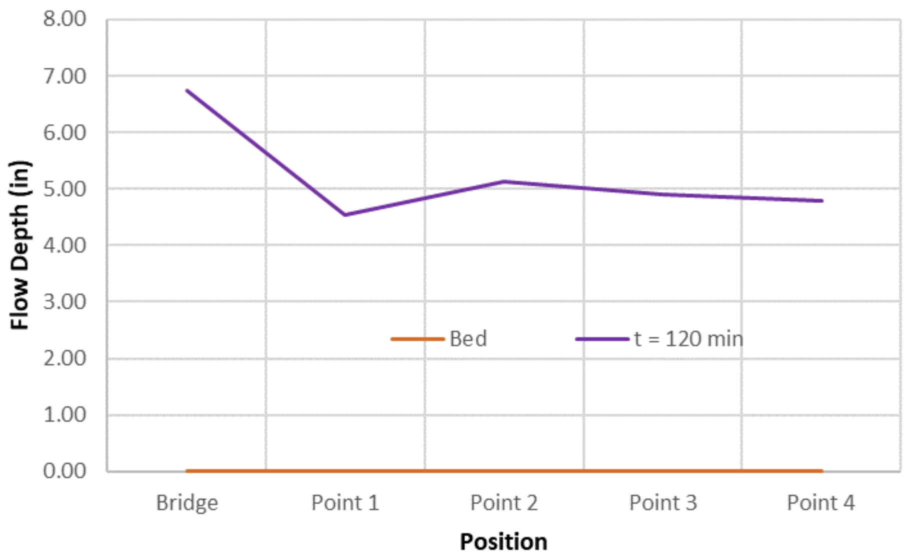

Figure 98: EXPT 01 Flow depth at 120 minutes

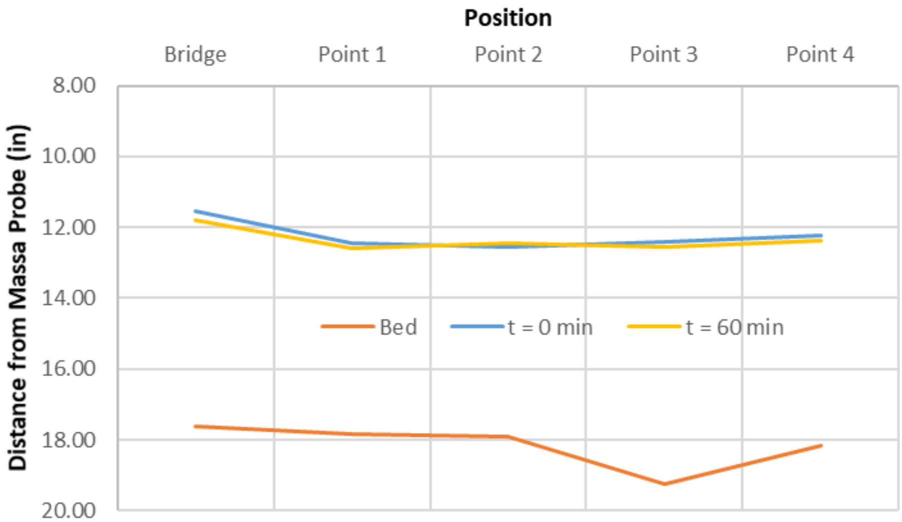

Figure 99: Before EXPT 02 Raw Massa Probe Data

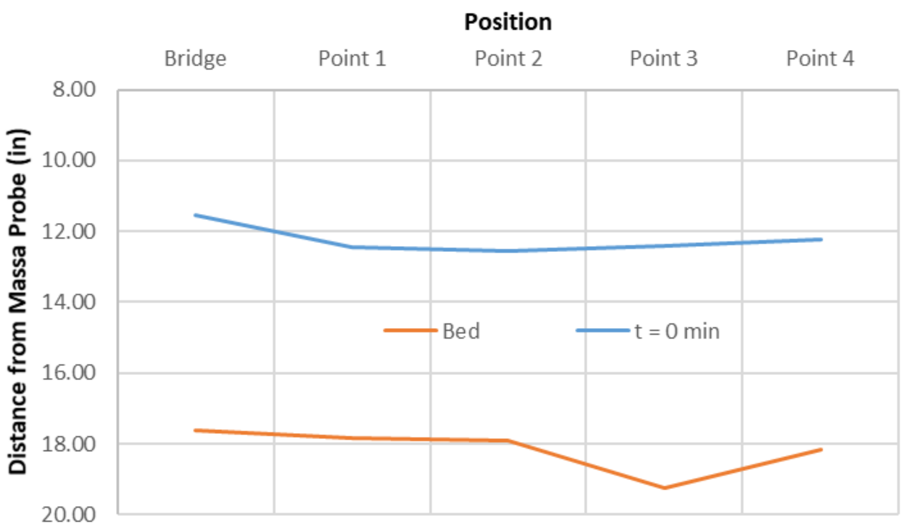

Figure 100: Before EXPT 02 Initial raw Massa probe data

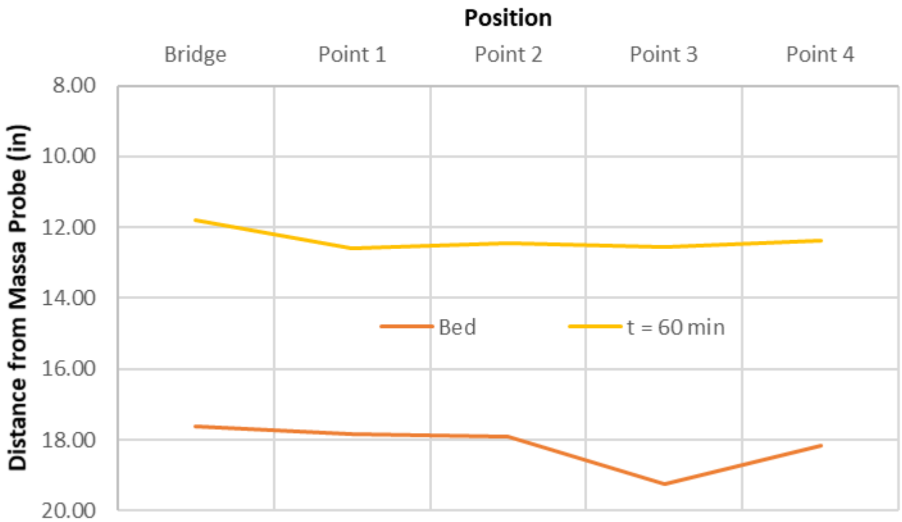

Figure 101: Before EXPT 02 Raw Massa probe data at 60 minutes

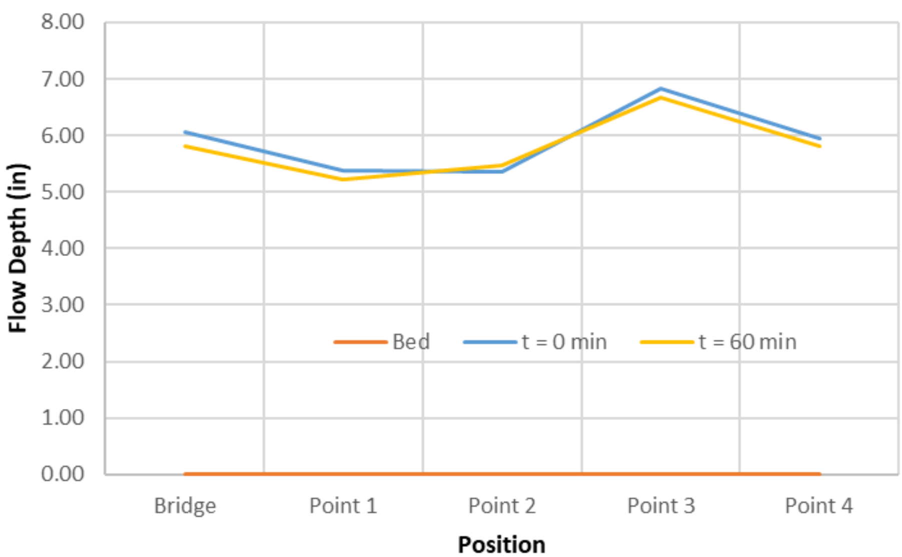

Figure 102: Before EXPT 02 Flow Depth

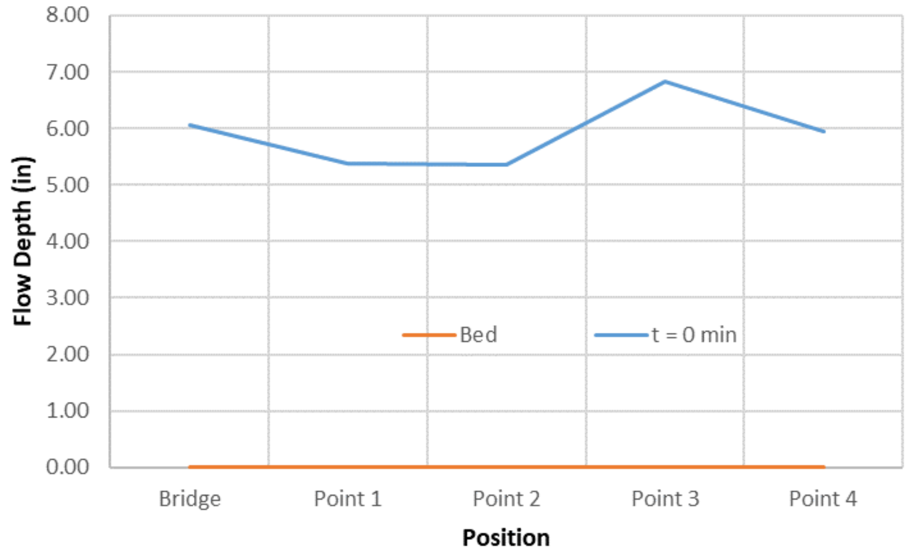

Figure 103: Before EXPT 02 Initial flow depth

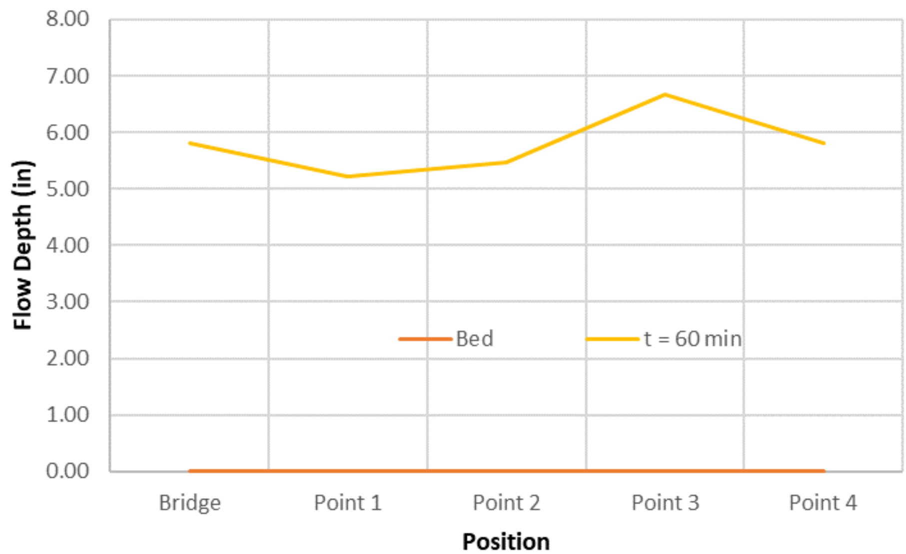

Figure 104: Before EXPT 02 Flow depth at 60 minutes

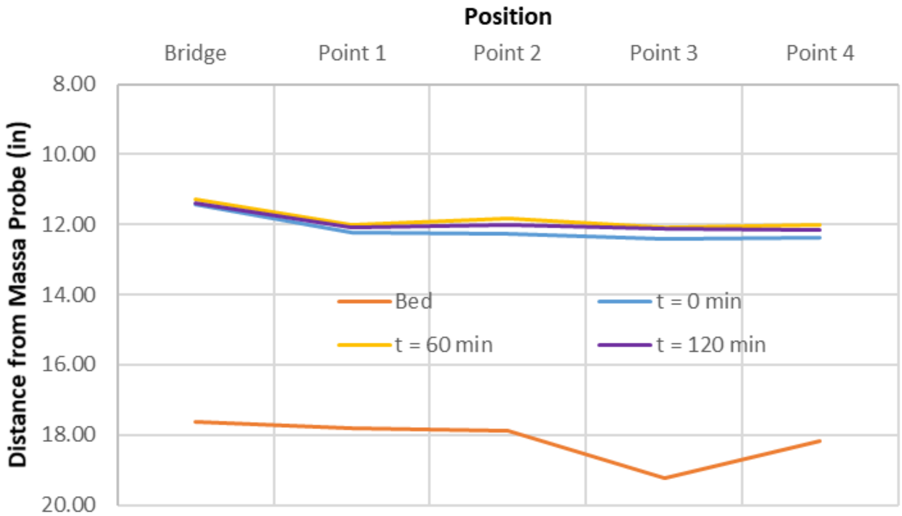

Figure 105: EXPT 02 Raw Massa Probe Data

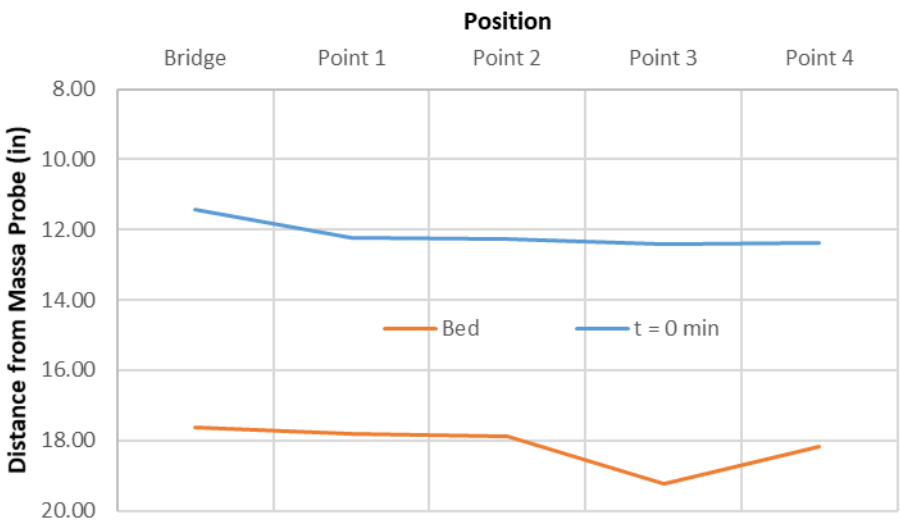

Figure 106: EXPT 02 Initial raw Massa probe data

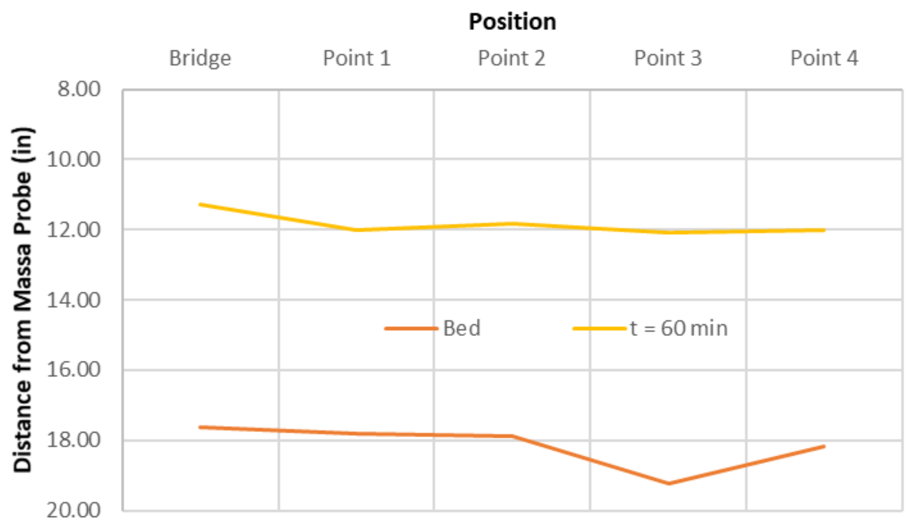

Figure 107: EXPT 02 Raw Massa probe data at 60 minutes

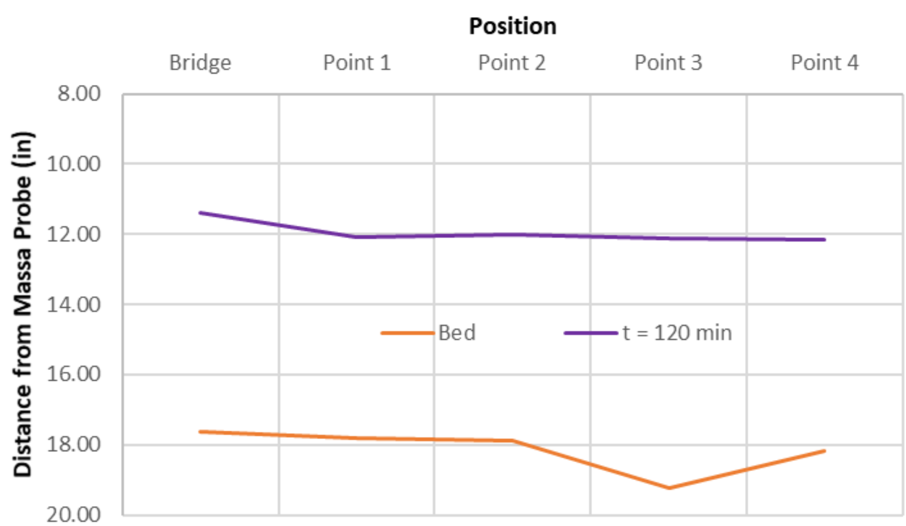

Figure 108: EXPT 02 Raw Massa probe data at 120 minutes

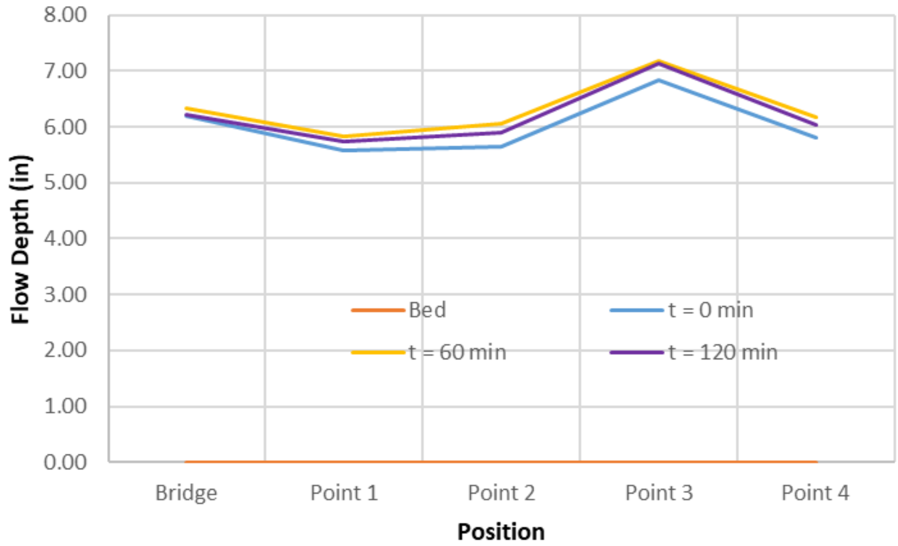

Figure 109: EXPT 02 Flow Depth

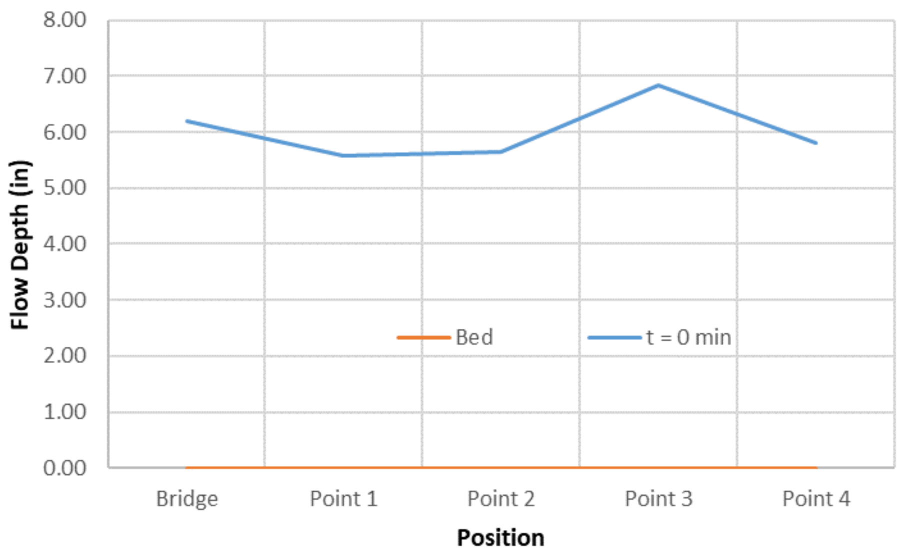

Figure 110: EXPT 02 Initial flow depth

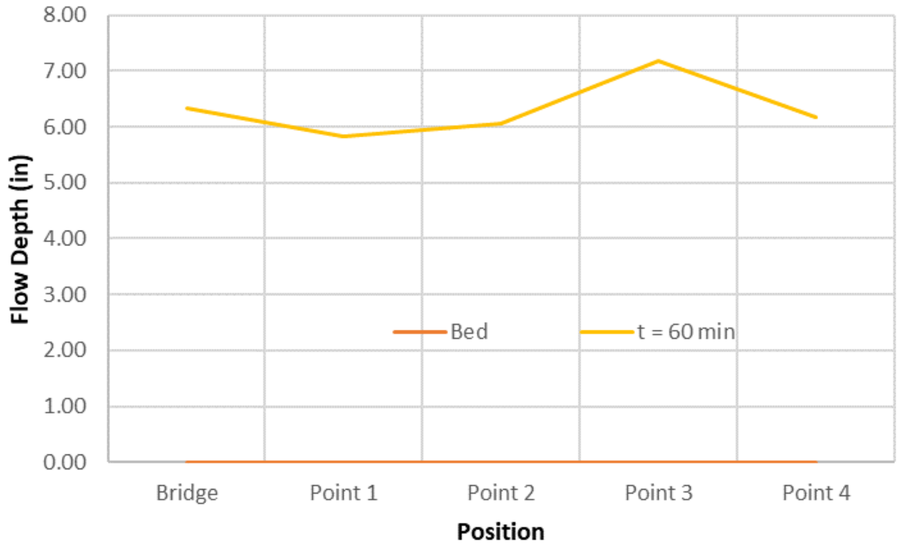

Figure 111: EXPT 02 Flow depth at 60 minutes

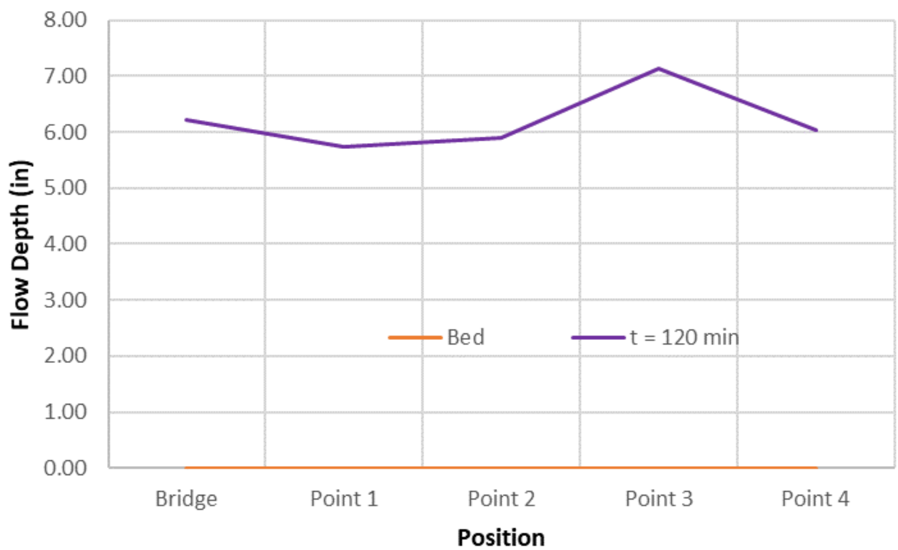

Figure 112: EXPT 02 Flow depth at 120 minutes

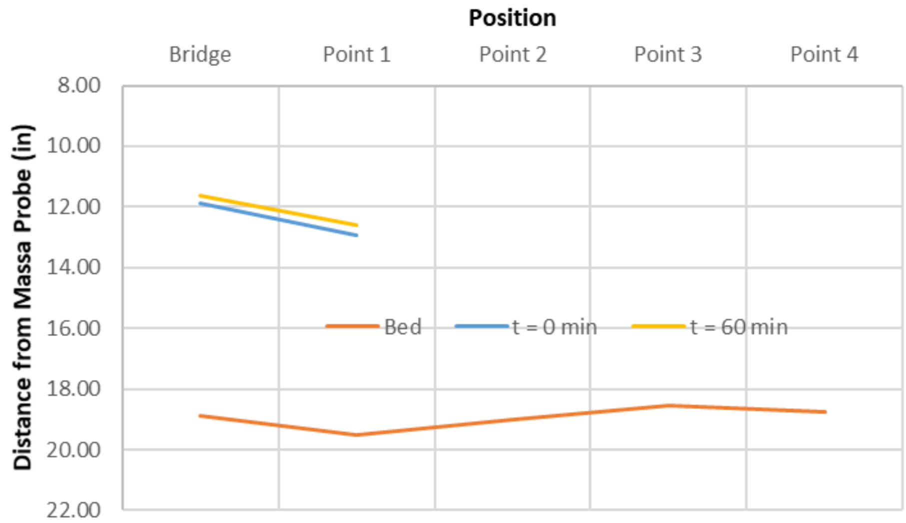

Figure 113: Before EXPT 03 Raw Massa Probe Data

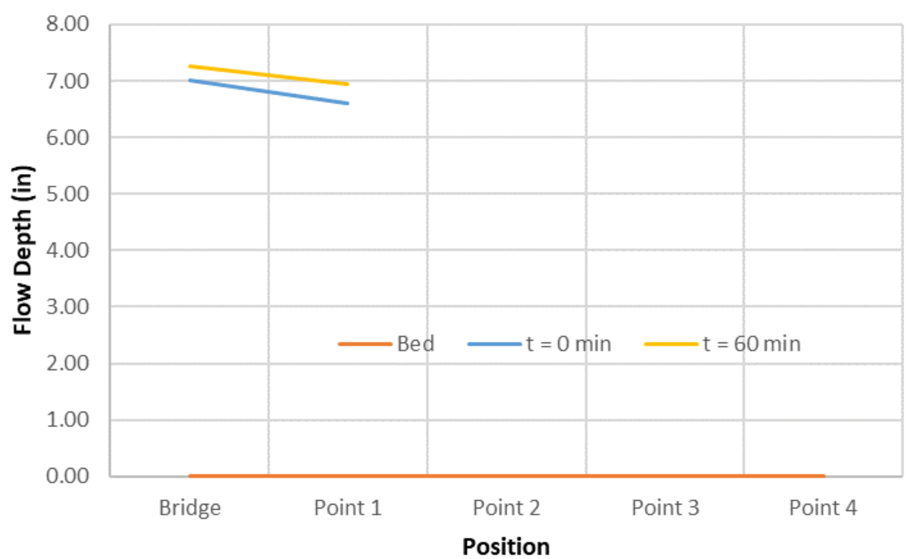

Figure 114: Before EXPT 03 Flow Depth

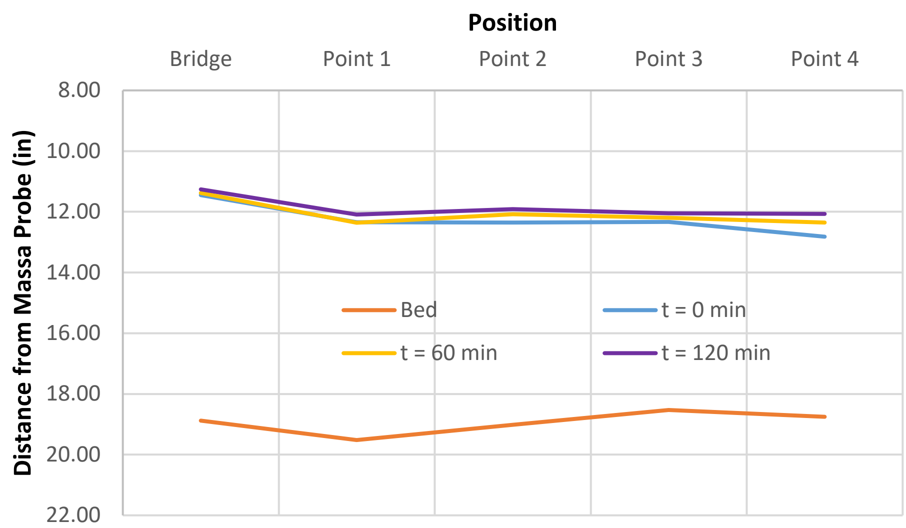

Figure 115: EXPT 03 Raw Massa Probe Data

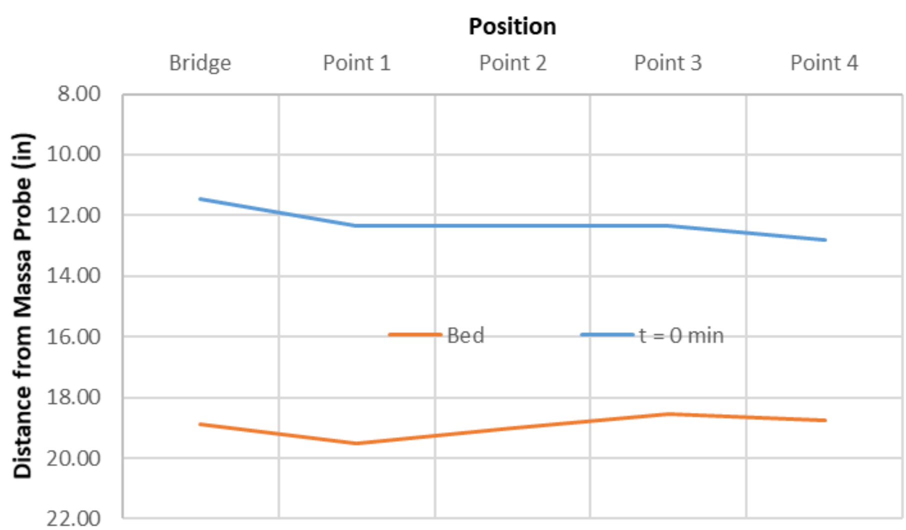

Figure 116: EXPT 03 Initial raw Massa probe data

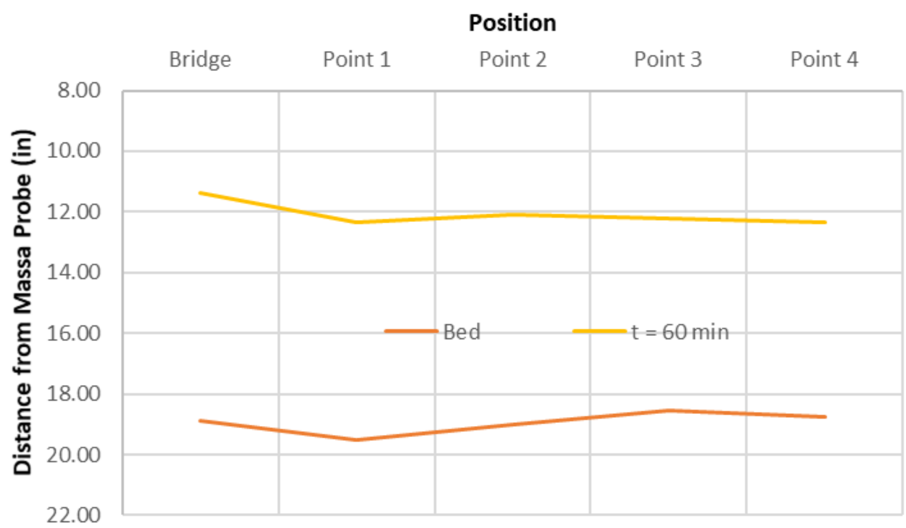

Figure 117: EXPT 03 Raw Massa probe data at 60 minutes

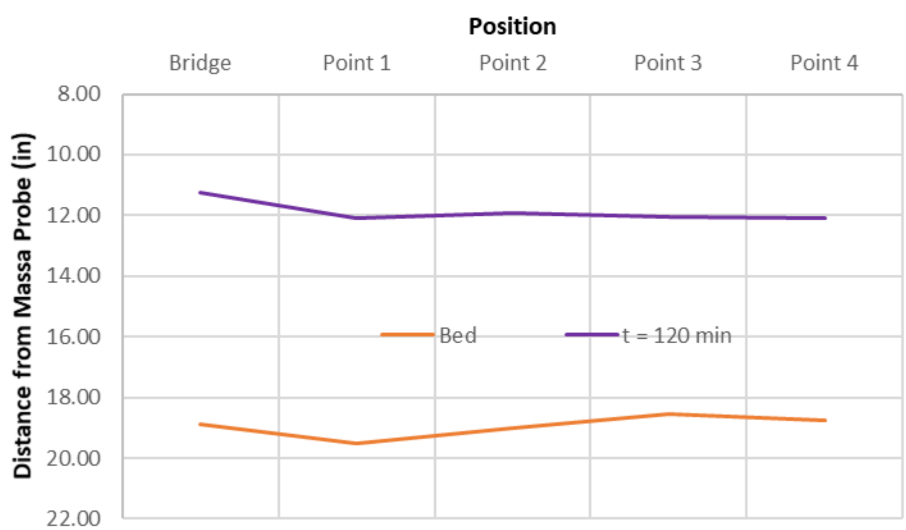

Figure 118: EXPT 03 Raw Massa probe data at 120 minutes

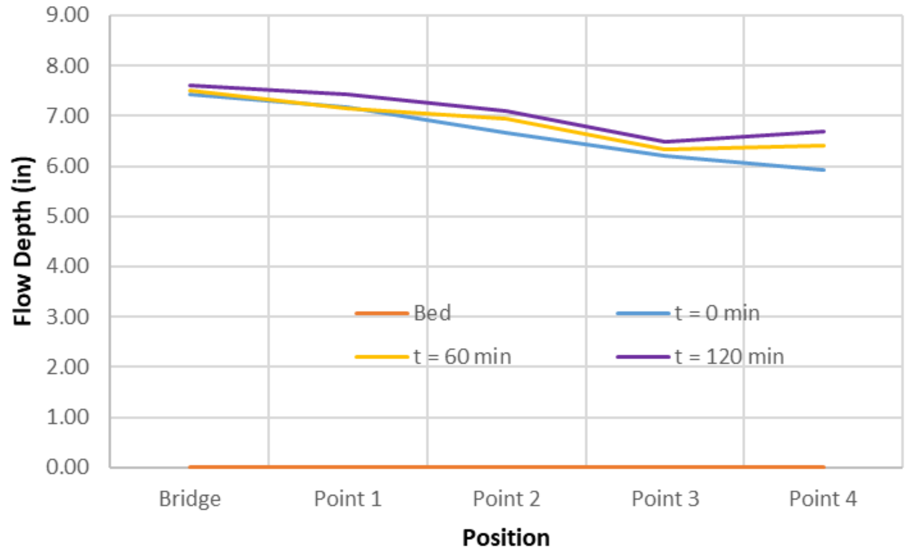

Figure 119: EXPT 03 Flow Depth

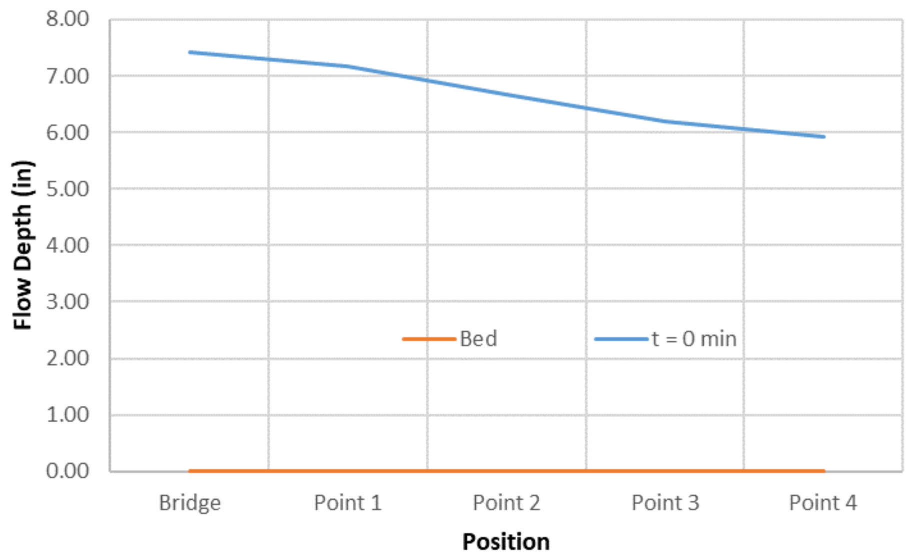

Figure 120: EXPT 03 Initial flow depth

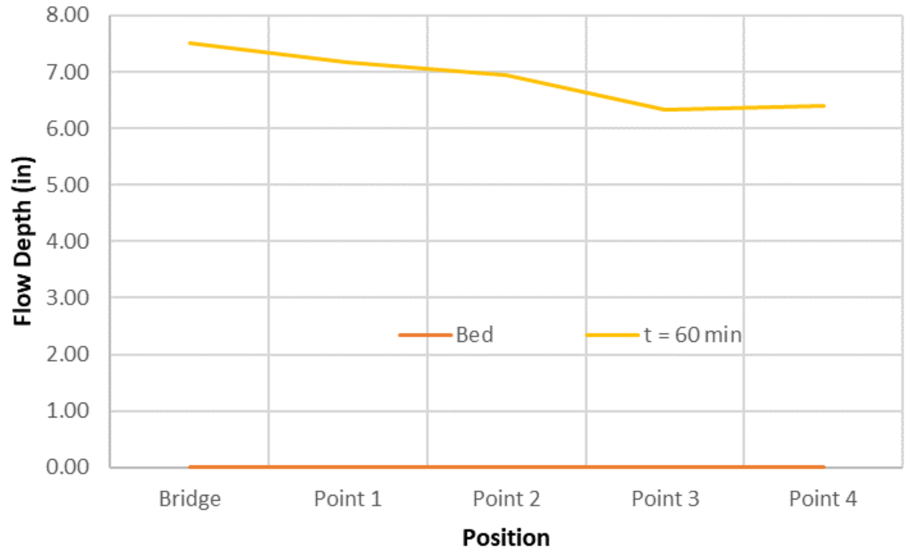

Figure 121: EXPT 03 Flow depth at 60 minutes

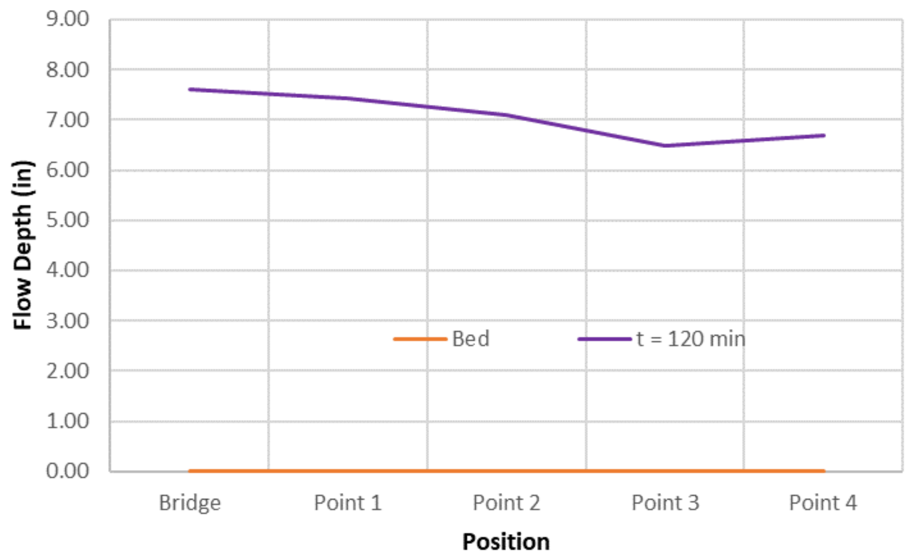

Figure 122: EXPT 03 Flow depth at 120 minutes

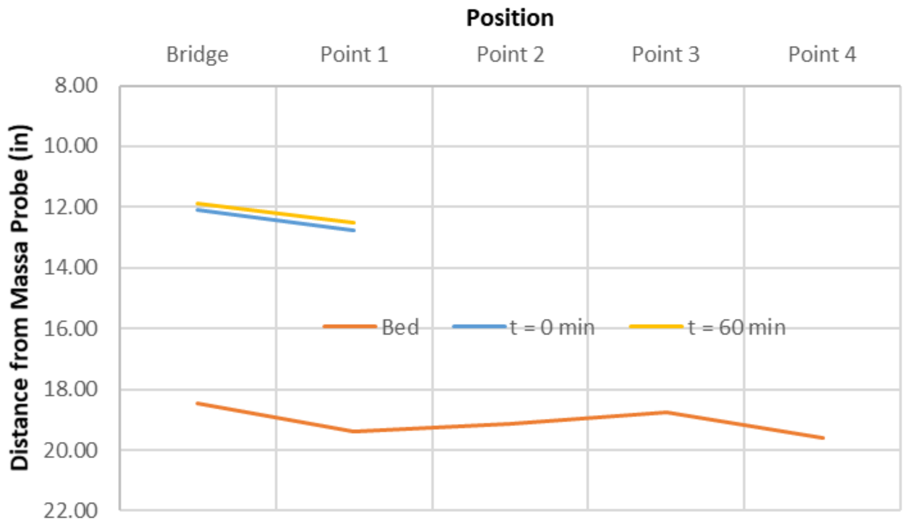

Figure 123: Before EXPT 04 Raw Massa Probe Data

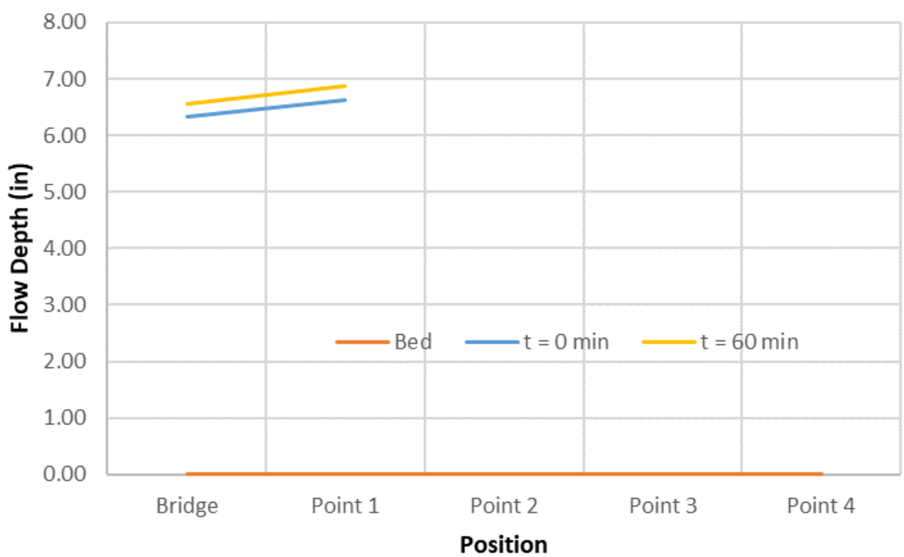

Figure 124: Before EXPT 04 Flow Depth

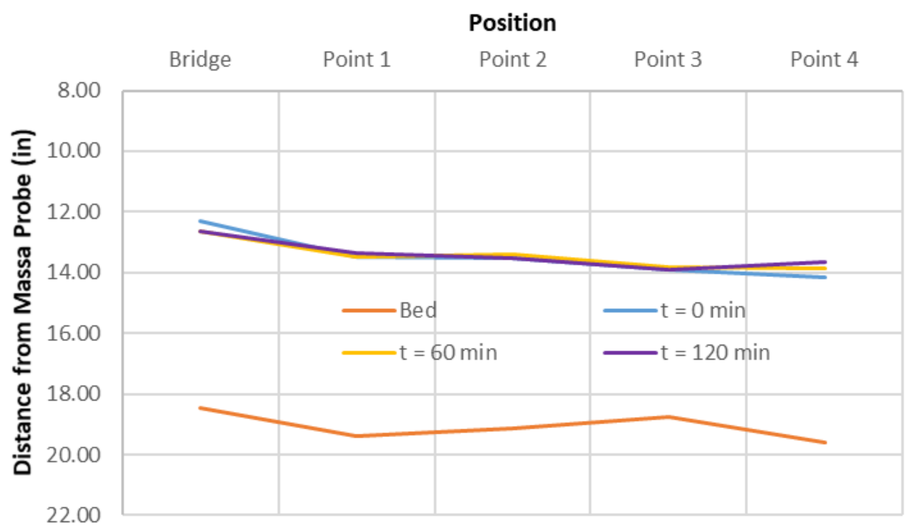

Figure 125: EXPT 04 Raw Massa Probe Data

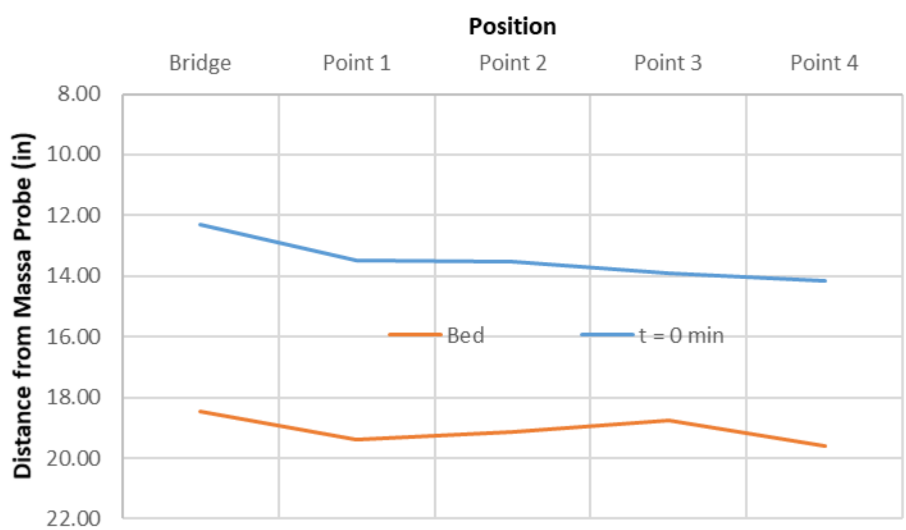

Figure 126: EXPT 04 Initial raw Massa probe data

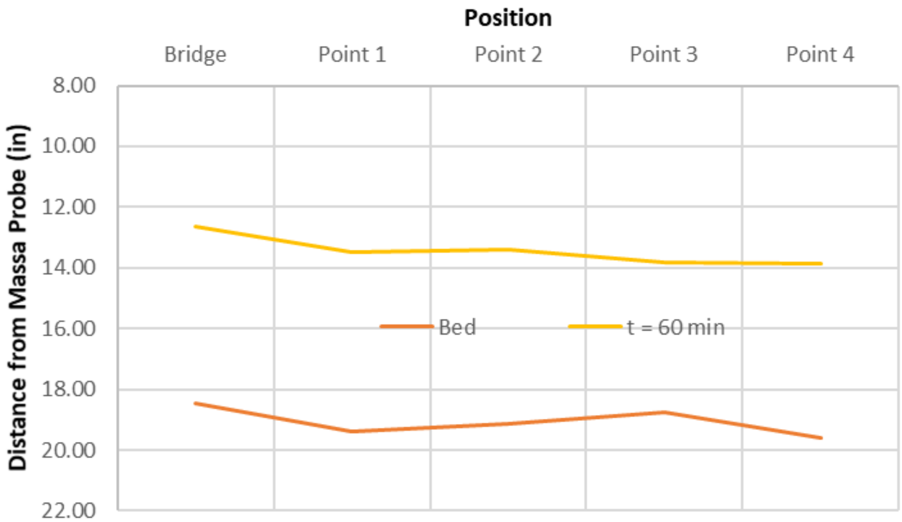

Figure 127: EXPT 04 Raw Massa probe data at 60 minutes

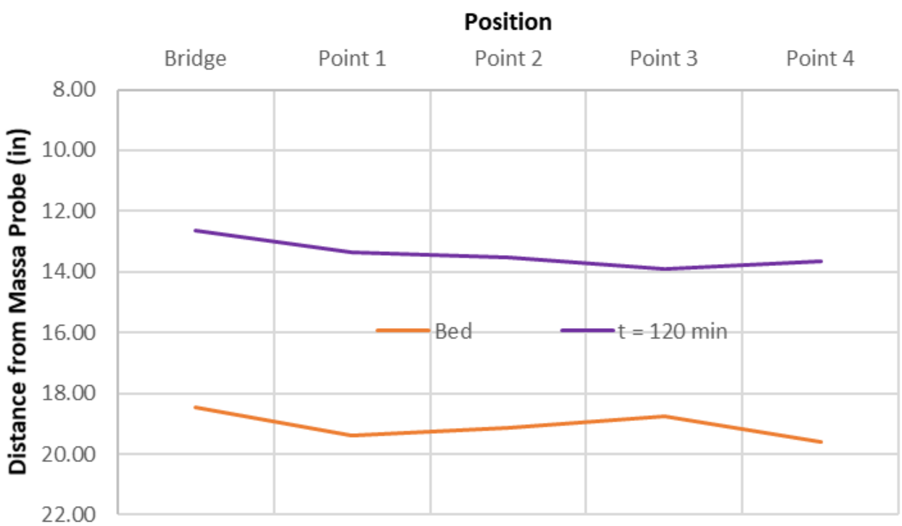

Figure 128: EXPT 04 Raw Massa probe data at 120 minutes

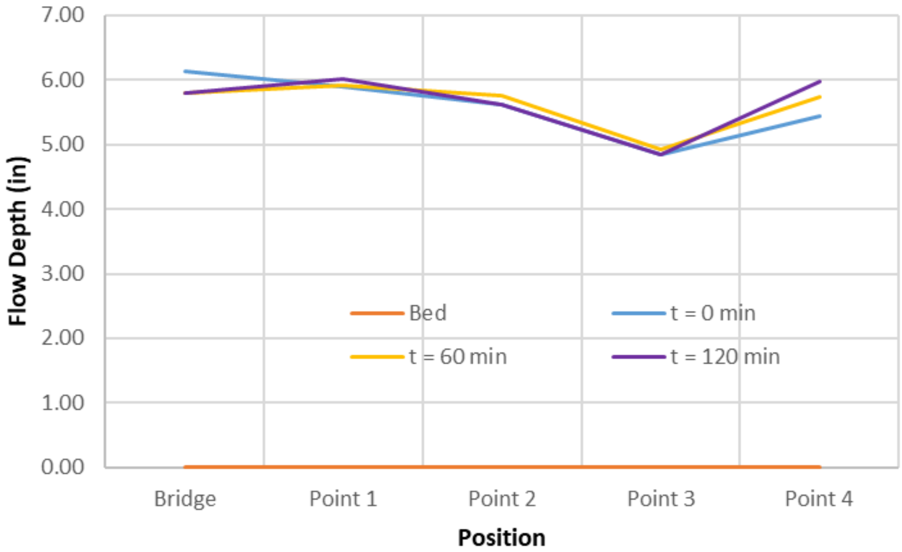

Figure 129: EXPT 04 Flow Depth

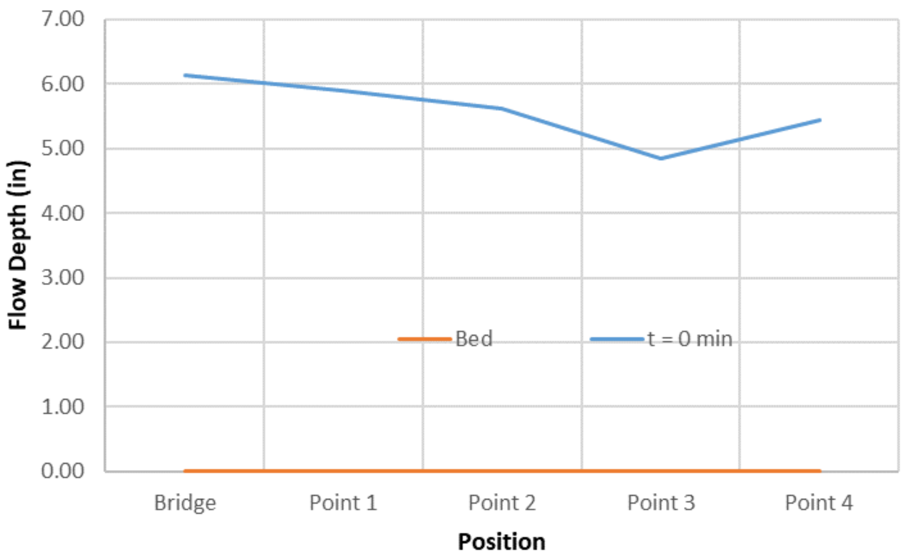

Figure 130: EXPT 04 Initial flow depth

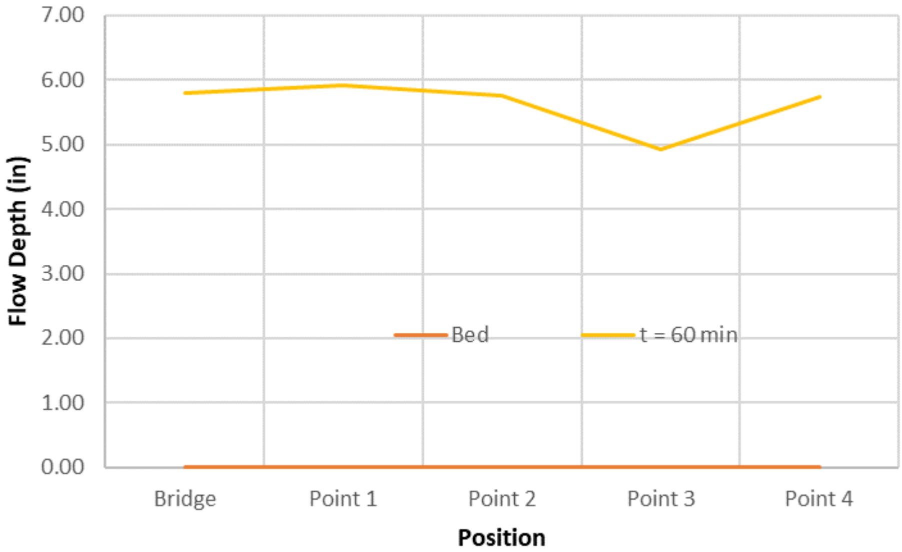

Figure 131: EXPT 04 Flow depth at 60 minutes

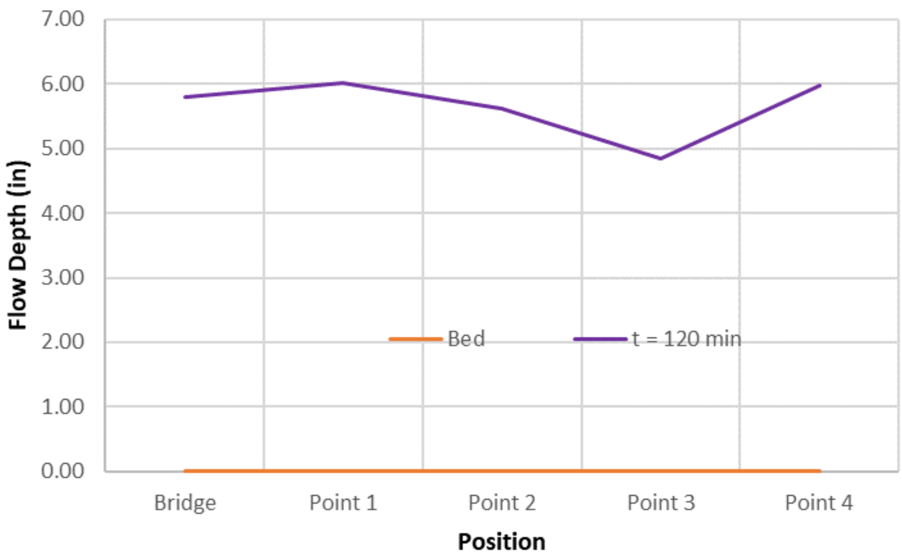

Figure 132: EXPT 04 Flow depth at 120 minutes

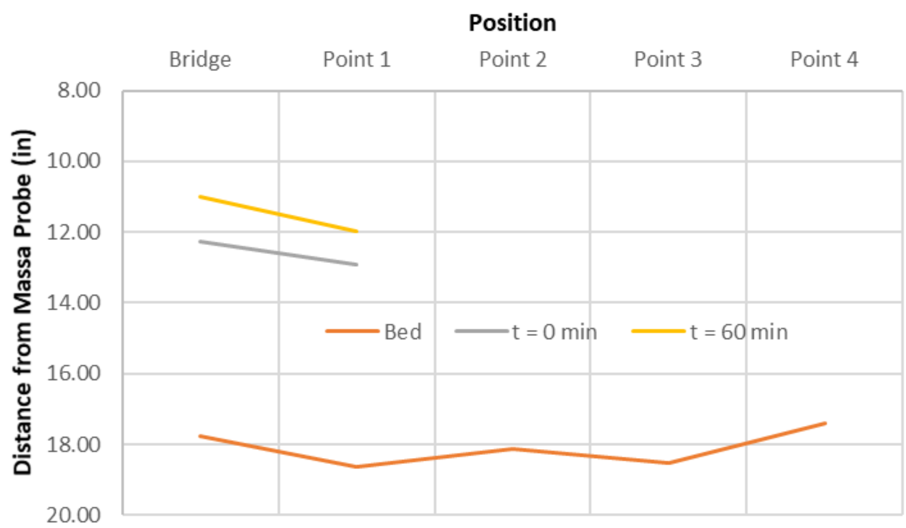

Figure 133: Before EXPT 05 Raw Massa Probe Data

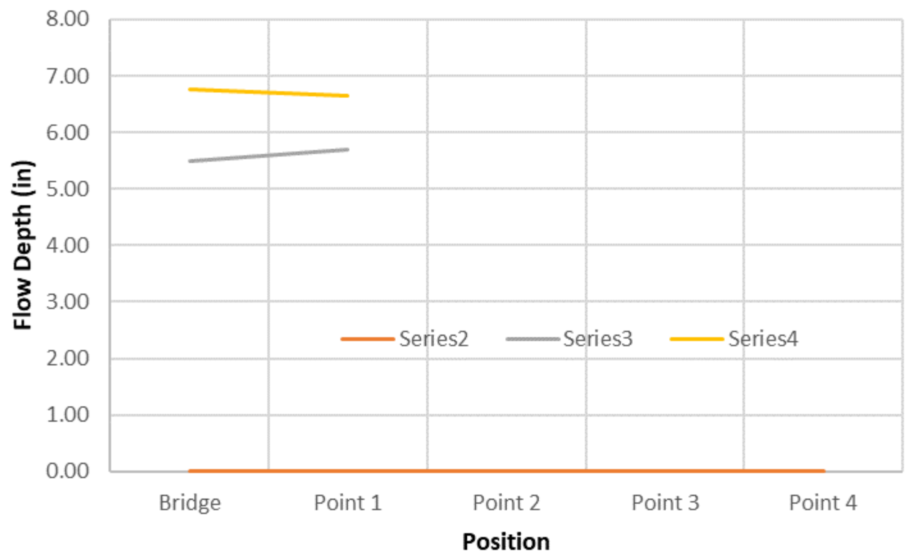

Figure 134: Before EXPT 05 Flow Depth

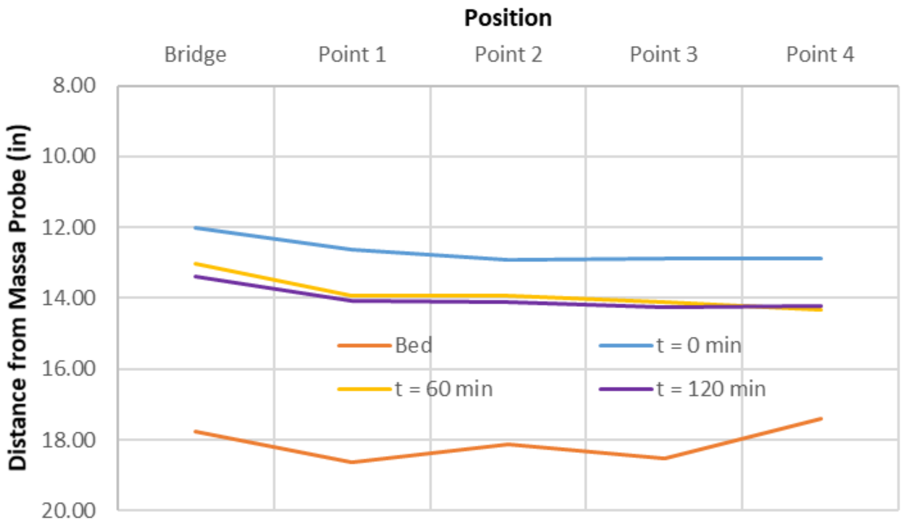

Figure 135: EXPT 05 Raw Massa Probe Data

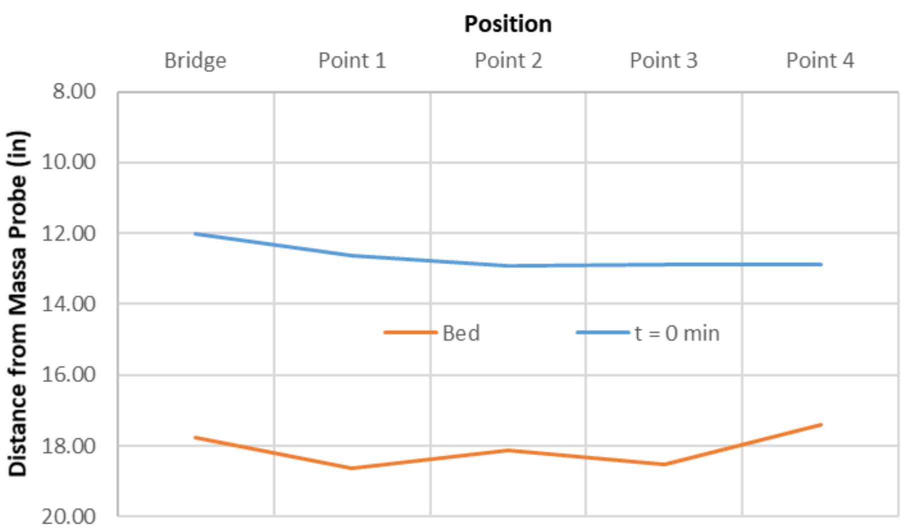

Figure 136: EXPT 05 Initial raw Massa probe data

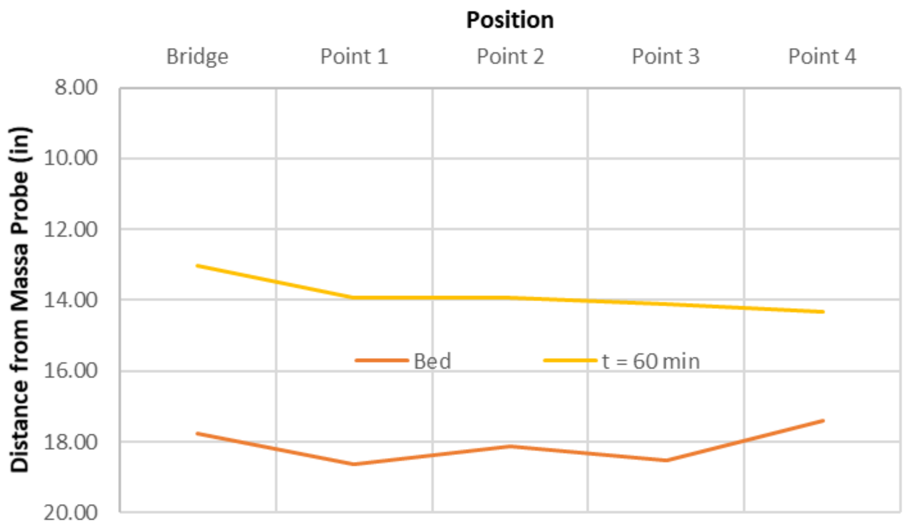

Figure 137: EXPT 05 Raw Massa probe data at 60 minutes

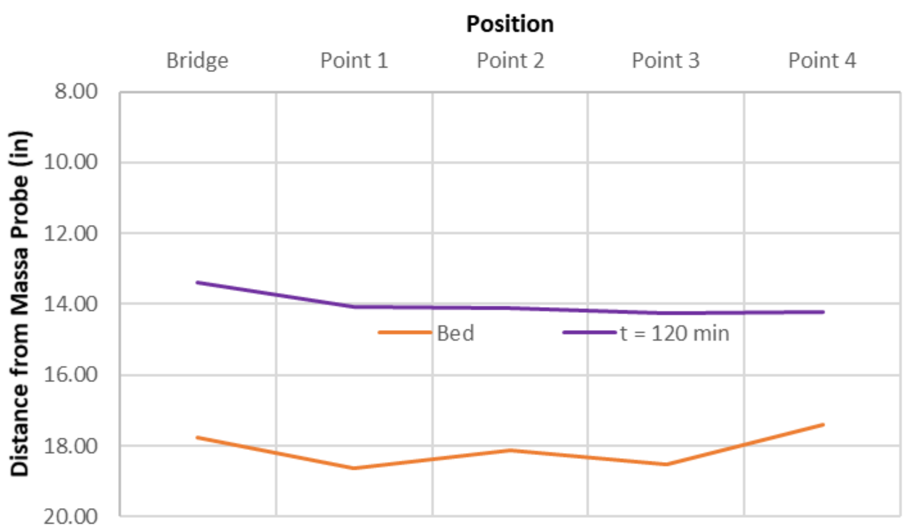

Figure 138: EXPT 05 Raw Massa probe data at 120 minutes

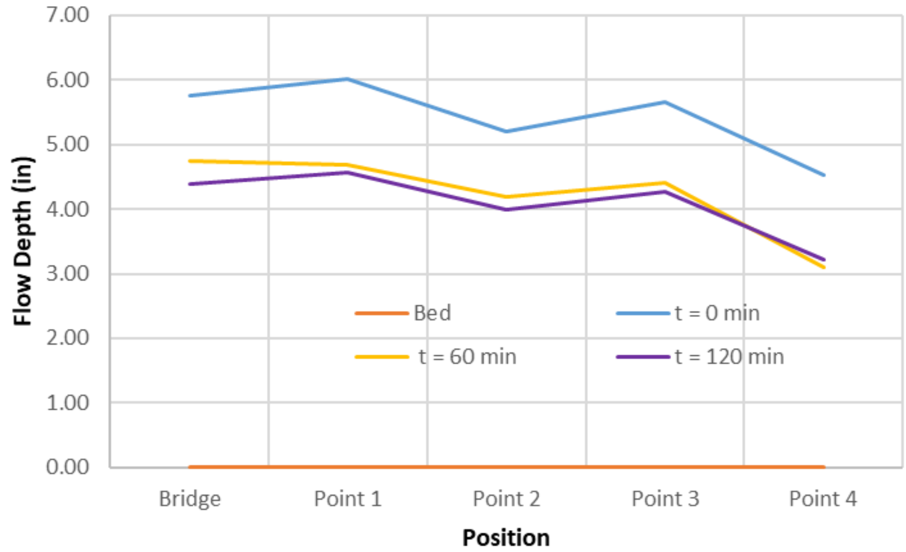

Figure 139: EXPT 05 Flow Depth

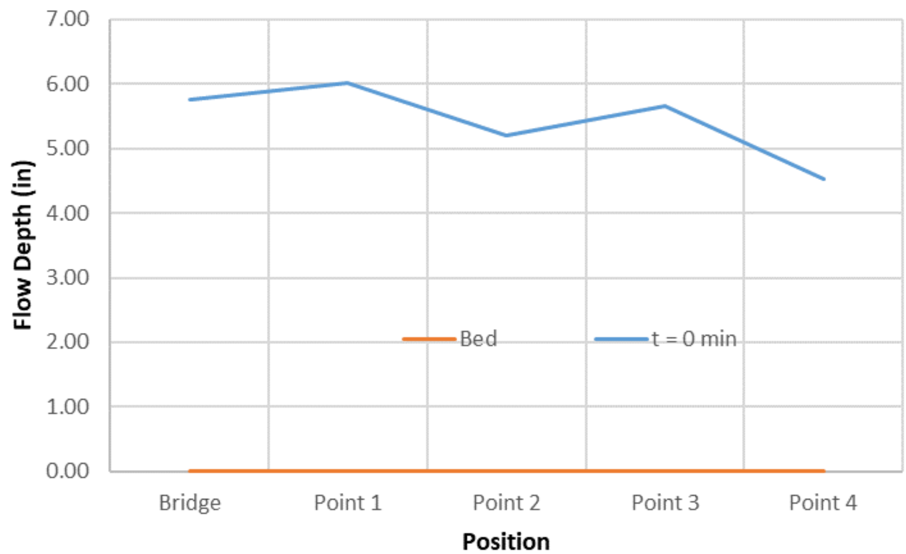

Figure 140: EXPT 05 Initial flow depth

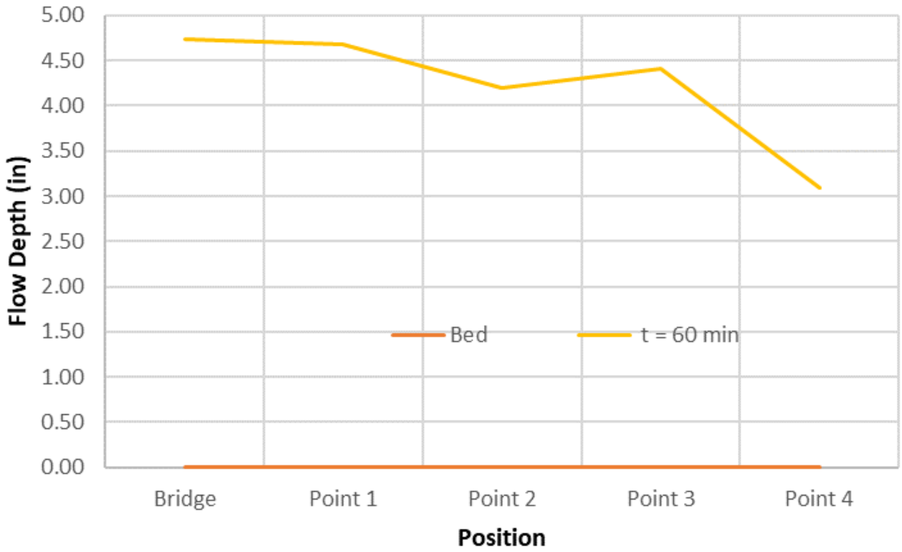

Figure 141: EXPT 05 Flow depth at 60 minutes

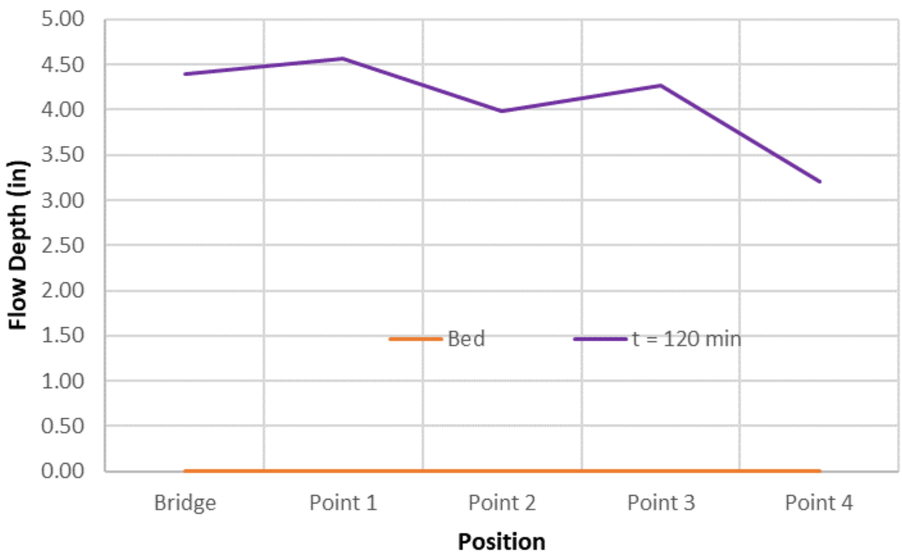

Figure 142: EXPT 05 Flow depth at 120 minutes

LIST OF ABBREVIATIONS

ADV	Acoustic Doppler Velocimetry
BW	Bendway Weir
CFD	Computational Flow Dynamics
CSU	Colorado State University
EXPT	Experiment
FLOW-3D	3D CFD model by Flow Science, Inc.
LiDAR	Light Detection and Ranging Survey System
LSPIV	Large-Scale Particle Image Velocimetry
MPM	Meyer-Peter & Müller
RV	Rock Vane
SRH-2D	Sedimentation and River Hydraulics – two dimensional
USBR	United States Bureau of Reclamation
WSE	Water Surface Elevation